Development and Application of Lysate Microarray Technology for Quantitative Analysis of Human Disease

(Article begins on next page)

Dissertation Advisor: Professor Gavin MacBeath

Albert Shanbuo Ye

Advisor: Professor Michael B. Yaffe

May 13, 2013

Harvard University

Development and Application of Lysate Microarray Technology for Quantitative Analysis of Human Disease

Abstract

Reductionist biology has yielded tremendous insight into the basis of biochemistry and genetic disease. However, the remarkable failure of reductionist biology to explain complex problems, especially cancer, has led to the development of systems biology. The vast complexity of biological systems remains the most difficult problem in biology today. In order to understand this complexity, we need tools to massively multiplex measurements of a signaling network. Therefore, we developed lysate microarray technology to fill this need. In this work, we discuss three ways in which lysate microarrays were applied to human disease.

In the first work, we discuss a key stage in malaria development. The liver-stage malaria parasite represents a promising target for intervention, and we present the first use of lysate microarray technology as a screening tool for host-parasite interactions in an infectious disease. We identified three cancer-related pathways that are modified in malaria infection, and studied the p53 pathway in depth. Our finding that the parasite downregulates p53 and that treatment with Nutlin-3 strongly decreases parasite load may lead to the development of a prophylactic malaria vaccine.

In the second work, we began by screening drug combinations and varying dosing schedule in triple-negative breast cancers (TNBCs). We systematically explored stimulation space and

collected a large lysate microarray dataset, which was used for statistical analysis. We identified a sensitization effect when a growth factor signaling inhibitor was presented before a genotoxic agent. This sensitization was generalizable among a subset of TNBCs and may generally be important for cancers driven by growth factor signaling, as we found the effect extends to non-TNBC cancers. We hope this data will be useful in guiding cancer treatment strategies in patients.

In the third work, we study the changing role of the DNA Damage Response (DDR) as a cell line evolves towards cancer. We used the MCF10A progression series and studied how these cell lines respond to genotoxic agents. We identified differences in cell fates after treatment, and collected a large lysate microarray dataset for statistical analysis. Early analysis of the data indicates gross rewiring within the DDR between the MCF10A cell lines.

To

My Family, Both Blood and Scientific,

Who Have Supported Me

In Everything, Always

Acknowledgements

A PhD is never produced by a single person. While my name is on the cover, I am hardly the only person who contributed to this work. I want to deeply thank, from the deepest part of my soul, everyone who I have met, spent time or broken bread with, or worked with, along the way. It's been a long road, and without fellow travelers it would have been lonely indeed.

I need to start by thanking my advisor, Dr. Gavin MacBeath, for everything he has done for me. Gavin has endlessly supported my work, with boundless optimism, enthusiasm, humor, and guidance. He has always allowed me the freedom to pursue whatever risk I wanted, and yet was always there with a smile and a fresh view when I needed it. He promoted collegial, open, and friendly collaboration within his lab, which was crucial to my graduate school experience. Gavin taught me to think more rigorously and speak more carefully, skills that I will take with me for the rest of my life. Finally, he bravely stood by his students when dark days befell the lab, for which we are all deeply appreciative.

I also need to thank my MacBeath lab colleagues, among whom I count some of my closest friends. In particular, I would like to mention by name Drs. Mark Sevecka, Alejandro Wolf-Yadlin, Jordan Krall, Elsa Beyer, Alexis Kaushansky, Grigoriy Koytiger, Taran Gujral, and Marina Chan.

To Mark and Ale: Thanks for collectively teaching me everything I know about preparing, printing, probing, quantifying, and interpreting lysate microarrays. Your endless banter and antics are the stuff of legend.

To Jordan and Elsa: As I had worked exclusively in microbiology prior to joining the MacBeath lab, I am indebted to you for giving me the crash course in mammalian cell culture.

To Alexis: Thanks for all the conversations through the years. You've made me an incorrigible coffee snob, for which I'm not so sure I'm grateful. I am definitely glad, however, that we ended up working together and the project went where it did.

To Greg: Your sharp wit and sarcasm are always a breath of fresh air. Thanks for the friendship, conversations, and perceptive insight in all walks of life.

To Taran: Your unshakable calm was the perfect antidote to my sometimes passionate outbursts. We shared many trials and tribulations, and I wish you all the best in your future science. Thanks also for always being so accommodating and working with me whenever I needed help.

To Marina: You've brightened the lab ever since you arrived, and you're everything a friend could be. I immensely enjoyed our frequent conversations, and though we disagreed often, I hope we both came away having learned from each other. I certainly did.

Without these other friends, I would have gone insane long ago. To Rosa, Srinjan, Dina, Bryan, Dario, and Liz: thanks for all the memories: may the friendships never end. Thanks also to Team Potato for the years of laughter and terribly convoluted inside jokes, most of which defy explanation. To Mark, Jon, and Bradford: GG.

Next, I need to thank my committee members, past and present: Professors Andrew Murray, Mike Yaffe, Alan Saghatelian, Peter Sorger, and Tim Mitchinson. Our meetings, though difficult to set up, were certainly useful and greatly accelerated my research. You all also taught me to be more explicit in my thought process, for which I always be thankful.

I need to thank Prof. Yaffe for working with me as a collaborator at first, then later having me join his lab as a visiting student. The final work in my graduate career would never have happened without his support, be it intellectual, material, or emotional. Here I should also mention my collaborators Drs. Andrea Tentner and Michael Lee, who have both remained colleagues and

friends, and from whom I learned much. In addition, I should thank Dr. Duaa Mohammad for making me feel welcome and for being the best friend I could ask for.

Last here but foremost in my thoughts, I need to thank my family, to whom I owe everything and to whom I dedicate this work. The most important thing to me has always been family. They have always encouraged me to achieve, and driven me to strive ever higher.

Table of Contents

Part 1

Introduction: Lysate Microarray Technology and Applications for

Human Health in Malaria and Cancer

Part 2

Application of Lysate Microarray Technology For High-Throughput Profiling

and Drug Target Identification In Liver-Stage Malaria Infection

Part 3

Application of Lysate Microarray Technology

For High-Throughput Profiling Of Apoptotic Signaling Networks

Part 4

Application of Lysate Microarray Technology For Understanding

the DNA Damage Response In the Context of Tumor Progression

List of Figures

List of Tables

List of Equations

Part 1

Introduction: Motivations for

Lysate Microarray Technology

And Applications for Human Health

In Malaria and Cancer

1.1. Motivations For Deep Network Analysis

Biological research has historically proceeded in a strongly linear fashion, with research frequently limited in scope to a single gene, protein, or signaling event. Signaling networks were painstakingly built, with phosphorylation events and genetic targets carefully identified. This wealth of knowledge has yielded many insights into the inner workings of both normal and abnormal biology.

The modern rational drug design approach in the fields of infectious disease and cancer have met with mixed results. We see problems with both, and present alternative strategies to avoiding the major difficulties in these approaches to human health and drug development.

1.1.1. Infectious Disease

There is little doubt that antimicrobials have greatly improved human health, but it is also evident that our strategies are far from optimal. Infectious disease researchers have traditionally worked in 3 major arenas: identification of the infectious agent, elucidation of key events in its natural history, and screening of natural products or synthetic compounds which inhibit its growth, infectivity, or virulence while minimally affecting the host. It is this last arena of research that has produced the vast pharmacopeia of antimicrobial agents and has largely eliminated many ancient diseases from daily life, at least in the regions of the world where the medicines are readily available.

Unfortunately, despite their remarkable successes, these approaches also pave the way to their own demise. The drugs commonly attack critical metabolic or signaling pathways in the pathogen itself, so mutation within the target protein, often a single amino acid in the drug binding site, can confer complete resistance (Wilcox et al., 2001). Overuse and incomplete killing efficiently select

for resistance, greatly accelerating the propagation of multiply-resistant strains. These effects have combined to render nearly obsolete such once-potent antimicrobials as tetracycline and ampicillin.

Historically, the pharmaceutical response to the evolution of resistance is to treat the symptom rather than the fundamental problem. Much effort has been spent into expanding the pharmacopeia by finding new antimicrobials and derivatizing existing drugs, in a never-ending and costly arms race that inevitably promotes the evolution of totally-resistant pathogens (Babu and Laxminarayan, 2012). The list of candidate molecules is finite, and the rate of new drugs coming on the market has stagnated while the need for new antimicrobials continues to increase (Coates and Halls, 2012; Pieren and Tigges, 2012). Indeed, in 2011 the World Health Organization declared antimicrobial resistance to be a primary threat to public health worldwide, and has published a book highlighting in part the importance of innovation in drug development (WHO, 2013).

We propose a new plan of attack focusing not on intra-pathogen signaling and biochemistry, but rather on pathogen-host interactions. An intervention that targets a host signaling pathway required for the parasite life cycle will be far more recalcitrant to evolution of resistance. We therefore chose malaria, a disease that the WHO identifies as critically in danger of reverting to a pre-antimicrobial era, and specifically focused on the liver-stage, when the parasite requires a host cell for metabolism. We developed a novel assay to measure host signaling in response to malarial infection and identify a prominent host target that the parasite manipulates in order to evade apoptosis. We also demonstrate that this manipulation is required for malarial progression, and present evidence that a drug originally developed for cancer treatment has potential as a malaria vaccine.

1.1.2. Oncology

The history of the vast field of cancer research has been very fruitful in theory and biological insight, but relatively lackluster in actionable treatments. As evidence for the multiple-hit hypothesis accumulated, cancer researchers increasingly focused their efforts on the particular mutations that could be shown to be correlated with cancer. Naturally, work focused heavily on frequently observed events such as aberrant kinase signaling and upregulated transcription factors. The frequency with which common lesions were observed also led to optimism that specific inhibitors against these targets would be magic bullets: if a cancer is driven by aberrant signaling through a particular protein, a drug inhibiting that protein would surely be an effective treatment. It is a sobering thought that most of these initially exciting treatments are less effective than expected.

If we have learned anything about cancer in the last 50 years, it is that cancer is a more complicated problem than anyone initially imagined. Genetic and epigenetic profiling has repeatedly shown that a single cancer carries hundreds, if not thousands, of abnormalities (Dawson and Kouzarides, 2012; Stratton et al., 2009). Even those drugs that do specifically and efficiently inhibit cancer signaling frequently do not succeed as monotherapies and must be used in combination therapies to achieve clinical efficacy (Awada et al., 2012; Saxena and Dwivedi, 2012). As the pharmacopeia of inhibitors grows, it becomes increasingly impractical to test all combinations for efficacy. The skyrocketing costs of these myriad clinical failures and the ongoing morbidity from cancer, combined with the ability to produce data from high-throughput multiplexed experiments, has left biologists looking for more nuanced approaches.

One of the great recent innovations in oncology is the application of network analysis to biological systems. It was recognized as early as 1957 that the well-understood and relatively simple 2-gene *lac* operon system was capable of non-linear behavior (Novick and Weiner, 1957),

4

so analyzing a single gene independently is insufficient to capture the full complexities and emergent properties of biological systems. Furthermore, it is increasingly clear that signaling in the cell does not usually proceed linearly, rather, cell decisions are more often made as a combination of multiple, competing, and highly dynamic molecular events. It is also clear that due to the many possible ways in which cancer can evolve, each tumor is unique. In an attempt to understand this complexity, beginning in the 1990s, biologists began to use mathematical network analysis and graph theory to model key molecular species and events in order to predict outcomes (Forrest and Curran, 1992). So far, this field is still young, but its applications are beginning to bear fruit.

The standard of cancer care at this time is paradoxically both high tech and coarse. For example, although we can identify that a particular patient's cancer carries a specific growth-promoting mutation, an otherwise good drug against that target may nonetheless have modest to no effect on tumor size (Burstein et al., 2008). When initial therapy fails or a tumor recurs, the standard of clinical care is an expensive and time-consuming trial-and-error where standard treatment regimens are tried until an efficacious one is found. While this process is underway, there is significant patient morbidity, astronomical cost, and degradation of quality of life with no guarantee of improvement or cure.

We believe that network analysis, when applied to cancer, can uniquely help this situation by identifying subtle non-intuitive approaches. We envision the ability to quickly measure the internal signaling network of cancer cells in a patient biopsy. We believe that analysis of such patient cancer networks can yield insights into the biological mechanisms unique to each tumor, as well as suggest potential routes of treatment. We also believe that by systematically stimulating

cells grown in culture and measuring the resulting network perturbations, we gain biological insight applicable to patients.

We therefore promote an approach that deeply studies the signaling state within the cell in order to identify those combinations of signaling events that represent growth and death. In Chapter 3, we use this strategy to identify a combination of drugs that efficiently primes cells to die, but only when given in a specific order and timing, and deeply probe the signaling events surrounding this decision. In Chapter 4, we extend this approach to understand, in the context of a tumor progression model, the specific signaling events that result from exposure to the poorly understood cancer drug doxorubicin.

Works Cited

Awada, A., Bozovic-Spasojevic, I., and Chow, L. (2012). New therapies in HER2-positive breast cancer: a major step towards a cure of the disease? Cancer treatment reviews *38*, 494-504.

Babu, G.R., and Laxminarayan, R. (2012). The unsurprising story of MDR-TB resistance in India. Tuberculosis (Edinb) *92*, 301-306.

Burstein, H.J., Storniolo, A.M., Franco, S., Forster, J., Stein, S., Rubin, S., Salazar, V.M., and Blackwell, K.L. (2008). A phase II study of lapatinib monotherapy in chemotherapy-refractory HER2-positive and HER2-negative advanced or metastatic breast cancer. Annals of oncology : official journal of the European Society for Medical Oncology / ESMO *19*, 1068-1074.

Coates, A.R.M., and Halls, G. (2012). Antibiotics in Phase II and III Clinical Trials. Handb Exp Pharmacol *211*, 167-183.

Dawson, M.A., and Kouzarides, T. (2012). Cancer epigenetics: from mechanism to therapy. Cell *150*, 12-27.

Forrest, D., and Curran, T. (1992). Crossed signals: oncogenic transcription factors. Curr Opin Genet Dev *2*, 19-27.

Novick, A., and Weiner, M. (1957). Enzyme Induction as an All-or-None Phenomenon. Proc Natl Acad Sci U S A *43*, 553-566.

Pieren, M., and Tigges, M. (2012). Adjuvant strategies for potentiation of antibiotics to overcome antimicrobial resistance. Current opinion in pharmacology *12*, 551-555.

Saxena, R., and Dwivedi, A. (2012). ErbB family receptor inhibitors as therapeutic agents in breast cancer: Current status and future clinical perspective. Medicinal Research Reviews *32*, 166-215.

Stratton, M.R., Campbell, P.J., and Futreal, P.A. (2009). The cancer genome. Nature *458*, 719-724.

WHO (2013). The evolving threat of antimicrobial resistance - Options for action (WHO Press).

Wilcox, S.K., Cavey, G.S., and Pearson, J.D. (2001). Single ribosomal protein mutations in antibiotic-resistant bacteria analyzed by mass spectrometry. Antimicrobial agents and chemotherapy *45*, 3046-3055.

1.2. Lysate Microarray Technology

1.2.1. Motivation for and Invention of Microarraying Technology

Microarray technology refers to a technique to deposit a large number of samples in a miniaturized format onto a small solid support. The idea grew naturally out of Southern blotting, with the first reported use of the approach dating back to 1982 when 378 samples were assayed at once for expression of genes in normal and tumor tissue (Augenlicht and Kobrin, 1982). The concept was adapted to produce DNA microarray technology, a powerful technique that can quantify mRNA transcript levels across the entire genome.

As sequencing efforts such as the Human Genome Project began to pay off, anticipation for DNA microarray technology grew.   The ability of DNA microarrays to measure, in a single experiment, expression levels over the entire genome, was too powerful to ignore. Whole genome DNA microarrays became available for the yeast *Sacchromyces cerevisae* in 1997 (Lashkari et al., 1997) with the human version following in 2001, hot on the heels of the publication of the human genome (Shoemaker et al., 2001). The ensuing explosion of large dataset production can be described as the advent of –omics level biology, with widespread optimism that functional genomics would enlighten many obscure features of biology.

However, DNA microarrays have a major caveat: they only reliably measure mRNA levels, which are assumed to be a proxy for protein level and function. Unfortunately, this has proven over and over to be a false assumption, as protein levels frequently do not correlate with mRNA levels (Gygi et al., 1999; Kopf and Zharhary, 2007; Zhu and Snyder, 2001), and it is the translated protein that fundamentally carries out gene function. Additionally, signaling events such as phosphorylation or protein cleavage can have profound effects on protein function and cannot be

accounted for in DNA microarrays. These problems can render DNA microarray datasets difficult to interpret, and underline the need for multiplexed assays for protein function.

1.2.2. Development of Lysate Microarray Technology

Lysate microarrays, sometimes also known as reverse phase protein arrays (RPPA), were specifically designed to analyze many samples for more proximal markers of protein function. Cellular lysates are adsorbed onto a solid support, usually made of PVDF or nitrocellulose, which is attached to a glass slide. These slides are then probed with unique antibodies against targets of interest, visualized, quantified, and normalized.

Lysate microarrays were initially used to profile signaling within primary tumor samples, though it was soon also harnessed to study cells in culture. Three early reports from the Liotta lab (Grubb et al., 2003; Paweletz et al., 2001; Wulfkuhle et al., 2003) surveyed the native signaling in prostate and ovarian cancers and showed that data acquired by microarray recapitulates data from other sources, including immunoblotting. These pioneering experiments notably used laser capture microdissection to subdivide a sample into cellular subclasses by histology and spotted them separately, an idea we echo in our malaria experiments in Chapter 2, though we utilized fluorescence activated cell sorting (FACS). The first application of lysate microarrays to cell lines was also published in 2003 (Nishizuka et al., 2003), with perturbation studies of drug treatment immediately following (Belluco et al., 2005).

Further innovations came from improvements in spotting technology, quantification, and arsenal of antibody probes against signaling proteins. The first experiments printed less than 1000 spots on a standard 25×75mm slide, while modern contact arrayers such as the 2470 Aushon microarray can easily fit 6000 samples in quadruplicate on the same slide. This increase in density

has greatly improved the throughput of the technique. In addition, initial experiments were performed with enzymatic readouts, which have been replaced by fluorescently conjugated antibodies. Fluorescence results in a larger dynamic range in which signal remains relatively linear, and is also easily quantified by fluorescence imagers. Surprisingly, the original papers report near linearity of enzymatic signal with concentration of sample in all cases, while we now know that signals resulting from an adsorption source should follow a sigmoidal curve (Zhang et al., 2009). Finally and perhaps most importantly, while the original papers each used 6 antibodies against known cancer signaling targets, we have today expanded the repertoire of antibodies that can be used in microarrays to over 300.

Today, lysate microarrays are a popular and inexpensive technique to measure target proteins in medium throughput in against biological samples in high throughput. They have been explored for diagnostic use (Theranostics Health Inc), biomarker discovery (Gonzalez-Angulo et al., 2011), and basic science applications such as perturbation analysis (Gujral et al., 2012). In this work we discuss three distinct uses of the technology, each of which contributes to human health in a different way.

1.2.3. Strengths and Weaknesses of Lysate Microarray Technology as Compared to Other Massively Multiplexed Techniques

The strengths of lysate microarrays are several: cheap cost, ease of use, small amount of biological material consumed, ability to discriminate post-translational modifications, and agnosticism toward type of biological sample. As compared to other comparable techniques such as Luminex™ (Luminex Corp (Austin, TX)) or immunoblotting, lysate microarray technology has some major selling points.

The only specialized hardware needed for the entire process is the arrayer, an investment that quickly pays for itself. Once the upfront cost of acquiring an arrayer has been paid, the incremental cost of printing more arrays is only the cost of the glass slide, on the order of $30/antibody probed, as compared to thousands of dollars for other techniques. Given that the consumables for a moderately sized Luminex or immunoblotting experiment may quickly run into the tens of thousands, the cost of the arrayer is quickly recouped.

Lysate microarrays, once printed, are easy to store, handle, probe, and quantify. Indeed, once the samples have been collected in denaturing buffer, they can be stored indefinitely at -80°C and can even be thawed to print more arrays or analysis by other techniques. Furthermore, the printing process is relatively quick: 10,000 samples can be comfortably printed onto 30 slides in a week with minimal human intervention on the arrayer. Once printed, the slides are inert and may be stored dry, at room temperature, indefinitely. Probing the arrays involves no harsh, specialized, expensive, or dangerous chemicals, and the protocol is not labor intensive. Finally, the quantification of microarrays is largely automated through the use of software specifically designed for image recognition of grids of spots. For the purposes of our work, we made extensive use of ArrayPro Analyzer by MediaCybernetics Inc (Rockville, MD), as well as MicroVigene by VigeneTech (Carlisle, MA).

Another advantage of lysate microarrays is the very small amount of sample consumed per experiment. The amount of lysate consumed per spot is only on the order of nanoliters. This means that a very small amount of sample can be used to print a large number of identical arrays, each of which can be probed uniquely with a primary antibody directed against a protein of interest to quantify each lysate for that protein. This also means that if there are many samples to be probed in parallel, only a small amount of sample need be created, cutting down on the cost to create those

samples. We exploit this feature in the experiments presented in Chapter 2 studying malaria, where it is vastly impractical to make enough volume of lysate in high enough concentration to perform more common techniques such as immunoblotting. We are not aware of any alternative technique that we could have used to discover the biological insights we gained through our experiment.

Perhaps most importantly for our work, lysate microarray technology can discern post-translational modifications that can mean the difference between inactive and active protein. Kinases frequently sit atop vast networks of signaling that can determine the behavior of entire organisms, and yet the immediate consequences of their activity are only on the level of phosphorylation. Luckily, many antibodies are commercially available that can discriminate between phosphorylated and non-phosphorylated versions of their target proteins. Experiments using antibodies that are specific for phosphorylation are often more likely to yield useful mechanistic information than measurements of bulk protein level.

A final feature of lysate microarrays is that it can be applied many kinds of lysate collection techniques, fractionation, buffer compositions, cellular or tissue sources, and stimulations. In our work we apply the technique to whole cell lysates of several different cell lines, including cells that have been infected with live malaria parasite. Because the denaturing 2% SDS lysis buffer totally inactivates all cellular components including lipids, nuclei acids, and proteins, the lysate is not hazardous and is safe to handle without quarantine procedures.

However, lysate arrays do have one major drawback. Recognition of target protein is carried out with primary antibodies, as is secondary detection of the primary antibody. Antibodies are simultaneously ideal reagents and frustrating to work with, because while their unique ability to recognize just about any epitope lends great modularity and specificity, antibodies can also bind non-specifically to the surface or bind off-targets. In addition, antibodies can have avidity effects

12

on a surface and some do not bind their target at all. These effects all result in a non-linearity of signal, where a doubling of the target protein within a sample usually results in less than a doubling in output signal. In extreme cases where the amount of bound antibody is totally driven by off-targets or surface effects, or the target protein is not recognized, there may even be no change at all in output signal. These effects are cell-line specific and it is impossible to tell which antibodies will work in which cell lines without empirical testing (Sevecka et al., 2011). Therefore, it is crucial that careful preliminary work be done to extensively test antibodies against control lysates in both microarray and a gold standard, usually immunoblotting, to ensure quality of data. Key metrics must all be met for an antibody to be selected for use in microarrays: presence of only 1 target band of the correct size in immunoblots, high signal to background ratio on microarrays, high dynamic range, and linearity. With this in mind, we carefully validated all antibodies whenever practical; it was not practical in the malaria experiments due to constraints on ability to produce enough sample. In this case, we treated the experiment as a primary screen and carefully validated the results in several ways to confirm the hit.

This strict requirement of suitable antibodies is a fundamental drawback that severely limits the field of protein microarraying as a whole, and does not appear to be easily surmountable. We remain hopeful that as the availability of high quality antibodies increases and the cost of producing and acquiring new antibodies decreases, protein microarraying will continue to increase in utility. It is also worth noting that competitor techniques such as Luminex and immunoblotting also have this basic dependence on antibodies, though they are somewhat aggravated in lysate microarrays due to the lack of size separation. However, despite this major drawback, we find that lysate microarrays are a mature technology that can and should be used to discover basic biology, gain deep insights into network behavior, and suggest routes to improve human health.

13

Works Cited

Augenlicht, L.H., and Kobrin, D. (1982). Cloning and screening of sequences expressed in a mouse colon tumor. Cancer Res *42*, 1088-1093.

Belluco, C., Mammano, E., Petricoin, E., Prevedello, L., Calvert, V., Liotta, L., Nitti, D., and Lise, M. (2005). Kinase substrate protein microarray analysis of human colon cancer and hepatic metastasis. Clinica chimica acta; international journal of clinical chemistry *357*, 180-183.

Gonzalez-Angulo, A.M., Hennessy, B.T., Meric-Bernstam, F., Sahin, A., Liu, W., Ju, Z., Carey, M.S., Myhre, S., Speers, C., Deng, L.*, et al.* (2011). Functional proteomics can define prognosis and predict pathologic complete response in patients with breast cancer. Clinical proteomics *8*, 11.

Grubb, R.L., Calvert, V.S., Wulkuhle, J.D., Paweletz, C.P., Linehan, W.M., Phillips, J.L., Chuaqui, R., Valasco, A., Gillespie, J., Emmert-Buck, M.*, et al.* (2003). Signal pathway profiling of prostate cancer using reverse phase protein arrays. Proteomics *3*, 2142-2146.

Gujral, T.S., Karp, R.L., Finski, A., Chan, M., Schwartz, P.E., Macbeath, G., and Sorger, P. (2012). Profiling phospho-signaling networks in breast cancer using reverse-phase protein arrays. Oncogene.

Gygi, S.P., Rochon, Y., Franza, B.R., and Aebersold, R. (1999). Correlation between protein and mRNA abundance in yeast. Mol Cell Biol *19*, 1720-1730.

Kopf, E., and Zharhary, D. (2007). Antibody arrays--an emerging tool in cancer proteomics. The international journal of biochemistry & cell biology *39*, 1305-1317.

Lashkari, D.A., DeRisi, J.L., McCusker, J.H., Namath, A.F., Gentile, C., Hwang, S.Y., Brown, P.O., and Davis, R.W. (1997). Yeast microarrays for genome wide parallel genetic and gene expression analysis. Proc Natl Acad Sci U S A *94*, 13057-13062.

Nishizuka, S., Charboneau, L., Young, L., Major, S., Reinhold, W.C., Waltham, M., Kouros-Mehr, H., Bussey, K.J., Lee, J.K., Espina, V.*, et al.* (2003). Proteomic profiling of the NCI-60 cancer cell lines using new high-density reverse-phase lysate microarrays. Proceedings of the National Academy of Sciences of the United States of America *100*, 14229-14234.

Paweletz, C.P., Charboneau, L., Bichsel, V.E., Simone, N.L., Chen, T., Gillespie, J.W., Emmert-Buck, M.R., Roth, M.J., Petricoin, E.F., and Liotta, L.A. (2001). Reverse phase protein microarrays which capture disease progression show activation of pro-survival pathways at the cancer invasion front. Oncogene *20*, 1981-1989.

Sevecka, M., Wolf-Yadlin, A., and G., M. (2011). Lysate microarrays enable high-throughput, quantitative investigations of cellular signaling. Mol Cell Proteomics *10*.

Shoemaker, D.D., Schadt, E.E., Armour, C.D., He, Y.D., Garrett-Engele, P., McDonagh, P.D., Loerch, P.M., Leonardson, A., Lum, P.Y., Cavet, G.*, et al.* (2001). Experimental annotation of the human genome using microarray technology. Nature *409*, 922-927.

Wulfkuhle, J.D., Aquino, J.A., Calvert, V.S., Fishman, D.A., Coukos, G., Liotta, L.A., and Petricoin, E.F., 3rd (2003). Signal pathway profiling of ovarian cancer from human tissue specimens using reverse-phase protein microarrays. Proteomics *3*, 2085-2090.

Zhu, H., and Snyder, M. (2001). Protein arrays and microarrays. Curr Opin Chem Biol *5*, 40-45.

1.3. The Mammalian DNA Damage Response at a Glance

The DNA Damage Response (DDR) is an evolutionarily conserved feature among all kingdoms of life, and is directly responsible for preserving the integrity of the most important molecule in that cell: its DNA genetic code. DNA damage occurs constantly in cells due to replication errors and normal metabolism (Lindahl and Barnes, 2000), are sometimes the result of specific cellular processes such as meiosis or VDJ recombination, and can also result from environmental exposure to radiation or mutagens (Upton, 2010; Valko et al., 2006), making the DDR one of the most critical pathways in the cell. If a replication error or damaged strand of DNA is allowed to persist into daughter cells, mutations may occur. Conversely, an overactive repair pathway may also introduce heritable mutations, so strict control must be maintained to prevent inappropriate repair or recombination events. While in single-celled organisms a certain level of mutation might be tolerable or even desirable, the DNA damage response in multicellular organisms has an additional role over its unicellular counterpart: it also serves as a primary safeguard against cancers which can result from such mutation events.

The DNA Damage Response encompasses at least seven major distinct repair pathways and responses, each targeted against a different kind of lesion. These include Nucleotide Excision Repair (NER), Base Excision Repair (BER), MisMatch Repair (MMR), TransLesion Synthesis (TLS), and Double Strand Break Repair (DSBR), which is further broken down into Non-Homologous End Joining (NHEJ), Homologous Recombination (HR), and the less well-understood Microhomology-Mediated End Joining (MMEJ).

For the purposes of our work, we focus foremost on DSBR, which targets the most dangerous type of DNA lesion: Double Strand Breaks (DSB). While DSBs repaired by HR typically do not cause mutation, the process requires a crossover event with the sister chromatid and can only be

performed in S/G2 phase. By contrast, NHEJ is the dominant pathway by which mammalian cells perform DSBR, and while NHEJ can rejoin any two ends at any time, the ends are usually first partially digested by DNAses, resulting in deletion of genetic material (Hefferin and Tomkinson, 2005). Furthermore, when more than 2 ends exist, NHEJ can join ends at random, resulting in aberrations such as deletions, inversions, and gross chromosomal rearrangements.

DSBs can form as a result of natural metabolism or environmental exposure, and are the most genotoxic as well as mutagenic type of DNA lesion. A DSB forms when both strands of a DNA duplex are broken and can lead to genomic rearrangements such as duplication or loss of genomic segments. DSBs form at sites of replication, especially upon replication fork collapse (Lehmann and Fuchs, 2006), or as a result of exposure to radiation (Shah et al., 2012). Finally, as cancers frequently feature mutations in their DDR pathways and are thus particularly unable to tolerate DNA damage, many of our best antineoplastic drugs directly cause DNA damage as their mechanism of action. We investigate a specific class of clinically important Topoisomerase inhibitors in Chapters 3 and 4, in order to understand their effects in both pre-cancer and cancer cells.

The DSBR can be broadly broken down into 3 stages: (1) the site of physical damage is sensed and protected, and a focus is formed, (2) the signal at the break is amplified and signaling information is integrated into central decision making proteins, which make the critical decision between possible outcomes, including (3) recruitment of repair enzymes and engaging cell cycle checkpoints to prevent propagation of aberrant genomic material, commitment to cellular suicide through apoptosis, or other exotic and controversial cellular phenotypes such as necroptosis, senescence, or autophagy.

In the next several sections, we will briefly discuss some of the key events in the control of the DSBR, with special focus on the signaling that is mediated by the interplay of kinases and p53. Many of the specific repair mechanisms have been omitted for simplicity, though coordination of their precise enzymatic activities no less important than the cell cycle checkpoints.
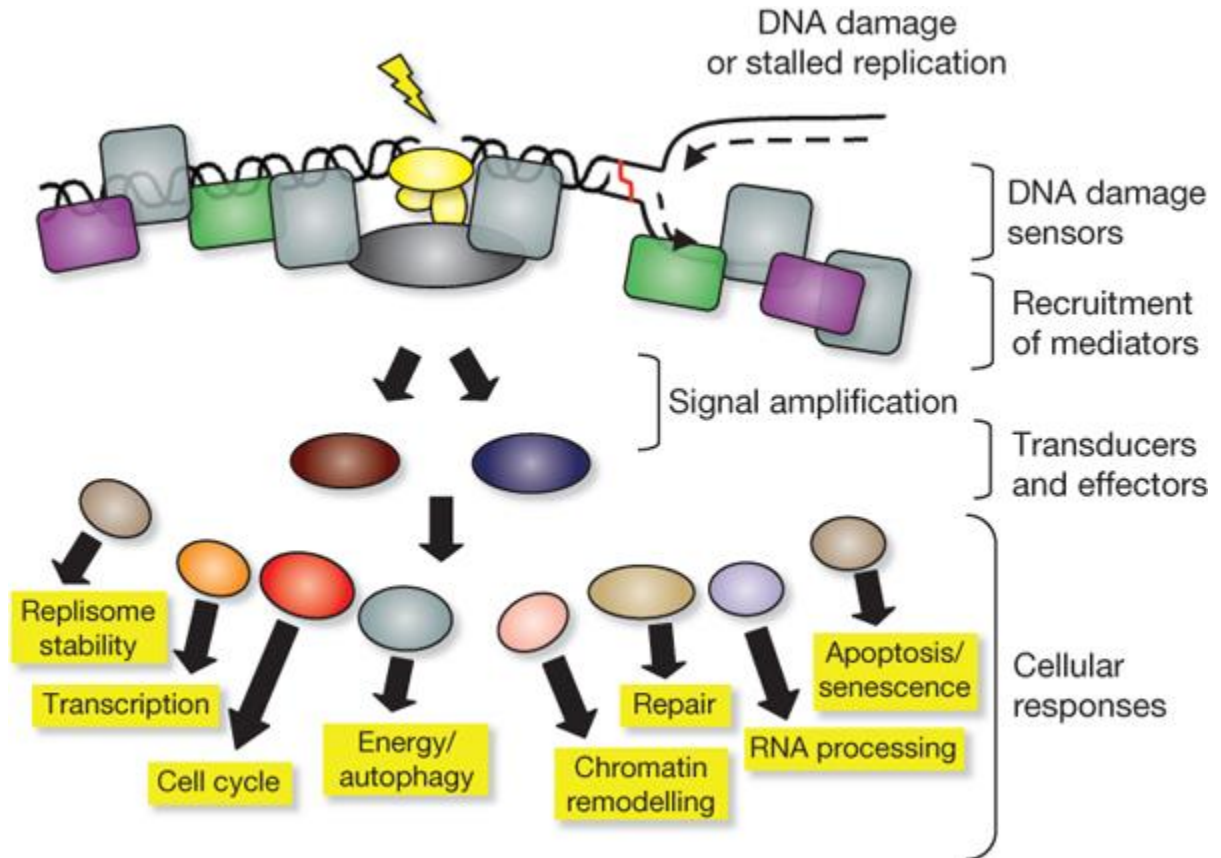
Figure 1.1. A schematic of the DNA damage response depicting the early sensory stage, signal transduction stage, and cellular response stage. Reproduced with permission from (Jackson and Bartek, 2009).

Works Cited

Hefferin, M.L., and Tomkinson, A.E. (2005). Mechanism of DNA double-strand break repair by non-homologous end joining. DNA repair *4*, 639-648.

Jackson, S.P., and Bartek, J. (2009). The DNA-damage response in human biology and disease. Nature *461*, 1071-1078.

Lehmann, A.R., and Fuchs, R.P. (2006). Gaps and forks in DNA replication: Rediscovering old models. DNA repair *5*, 1495-1498.

Lindahl, T., and Barnes, D.E. (2000). Repair of Endogenous DNA Damage. Cold Spring Harbor Symposia on Quantitative Biology *65*, 127-134.

Shah, D.J., Sachs, R.K., and Wilson, D.J. (2012). Radiation-induced cancer: a modern view. The British journal of radiology *85*, e1166-1173.

Upton, A.C. (2010). Carcinogenic Effects of Ionising Radiation. Cancer Growth and Progression *12*, 43-61.

Valko, M., J., R.C., Moncol, J., Izakovic, M., and Mazur, M. (2006). Free radicals, metals and antioxidants in oxidative stress-induced cancer. Chem Biol Interact *160*, 1-40.

1.4. The Early DNA Damage Response: Sensing, Protecting, and Marking the Point of Physical Damage

Initial sensing in the DSBR has 3 main goals: (1) to quickly find the damage and protect the DNA, (2) to recruit downstream events, and (3) to ensure a robust response that is not spontaneously lost. Many molecules have been implicated in the early stage, but here we will discuss the key events that occur in the early DSBR. The early events in the DNA damage response revolve around the creation and maintenance of a highly stable protein complex known as the ionizing-radiation induced focus (IRIF), whose protein composition is quite dynamic, dependent on cellular context, and will vary greatly throughout the repair process.

Naked double-stranded DNA is rapidly degraded within a cell, so speed is paramount in the initial task of finding and protecting the damaged DNA end. Indeed, the presence of double-stranded DNA exonucleases within cells is an evolutionarily ancient mechanism of viral defense (Zhang et al., 2011). Therefore, once a break occurs, there is a literal race for the DDR to respond and protect the DNA fragment before it is irrecoverably destroyed.

Two distinct protein complexes are known to arrive within seconds of a break occurring. These complexes are known as MRN (Mre11-Rad50-Nbs1) and Ku (Ku70-Ku80) (de Jager et al., 2001; de Jager et al., 2002; Kim et al., 2005). Mre11 and Rad50 were originally discovered in genetic screens in *S. cerevisiae*, mutants in these genes being deficient in meiotic recombination (Ajimura et al., 1993) and sensitivity to radiation (Parry et al., 1976), respectively. Nbs1 was discovered through its interactions with the human Mre11 and Rad 50 proteins, and because mutations in Nbs1 causes Nijmegen Breakage Syndrome, a disease causing high cancer incidence and radiosensitivity (Carney et al., 1998). The Ku proteins were discovered when patients suffering from systemic lupus erythematosus were found to have autoantibodies that had a

speckled nuclear localization. In laser-stripe fluorescence experiments, both MRN and Ku70/80 complexes have been seen to be present at damage sites within seconds. As downstream events are strictly dependent on the presence of MRN or Ku at the break, and given that deletions of all of these genes have severe phenotypes including embryonic lethality, it is believed that recruitment of these complexes represents the first, most critical, signaling step in the DSBR.

The MRN and Ku complexes, once bound to DNA, rapidly recruit signaling kinases that amplify the original signal as well as recruit further factors. The three major kinases recruited at this stage (ATM, ATR, and DNA-PK$_{cs}$) are all very large (>300 kDa), and belong to the family of protein serine/threonine kinases known as the phosphoinositide 3-kinase related kinases (PIKKs). ATM and ATR with its obligatory interaction partner ATRIP (Cortez et al., 2001) generally promote HR (Thompson, 2012), while DNA-PK$_{cs}$ combines with the Ku complex to form the DNA-PK holoenzyme which helps to position the ends and recruit additional NHEJ factors (DeFazio et al., 2002; Mimori and Hardin, 1986; Spagnolo et al., 2006). Active ATM monomers are primarily recruited by interactions through MRN (Lee and Paull, 2005; Suzuki et al., 1999), while ATR-ATRIP is primarily recruited through interactions with Replication Protein A (RPA) that rapidly coats single-stranded DNA (ssDNA), commonly present at sites of DSBs associated with distressed or normal replication (Dart et al., 2004; Lupardus et al., 2002; Zou and Elledge, 2003).

Despite sharing clear evolutionary relationship to PI3K, the PIKK family exclusively phosphorylate proteins rather than lipids. The PIKK family came to prominence in a flurry of reports in the mid-1990s following the discovery of mTOR (Brown et al., 1994). Using homology in the kinase domain, ATM was soon discovered as the causative mutation in the disease Ataxia

Telangiectasia (Savitsky et al., 1995), with the discoveries of ATR (Cimprich et al., 1996), and DNA-PK$_{cs}$ (Hartley et al., 1995) immediately following.

Biochemical analysis of the DDR PIKKs suggests that they may be at least partially redundant. The consensus sequence for all PIKKs is an invariant requirement of an S/T-Q motif (Kim et al., 1999), with the notable exception of mTOR. The mechanisms by which these kinases are activated remain controversial, for ATM seems to involve but not require phosphorylation of serine 1981, causing dimer dissociation into active monomers (Bakkenist and Kastan, 2003; Pellegrini et al., 2006). Both ATR and ATRIP are known to be phosphorylated (Cortez et al., 2001; Liu et al., 2011), though significantly less is known about the specific mechanism of activation. The mediator protein TopBP1 is recruited to ssDNA-RPA by the PCNA-like Rad9-Rad1-Hus1 checkpoint clamp and activates ATR activity, but exactly how this occurs is controversial (Delacroix et al., 2007). A study to exhaustively identify direct ATM/ATR substrates *in vivo* found over 900 phosphorylation sites on over 700 proteins (Matsuoka et al., 2007), supporting the idea that PIKKs act much as coordinators of the early DDR.

Once activated and present at the IRIF, ATM, ATR, and DNA-PK$_{cs}$ have all been shown to phosphorylate the histone variant H2AX on serine 139, which when phosphorylated is known as γ-H2AX (Celeste et al., 2003; Matsuoka et al., 2007; Paull et al., 2000; Rogakou et al., 1998; Stiff et al., 2004). Histone 2A has several variants, but the evolutionarily conserved H2AX has a special role in the DDR. H2AX constitutes between 4-25% of total H2A protein, depending on species and tissue type (Rogakou et al., 1998), but always contains the invariant SQ motif followed by 2 residues on the exposed C-terminal tail. This phosphorylation site on γ-H2AX is a binding site for the BRCT domains of MDC1 (Lou et al., 2006; Stucki et al., 2005). Binding of MDC1 to the IRIF completes a positive feedback loop ensuring robust signaling at the break, because MDC1 acts as

an adapter by recruiting further MRN and ATM complexes (Chapman and Jackson, 2008; Melander et al., 2008). Indeed, this positive feedback can result in massive γ-H2AX structures propagating to over a megabase away from the actual site of damage (Rogakou et al., 1999). Why these structures are so massive is controversial, though it may be to ensure robust constant signal as long as a break persists.

Another important function of PIKKs is to activate downstream kinases. Activated ATM phosphorylates Chk2 on threonine 68 (Ahn et al., 2000), which resides in an N-terminal region rich in SQ/TQ motifs. Upon T68 phosphorylation, Chk2 transiently homodimerizes through interactions *in trans* requiring the forkhead-associated (FHA) domain, causing intermolecular loop phosphorylation, and full kinase activation (Ahn et al., 2002; Cai et al., 2009; Oliver et al., 2006). By contrast, activated ATR phosphorylates Claspin, normally present at replication forks (Lee et al., 2003), in a short repeated motif, that once phosphorylated, binds Chk1 and allows ATR to activate Chk1 (Guo, 2000; Jeong et al., 2003). Some of these mechanistic events are not well characterized, though it is clear that the end result is phosphorylation of Chk1 within its C-terminal domain, most notably on serines 317 and 345, widely regarded as markers for Chk1 activation (Niida et al., 2007; Walker et al., 2009). Once activated, both Chk1 and Chk2 are thought to dissociate from their respective complexes, and each has many targets that will be discussed in detail in the next section.

All events so far discussed happen within 1-2 minutes of the damage event (Bakkenist and Kastan, 2003; Pellegrini et al., 2006). The next wave of protein recruitment occurs through the recruitment of ubiquitin ligase RNF8 by MDC1 (Pellegrini et al., 2006), resulting in a cascade of ubiquitinylation on histones H2A and H2AX (Huen et al., 2007; Wang and Elledge, 2007) and chromatin rearrangement (Price and D'Andrea, 2013). Immediately following these changes to

chromatin structure, further factors such as 53BP1 and BRCA1 can be then be detected at the IRIF, arriving after a short but significant 1-2 minute lag after MDC1 (Pellegrini et al., 2006). These factors are thought to have important roles in maintenance of the IRIF as well as recruitment of enzymes that perform the enzymatic repair of damage. However, we were most interested in control of the cell cycle and the decision between apoptosis and survival, so we will shift our focus to the events downstream of activated ATM/ATR/Chk1/Chk2.

Works Cited

Ahn, J.Y., Li, X., Davis, H.L., and Canman, C.E. (2002). Phosphorylation of threonine 68 promotes oligomerization and autophosphorylation of the Chk2 protein kinase via the forkhead-associated domain. The Journal of biological chemistry *277*, 19389-19395.

Ahn, J.Y., Schwarz, J.K., Piwnica-Worms, H., and Canman, C.E. (2000). Threonine 68 phosphorylation by ataxia telangiectasia mutated is required for efficient activation of Chk2 in response to ionizing radiation. Cancer Res *60*, 5934-5936.

Ajimura, M., Leem, S.H., and Ogawa, H. (1993). Identification of new genes required for meiotic recombination in Saccharomyces cerevisiae. Genetics *133*, 51-66.

Bakkenist, C.J., and Kastan, M.B. (2003). DNA damage activates ATM through intermolecular autophosphorylation and dimer dissociation. Nature *421*, 499-506.

Brown, E.J., Albers, M.W., Shin, T.B., Ichikawa, K., Keith, C.T., Lane, W.S., and Schreiber, S.L. (1994). A mammalian protein targeted by G1-arresting rapamycin-receptor complex. Nature *369*, 756-758.

Cai, Z., Chehab, N.H., and Pavletich, N.P. (2009). Structure and activation mechanism of the CHK2 DNA damage checkpoint kinase. Molecular cell *35*, 818-829.

Carney, J.P., Maser, R.S., Olivares, H., Davis, E.M., Le Beau, M., Yates, J.R., Hays, L., Morgan, W.F., and Petrini, J.H. (1998). The hMre11/hRad50 protein complex and Nijmegen breakage syndrome: linkage of double-strand break repair to the cellular DNA damage response. Cell *93*, 477-486.

Celeste, A., Fernandez-Capetillo, O., Kruhlak, M.J., Pilch, D.R., Staudt, D.W., Lee, A., Bonner, R.F., Bonner, W.M., and Nussenzweig, A. (2003). Histone H2AX phosphorylation is dispensable for the initial recognition of DNA breaks. Nat Cell Biol *5*, 675-679.

Chapman, J.R., and Jackson, S.P. (2008). Phospho-dependent interactions between NBS1 and MDC1 mediate chromatin retention of the MRN complex at sites of DNA damage. EMBO reports *9*, 795-801.

Cimprich, K.A., Shin, T.B., Keith, C.T., and Schreiber, S.L. (1996). cDNA cloning and gene mapping of a candidate human cell cycle checkpoint protein. Proc Natl Acad Sci USA *93*, 2850-2855.

Cortez, D., Guntuku, S., Qin, J., and Elledge, S.J. (2001). ATR and ATRIP: partners in checkpoint signaling. Science *294*, 1713-1716.

Dart, D.A., Adams, K.E., Akerman, I., and Lakin, N.D. (2004). Recruitment of the cell cycle checkpoint kinase ATR to chromatin during S-phase. The Journal of biological chemistry *279*, 16433-16440.

de Jager, M., van Noort, J., van Gent, D.C., Dekker, C., Kanaar, R., and Wyman, C. (2001). Human Rad50/Mre11 is a flexible complex that can tether DNA ends. Molecular cell *8*, 1129-1135.

de Jager, M., Wyman, C., van Gent, D.C., and Kanaar, R. (2002). DNA end-binding specificity of human Rad50/Mre11 is influenced by ATP. Nucleic Acids Res *30*, 4425-4431.

DeFazio, L.G., Stansel, R.M., Griffith, J.D., and Chu, G. (2002). Synapsis of DNA ends by DNA-dependent protein kinase. EMBO J *21*, 3192-3200.

Delacroix, S., Wagner, J.M., Kobayashi, M., Yamamoto, K., and Karnitz, L.M. (2007). The Rad9-Hus1-Rad1 (9-1-1) clamp activates checkpoint signaling via TopBP1. Genes & development *21*, 1472-1477.

Guo, Z. (2000). Requirement for Atr in phosphorylation of Chk1 and cell cycle regulation in response to DNA replication blocks and UV-damaged DNA in Xenopus egg extracts. Genes & development *14*, 2745-2756.

Hartley, K.O., Gell, D., Smith, G.C., Zhang, H., Divecha, N., Connelly, M.A., Admon, A., Lees-Miller, S.P., Anderson, C.W., and P., J.S. (1995). DNA-dependent protein kinase catalytic subunit: A relative of phosphatidylinositol 3-kinase and the ataxia telangiectasia gene product. Cell *82*, 849-856.

Huen, M.S., Grant, R., Manke, I., Minn, K., Yu, X., Yaffe, M.B., and Chen, J. (2007). RNF8 transduces the DNA-damage signal via histone ubiquitylation and checkpoint protein assembly. Cell *131*, 901-914.

Jeong, S.Y., Kumagai, A., Lee, J., and Dunphy, W.G. (2003). Phosphorylated claspin interacts with a phosphate-binding site in the kinase domain of Chk1 during ATR-mediated activation. The Journal of biological chemistry *278*, 46782-46788.

Kim, J.S., Krasieva, T.B., Kurumizaka, H., Chen, D.J., Taylor, A.M., and Yokomori, K. (2005). Independent and sequential recruitment of NHEJ and HR factors to DNA damage sites in mammalian cells. The Journal of cell biology *170*, 341-347.

Kim, S.T., Lim, D.S., Canman, C.E., and B., K.M. (1999). Substrate specificities and identification of putative substrates of ATM kinase family members. J Biol Chem *274*, 37538-37543.

Lee, J., Kumagai, A., and Dunphy, W.G. (2003). Claspin, a Chk1-regulatory protein, monitors DNA replication on chromatin independently of RPA, ATR, and Rad17. Molecular cell *11*, 329-340.

Lee, J.H., and Paull, T.T. (2005). ATM activation by DNA double-strand breaks through the Mre11-Rad50-Nbs1 complex. Science *308*, 551-554.

Liu, S., Shiotani, B., Lahiri, M., Marechal, A., Tse, A., Leung, C.C., Glover, J.N., Yang, X.H., and Zou, L. (2011). ATR autophosphorylation as a molecular switch for checkpoint activation. Molecular cell *43*, 192-202.

Lou, Z., Minter-Dykhouse, K., Franco, S., Gostissa, M., Rivera, M.A., Celeste, A., Manis, J.P., van Deursen, J., Nussenzweig, A., Paull, T.T.*, et al.* (2006). MDC1 maintains genomic stability by participating in the amplification of ATM-dependent DNA damage signals. Molecular cell *21*, 187-200.

Lupardus, P.J., Byun, T., Yee, M.C., Hekmat-Nejad, M., and Cimprich, K.A. (2002). A requirement for replication in activation of the ATR-dependent DNA damage checkpoint. Genes & development *16*, 2327-2332.

Matsuoka, S., Ballif, B.A., Smogorzewska, A., McDonald, E.R., 3rd, Hurov, K.E., Luo, J., Bakalarski, C.E., Zhao, Z., Solimini, N., Lerenthal, Y.*, et al.* (2007). ATM and ATR substrate analysis reveals extensive protein networks responsive to DNA damage. Science *316*, 1160-1166.

Melander, F., Bekker-Jensen, S., Falck, J., Bartek, J., Mailand, N., and Lukas, J. (2008). Phosphorylation of SDT repeats in the MDC1 N terminus triggers retention of NBS1 at the DNA damage-modified chromatin. The Journal of cell biology *181*, 213-226.

Mimori, T., and Hardin, J.A. (1986). Mechanism of interaction between Ku protein and DNA. J Biol Chem *261*, 10375-10379.

Niida, H., Katsuno, Y., Banerjee, B., Hande, M.P., and Nakanishi, M. (2007). Specific role of Chk1 phosphorylations in cell survival and checkpoint activation. Molecular and cellular biology *27*, 2572-2581.

Oliver, A.W., Paul, A., Boxall, K.J., E., B.S., Aherne, G.W., Garrett, M.D., Mittnacht, S., and Pearl, L.H. (2006). Trans-activation of the DNA-damage signalling protein kinase Chk2 by T-loop exchange. EMBO J *25*, 3179-3190.

Parry, J.M., Davies, P.J., and Evans, W.E. (1976). The effects of "cell age" upon the lethal effects of physical and chemical mutagens in the yeast, Saccharomyces cerevisiae. Mol Gen Genet *146*, 27-35.

Paull, T.T., Rogakou, E.P., Yamazaki, V., Kirchgessner, C.U., Gellert, M., and Bonner, W.M. (2000). A critical role for histone H2AX in recruitment of repair factors to nuclear foci after DNA damage. Curr Biol *10*, 886-895.

Pellegrini, M., Celeste, A., Difilippantonio, S., Guo, R., Wang, W., Feigenbaum, L., and Nussenzweig, A. (2006). Autophosphorylation at serine 1987 is dispensable for murine Atm activation in vivo. Nature *443*, 222-225.

Price, B.D., and D'Andrea, A.D. (2013). Chromatin remodeling at DNA double-strand breaks. Cell *152*, 1344-1354.

Rogakou, E.P., Boon, C., Redon, C., and Bonner, W.M. (1999). Megabase chromatin domains involved in DNA double-strand breaks in vivo. J Cell Biol *146*, 905-916.

Rogakou, E.P., Pilch, D.R., Orr, A.H., Ivanova, V.S., and Bonner, W.M. (1998). DNA double-stranded breaks induce histone H2AX phosphorylation on serine 139. J Biol Chem *273*, 5858-5868.

Savitsky, K., Bar-Shira, A., Gilad, S., Rotman, G., Ziv, Y., Vanagaite, L., Tagle, D.A., Smith, S., Uziel, T., Sfez, S.*, et al.* (1995). A single ataxia telangiectasia gene with a product similar to PI-3 kinase. Science *268*, 1749-1753.

Spagnolo, L., Rivera-Calzada, A., Pearl, L.H., and Llorca, O. (2006). Three-dimensional structure of the human DNA-PKcs/Ku70/Ku80 complex assembled on DNA and its implications for DNA DSB repair. Molecular cell *22*, 511-519.

Stiff, T., O'Driscoll, M., Rief, N., Iwabuchi, K., Löbrich, M., and Jeggo, P.A. (2004). ATM and DNA-PK function redundantly to phosphorylate H2AX after exposure to ionizing radiation. Cancer Res *64*, 2390-2396.

Stucki, M., Clapperton, J.A., Mohammad, D., Yaffe, M.B., Smerdon, S.J., and Jackson, S.P. (2005). MDC1 directly binds phosphorylated histone H2AX to regulate cellular responses to DNA double-strand breaks. Cell *123*, 1213-1226.

Suzuki, K., Kodama, S., and Watanabe, M. (1999). Recruitment of ATM protein to double strand DNA irradiated with ionizing radiation. J Biol Chem *274*, 25571-25575.

Thompson, L.H. (2012). Recognition, signaling, and repair of DNA double-strand breaks produced by ionizing radiation in mammalian cells: the molecular choreography. Mutation research *751*, 158-246.

Walker, M., Black, E.J., Oehler, V., Gillespie, D.A., and Scott, M.T. (2009). Chk1 C-terminal regulatory phosphorylation mediates checkpoint activation by de-repression of Chk1 catalytic activity. Oncogene *28*, 2314-2323.

Wang, B., and Elledge, S.J. (2007). Ubc13/Rnf8 ubiquitin ligases control foci formation of the Rap80/Abraxas/Brca1/Brcc36 complex in response to DNA damage. Proceedings of the National Academy of Sciences of the United States of America *104*, 20759-20763.

Zhang, D., Iyer, L.M., and Aravind, L. (2011). A novel immunity system for bacterial nucleic acid degrading toxins and its recruitment in various eukaryotic and DNA viral systems. Nucleic acids research *39*, 4532-4552.

Zou, L., and Elledge, S.J. (2003). Sensing DNA damage through ATRIP recognition of RPA-ssDNA complexes. Science *300*, 1542-1548.

1.5. The DNA Damage Response: Integrating Information and the Crucial Roles of p53 in the Context of DNA Damage

1.5.1. Discovery and Controversy: Is p53 an Oncogene or a Tumor Suppressor?

In the previous section, the early, chromatin-associated events following DNA damage were discussed in great detail. The activation of the kinases ATM, ATR, Chk1, and Chk2 marks the next stage of signaling events that converge on the tumor suppressor transcription factor Tp53.

p53 was first discovered in 1979 by 2 separate approaches. Virologists studying SV40-transformed cells found a 55 kDa protein that coprecipitated with the large-T antigen (Chang et al., 1979), which was not coded in the virus because it was also present in uninfected cells (Linzer and Levine, 1979). At the same time, oncologists studying carcinogen-induced tumor cell lines found a 54 kDa protein universally expressed in many transformed cell lines (DeLeo et al., 1979). In 1982 antibodies against p53 were reported in the blood sera of cancer patients (Crawford et al., 1982), further confusing the discussion of the biological function of the protein.

Initial work was highly contentious: first p53 was thought to be an oncogene, before its true role as a tumor suppressor was elucidated. The discoveries surrounding src and ras as drivers of proliferation and cancer in the early 1980s brought attention to genes that, when disregulated, could promote cancer (Ellis et al., 1982; Shih and Weinberg, 1982). Thus, when it was reported that proliferation was highly correlated with having a high intracellular p53 level (Reich and Levine, 1984), and that it could cooperate with ras to transform cells (Eliyahu et al., 1984), it was naturally classified as a dominant oncogene. However, by the late 1980s, it was known that p53 was frequently mutated (Mowat et al., 1985), and that it was overexpression of mutant p53 that promote proliferation and cancer (Finlay et al., 1988), while wild-type p53 actually suppressed transformation (Eliyahu et al., 1989). By the 1990s, it had been definitively demonstrated that
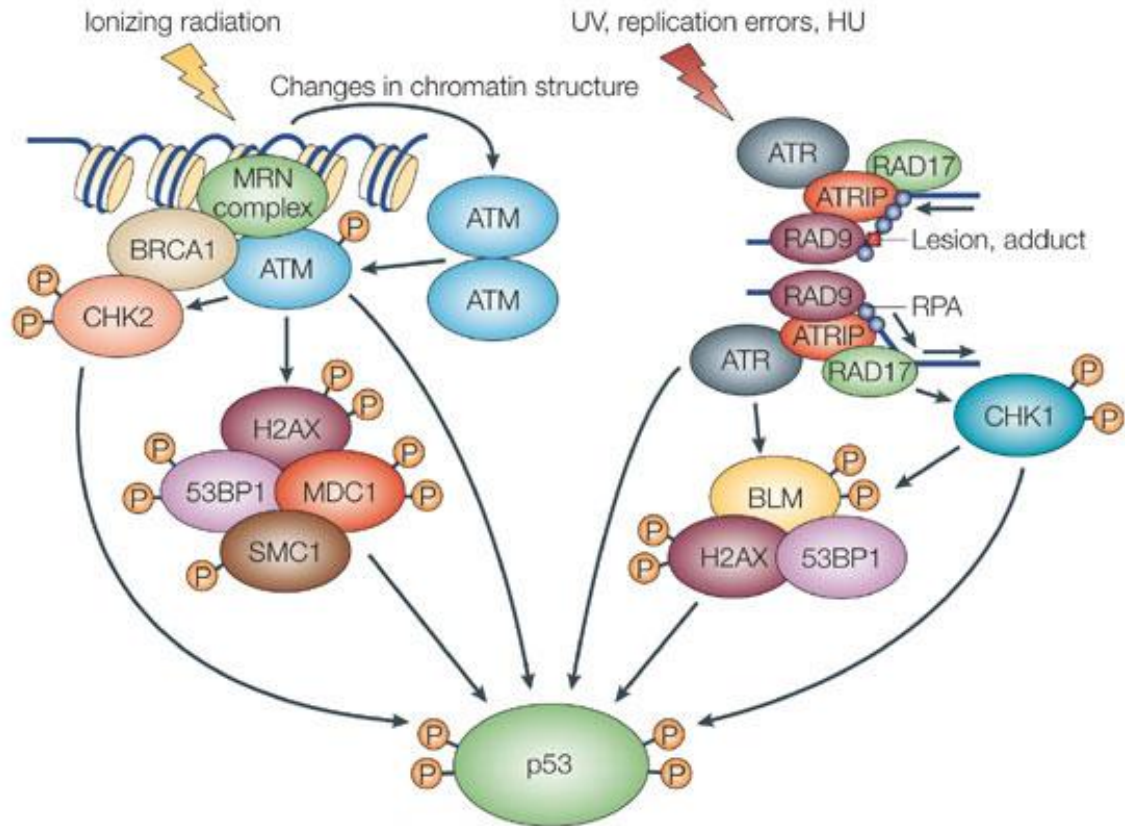
Figure 1.2. Schematic of the mechanisms of p53 activation in the context of DNA Damage. Adapted and reproduced from (Sengupta and Harris, 2005) with permission.

wild-type p53 is a tumor suppressor, while mutations in or deletions of p53 can act as a dominant

oncogene.

1.5.2. The Role of p53 in DSBR

p53 is a critical decision point at the convergence of several signaling pathways essential for

both cellular growth and apoptosis induced by many disparate genotoxic and non-genotoxic

stresses (Vogelstein et al., 2000). In normal unstressed cells, p53 is constantly expressed but levels

are held low by rapid degradation, most importantly by its E3 ubiquitin ligase Mdm2 (Momand et

al., 2000; Shieh et al., 1997). In the context of genotoxic stress, p53 is involved in all the major DDR pathways (reviewed in Sengupta and Harris (2005)).

The role of p53 in NHEJ is not straightforward. Activated DNA-PK phosphorylates p53 (Wang et al., 2000), but phosphorylation does not appear to be required (Jhappan et al., 2000; Jimenez et al., 1999). A direct role for p53 protein in precise end joining was demonstrated both *in vivo* and *in vitro* (Tang et al., 1999; Yang et al., 1997), indicating that its transcriptional activity was not required for NHEJ. However, careful analysis of end-joining assays and integration demonstrated that wild-type p53 inhibits NHEJ (Bill et al., 1997; Lee et al., 1999). Conversely, deletions of NHEJ factors such as Ku80 or Xrcc4 in mice cause a number of embryonic lethalities that can be rescued by p53 deletion, suggesting that p53 is critical for NHEJ (Frank et al., 2000; Gao et al., 2000). These data also emphasize the importance of NHEJ in normal mammalian development. It is also interesting to note that NHEJ-mutant mice are not usually cancer prone, and that it has been hypothesized that p53's role in NHEJ is more anti-aging than anti-cancer (reviewed in Hasty (2008)). Indeed, p53's role in cellular aging and senescence is only recently coming under study.

p53 is a key control point in HR, and its inactivation leads to increases in both spontaneous and stress-induced HR. Cancer-derived hotspot mutations at 281, 273, 248, 175, and 143 all increased recombination rates (Akyuz et al., 2002). HR involves the creation of a DNA heteroduplex structure known as a Holliday junction, and p53 tetramers bind and stabilize the strand-transfer intermediate (Janz et al., 2002). Importantly, p53 also directly interacts with Rad51, directly inhibiting its ability to polymerize (Buchhop et al., 1997; Linke et al., 2003). It is further hypothesized that wild-type p53 primarily protects cells by preventing recombinogenic lesions from forming in the first place (Kumari et al., 2004).

1.5.3. Phosphorylation of p53

In the last 20 years, p53 has been one of the most extensively studied proteins in the genome, and dozens of post-translational modifications have been identified. Importantly, though *in vitro* results are typically universally reproducible, *in vivo* results tend to be context specific, specifically with respect to cell type, tissue, genotype, and stimuli. Indeed, p53 is known to be phosphorylated, acetylated, methylated, mono- and poly- ubiquitinylated, SUMOylated, O-GlyNAcylated, Neddylated, demethylated, and ADP-ribosylated (reviewed in Gu and Zhu (2012). Phosphorylation occurs almost exclusively in the N-terminal transactivation domain (TAD), of which there are two, residues 1-40, and 41-61, or in the C-terminal, disordered regulatory domain (REG), residues 363-393. The TAD is not known to be modified in any way other than phosphorylation. The key phosphorylation events in the TAD occur rapidly in response to stress, and in a specific order: S15 phosphorylation usually precedes T18 phosphorylation and is required for S20 phosphorylation (Saito et al., 2003; Sakaguchi et al., 2000).

The effects of specific phosphorylation events were studied by knock-in mice models with mutations introduced at the mutation sites. Mutation of serine to alanine prevents phosphorylation, while mutation to aspartic acid mimics constitutive phosphorylation. $p53^{S18A}$, $p53^{S23A}$, and $p53^{S18A,S23A}$ mutant mice (S15 and S20 in human) all show reduced life span, though stabilization of p53 after stress is not significantly altered. However, all 3 mutant mice and derived cells did show defects in p53-dependent stress responses (Armata et al., 2007; Chao et al., 2006). In particular, $p53^{S18A/S23A}$ homozygous mutant mice were profoundly unable to activate p53-dependent apoptosis. Therefore, it seems that levels of p53 protein and its downstream activity by phosphorylated may not be directly correlated. In fact, careful analysis of $p53^{S18A,S23A/\ S18A,S23A}$

32

cells showed no difference from a p53$^{-/-}$ mouse in p53-dependent stress responses, though protein levels did not significantly differ from cells expressing wild-type protein (Chao et al., 2006). In contrast to these non-phosphorylatable mutants, a p53^{T21D,S23D} mutant mimics constitutive phosphorylation. A p53$^{T21D,S23D/-}$ mouse exhibits strongly accelerated aging, while a homozygous mutation is embryonic lethal. p53$^{T21D,S23D/-}$ cells showed significant p53-dependent transcription and apoptosis in the absence of stress as compared to p53$^{+/-}$ cells, but did not further induce these responses in the presence of DNA damage, and was lower than the response in p53$^{+/-}$ after damage. All in all, these knock-in experiments show the critical importance of the S18 and S23 (human S15 and S20) sites in activation of p53 somewhat independently of protein levels.

p53 phosphorylation affects its interactions with its negative regulator Mdm2 while also activating its downstream transcriptional activity. A published crystal structure of Mdm2 in complex with the TAD domain shows that the minimal binding region is a helix formed by residues 19-26 within the TAD (Kussie et al., 1996). Strikingly, this interaction is largely formed by highly conserved hydrophobic residues (F19, W23, L26) inserting into a deep hydrophobic cleft in Mdm2. Phosphorylation on p53 at S18 and S23, along with concurrent phosphorylation by ATM at S395 in Mdm2 (Maya et al., 2001), introduce bulky, negatively charged structures that inhibit the interaction, relieving the negative regulation while at the same time revealing a binding surface for p62 and CBP/p300 (Blau et al., 1996; Feng et al., 2009). p62 is a subunit of the transcription factor TFIIH and activates p53-dependent transcription (Blau et al., 1996), and CBP/p300 are a pair of homologous histone acetylases responsible for chromatin modification at sites of p53-dependent transcription and are required for p53-dependent apoptosis (Avantaggiati et al., 1997; Hsu et al., 2004).

1.5.4. Phosphorylation of p53 by ATM/Chk2 and ATR/Chk1

Given the importance of the phosphorylation events at serine 15 and 20, it is important to understand how they become phosphorylated and by which kinases. Perhaps unsurprisingly, the answer is not simple, and also has a significant timing component; different kinases appear to be required for different kinetic regimes of p53 phosphorylation.

It is well established that serine 15 phosphorylation is a benchmark for ATM activity, but this is perhaps an erroneous assumption. Indeed, A-T cells deficient for ATM activity do not phosphorylate p53 S15 at the initial phase of the DDR, but phosphorylation is nonetheless evident at later time points (Siliciano et al., 1997). This observation indicates other kinases, possibly ATR, also act upon p53 S15 at later time points. Other phosphorylation events in p53 such as serines 9, 20, and 46 are even more dependent on ATM than serine 15 (Saito et al., 2002), though ATM has weak affinity for those sites.

A parsimonious explanation for this apparent paradox would be an ATM-dependent kinase, namely Chk2, phosphorylates serines 9, 20, and 46, though this hypothesis also has problems. Chk2 has indeed been shown to phosphorylate S20 *in vitro* (Chehab et al., 2000; Shieh et al., 2000), but S20 is not a Chk2 consensus phosphorylation site and is in fact a poor Chk2 substrate (Ahn et al., 2003; Craig et al., 2003). Then again, Chk2^{-/-} mice appeared to be normal in both p53 stabilization and S23 phosphorylation, though downstream p53 transcriptional activity was defective (Takai et al., 2002). Further adding to the complexity of the problem, Chk1 has also been reported to have phosphorylation activity for S20 *in vitro* (Shieh et al., 2000). These complexities in mind, it is safe to conclude that phosphorylation of the N-terminus of p53 is not straightforward, and may well be context specific as well as combinatorial.

Works Cited

Ahn, J., Urist, M., and Prives, C. (2003). Questioning the role of checkpoint kinase 2 in the p53 DNA damage response. The Journal of biological chemistry *278*, 20480-20489.

Akyuz, N., Boehden, G.S., Susse, S., Rimek, A., Preuss, U., Scheidtmann, K.H., and Wiesmuller, L. (2002). DNA Substrate Dependence of p53-Mediated Regulation of Double-Strand Break Repair. Molecular and cellular biology *22*, 6306-6317.

Armata, H.L., Garlick, D.S., and Sluss, H.K. (2007). The ataxia telangiectasia-mutated target site Ser18 is required for p53-mediated tumor suppression. Cancer Res *67*, 11696-11703.

Avantaggiati, M.L., Ogryzko, V., Gardner, K., Giordano, A., Levine, A.S., and Kelly , K. (1997). Recruitment of p300/CBP in p53-dependent signal pathways. Cell *89*, 1175-1186.

Bill, C.A., Yu, Y., Miselis, N.R., Little, J.B., and Nickoloff, J.A. (1997). A role for p53 in DNA end rejoining by human cell extracts. Mutation research *385*, 21-29.

Blau, J., Xiao, H., McCracken, S., O'Hare, P., Greenblatt, J., and Bentley, D. (1996). Three functional classes of transcriptional activation domain. Molecular and cellular biology *16*, 2044-2055.

Buchhop, S., Gibson, M.K., Wang, X.W., Wagner, P., Stürzbecher, H.W., and Harris, C.C. (1997). Interaction of p53 with the human Rad51 protein. Nucleic acids research *25*, 3868-3874.

Chang, C., Simmons, D.T., Martin, M.A., and Mora, P.T. (1979). Identification and partial characterization of new antigens from simian virus 40-transformed mouse cells. J Virol *31*, 463-471.

Chao, C., Herr, D., Chun, J., and Xu, Y. (2006). Ser18 and 23 phosphorylation is required for p53-dependent apoptosis and tumor suppression. EMBO J *25*, 2615-2622.

Chehab, N.H., Malikzay, A., Appel, M., and Halazonetis, T.D. (2000). Chk2/hCds1 functions as a DNA damage checkpoint in G(1) by stabilizing p53. Genes & development *14*, 278-288.

Craig, A., Scott, M., Burch, L., Smith, G., Ball, K., and Hupp, T. (2003). Allosteric effects mediate CHK2 phosphorylation of the p53 transactivation domain. EMBO reports *4*, 787-792.

Crawford, L.V., Pim, D.C., and Bulbrook, R.D. (1982). Detection of antibodies against the cellular protein p53 in sera from patients with breast cancer. Int J Cancer *30*, 403-408.

DeLeo, A.B., Jay, G., Appella, E., Dubois, G.C., Law, L.W., and Old, L.J. (1979). Detection of a transformation-related antigen in chemically induced sarcomas and other transformed cells of the mouse. Proc Natl Acad Sci U S A *76*, 2420-2424.

Eliyahu, D., Michalovitz, D., Eliyahu, S., Pinhasi-Kimhi, O., and Oren, M. (1989). Wild-type p53 can inhibit oncogene-mediated focus formation. Proc Natl Acad Sci U S A *86*, 8763-8767.

Eliyahu, D., Raz, A., Gruss, P., Givol, D., and Oren, M. (1984). Participation of p53 cellular tumour antigen in transformation of normal embryonic cells. Nature *312*, 646-649.

Ellis, R.W., DeFeo, D., Furth, M.E., and Scolnick, E.M. (1982). Mouse cells contain two distinct ras gene mRNA species that can be translated into a p21 onc protein. Mol Cell Biol *2*, 1339-1345.

Feng, H., Jenkins, L.M., Durell, S.R., Hayashi, R., Mazur, S.J., Cherry, S., Tropea, J.E., Miller, M., Wlodawer, A., Appella, E., *et al.* (2009). Structural basis for p300 Taz2-p53 TAD1 binding and modulation by phosphorylation. Structure *17*, 202-210.

Finlay, C.A., W., H.P., Tan, T.H., Eliyahu, D., Oren, M., and Levine, A.J. (1988). Activating mutations for transformation by p53 produce a gene product that forms an hsc70-p53 complex with an altered half-life. Mol Cell Biol *8*, 531-539.

Frank, K.M., Sharpless, N.E., Gao, Y., Sekiguchi, J.M., Ferguson, D.O., Zhu, C., Manis, J.P., Horner, J., DePinho, R.A., and Alt, F.W. (2000). DNA ligase IV deficiency in mice leads to defective neurogenesis and embryonic lethality via the p53 pathway. Molecular cell *5*, 993-1002.

Gao, Y., Ferguson, D.O., Xie, W., Manis, J.P., Sekiguchi, J., Frank, K.M., Chaudhuri, J., Horner, J., DePinho, R.A., and Alt, F.W. (2000). Interplay of p53 and DNA-repair protein XRCC4 in tumorigenesis, genomic stability and development. Nature *404*, 897-900.

Gu, B., and Zhu, W.G. (2012). Surf the post-translational modification network of p53 regulation. International journal of biological sciences *8*, 672-684.

Hasty, P. (2008). Is NHEJ a tumor suppressor or an aging suppressor? 2008 *7*, 1139-1145.

Hsu, C.H., Chang, M.D., Tai, K.Y., Yang, Y.T., Wang, P.S., Chen, C.J., Wang, Y.H., Lee, S.C., Wu, C.W., and Juan, L.J. (2004). HCMV IE2-mediated inhibition of HAT activity downregulates p53 function. EMBO J *23*, 2269-2280.

Janz, C., Süsse, S., and Wiesmüller, L. (2002). p53 and recombination intermediates: role of tetramerization at DNA junctions in complex formation and exonucleolytic degradation. Oncogene *21*, 2130-2140.

Jhappan, C., Yusufzai, T.M., Anderson, S., Anver, M.R., and Merlino, G. (2000). The p53 response to DNA damage in vivo is independent of DNA-dependent protein kinase. Mol Cell Biol *20*, 4075-4083.

Jimenez, G.S., Bryntesson, F., Torres-Arzayus, M.I., Priestley, A., Beeche, M., Saito, S., Sakaguchi, K., Appella, E., Jeggo, P.A., Taccioli, G.E., *et al.* (1999). DNA-dependent protein kinase is not required for the p53-dependent response to DNA damage. Nature *400*, 81-83.

Kumari, A., Schultz, N., and Helleday, T. (2004). p53 protects from replication-associated DNA double-strand breaks in mammalian cells. Oncogene *23*, 2324-2329.

Kussie, P.H., Gorina, S., Marechal, V., Elenbaas, B., Moreau, J., Levine, A.J., and Pavletich, N.P. (1996). Structure of the MDM2 oncoprotein bound to the p53 tumor suppressor transactivation domain. Science *274*, 948-953.

Lee, H., Sun, D., Larner, J.M., and Wu, F.S. (1999). The tumor suppressor p53 can reduce stable transfection in the presence of irradiation. J Biomed Sci *6*, 285-292.

Linke, S.P., Sengupta, S., Khabie, N., Jeffries, B.A., Buchhop, S., Miska, S., Henning, W., Pedeux, R., Wang, X.W., Hofseth, L.J.*, et al.* (2003). p53 interacts with hRAD51 and hRAD54, and directly modulates homologous recombination. Cancer Res *63*, 2596-2605.

Linzer, D.I., and Levine, A.J. (1979). Characterization of a 54K dalton cellular SV40 tumor antigen present in SV40-transformed cells and uninfected embryonal carcinoma cells. Cell *17*, 43-52.

Maya, R., Balass, M., Kim, S.T., Shkedy, D., Leal, J.F., Shifman, O., Moas, M., Buschmann, T., Ronai, Z., Shiloh, Y.*, et al.* (2001). ATM-dependent phosphorylation of Mdm2 on serine 395: role in p53 activation by DNA damage. Genes & development *15*, 1067-1077.

Momand, J., Wu, H.H., and Dasgupta, G. (2000). MDM2--master regulator of the p53 tumor suppressor protein. Gene *242*, 15-29.

Mowat, M., Cheng, A., Kimura, N., Bernstein, A., and Benchimol, S. (1985). Rearrangements of the cellular p53 gene in erythroleukaemic cells transformed by Friend virus. Nature *314*, 633-636.

Reich, N.C., and Levine, A.J. (1984). Growth regulation of a cellular tumour antigen, p53, in nontransformed cells. Nature *308*, 199-201.

Saito, S., Goodarzi, A.A., Higashimoto, Y., Noda, Y., Lees-Miller, S.P., Appella, E., and Anderson, C.W. (2002). ATM mediates phosphorylation at multiple p53 sites, including Ser(46), in response to ionizing radiation. The Journal of biological chemistry *277*, 12491-12494.

Saito, S., Yamaguchi, H., Higashimoto, Y., Chao, C., Xu, Y., Fornace, A.J., Jr., Appella, E., and Anderson, C.W. (2003). Phosphorylation site interdependence of human p53 post-translational modifications in response to stress. The Journal of biological chemistry *278*, 37536-37544.

Sakaguchi, K., Saito, S., Higashimoto, Y., Roy, S., Anderson, C.W., and Appella, E. (2000). Damage-mediated phosphorylation of human p53 threonine 18 through a cascade mediated by a casein 1-like kinase. Effect on Mdm2 binding. J Biol Chem *275*, 9278-9283.

Sengupta, S., and Harris, C.C. (2005). p53: traffic cop at the crossroads of DNA repair and recombination. Nature reviews Molecular cell biology *6*, 44-55.

Shieh, S.Y., Ahn, J., Tamai, K., Taya, Y., and Prives, C. (2000). The human homologs of checkpoint kinases Chk1 and Cds1 (Chk2) phosphorylate p53 at multiple DNA damage-inducible sites. Genes & development *14*, 289-300.

Shieh, S.Y., Ikeda, M., Taya, Y., and Prives, C. (1997). DNA damage-induced phosphorylation of p53 alleviates inhibition by MDM2. Cell *91*, 325-334.

Shih, C., and Weinberg, R.A. (1982). Isolation of a transforming sequence from a human bladder carcinoma cell line. Cell *29*, 161-169.

Siliciano, J.D., Canman, C.E., Taya, Y., Sakaguchi, K., Appella, E., and Kastan, M.B. (1997). DNA damage induces phosphorylation of the amino terminus of p53. Genes & development *11*, 3471-3481.

Takai, H., Naka, K., Okada, Y., Watanabe, M., Harada, N., Saito, S., Anderson, C.W., Appella, E., Nakanishi, M., Suzuki, H.*, et al.* (2002). Chk2-deficient mice exhibit radioresistance and defective p53-mediated transcription. EMBO J *21*, 5195-5205.

Tang, W., Willers, H., and Powell, S.N. (1999). p53 directly enhances rejoining of DNA double-strand breaks with cohesive ends in gamma-irradiated mouse fibroblasts. Cancer Res *59*, 2562-2565.

Vogelstein, B., Lane, D., and Levine, A.J. (2000). Surfing the p53 network. Nature *408*, 307-310.

Wang, S., Guo, M., Ouyang, H., Li, X., Cordon-Cardo, C., Kurimasa, A., Chen, D.J., Fuks, Z., Ling, C.C., and Li, G.C. (2000). The catalytic subunit of DNA-dependent protein kinase selectively regulates p53-dependent apoptosis but not cell-cycle arrest. Proc Natl Acad Sci U S A *97*, 1584-1588.

Yang, T., Namba, H., Hara, T., Takmura, N., Nagayama, Y., Fukata, S., Ishikawa, N., Kuma, K., Ito, K., and Yamashita, S. (1997). p53 induced by ionizing radiation mediates DNA end-jointing activity, but not apoptosis of thyroid cells. Oncogene *14*, 1511-1519.

1.6. The DNA Damage Response: Checkpoints, Apoptosis, and Other Phenotypes

After DNA damage, cells can respond in several ways. Cells will choose between several possible fates, either to survive or die. The survival phenotype manifests as a pause in cell cycle progression at any of several checkpoints, designed to prevent replication of damaged DNA and propagation of mutations to daughter cells. By contrast, cells choosing cellular death will commit apoptosis if the damage is too extensive in an effort to prevent potential oncogenesis. Other, more exotic, and less-well understood phenotypes have also been described recently, including necrosis, senescence, necroptosis, and autophagy. There are 3 major checkpoints in mammalian cells: the G1-S, the intra-S, and the G2-M checkpoint. Here we discuss these checkpoints and apoptosis in detail, and briefly summarize the current thinking on the other less well understood cell fates.

1.6.1. The G1-S checkpoint

The G1-S transition marks a decision point where a cell begins to replicate its DNA, and is initiated by expression and buildup of CyclinD beginning immediately after mitosis. CyclinD forms a complex with either Cdk4 or Cdk6, depending on cellular context, which in its active state phosphorylates many targets, including pRB (reviewed in Coqueret (2002)). In the absence of phosphorylation, pRB binds and inhibits E2F transcription factor family members that are required for cell cycle progress. Upon poly-phosphorylation by activated CyclinD-Cdk4/6, pRB dissociates from E2F, allowing transcription of CyclinE. CyclinE-Cdk2 complexes further phosphorylate and activate pRB, completing a positive feedback loop to ensure a robust initiation to S-phase.

In the presence of DNA damage, cells can break this feedback loop in order to prevent G1-S progression. There are 2 known mechanisms by which this occurs, both requiring upstream activation of ATM. A fast acting pathway involves activated Chk2, which directly phosphorylates
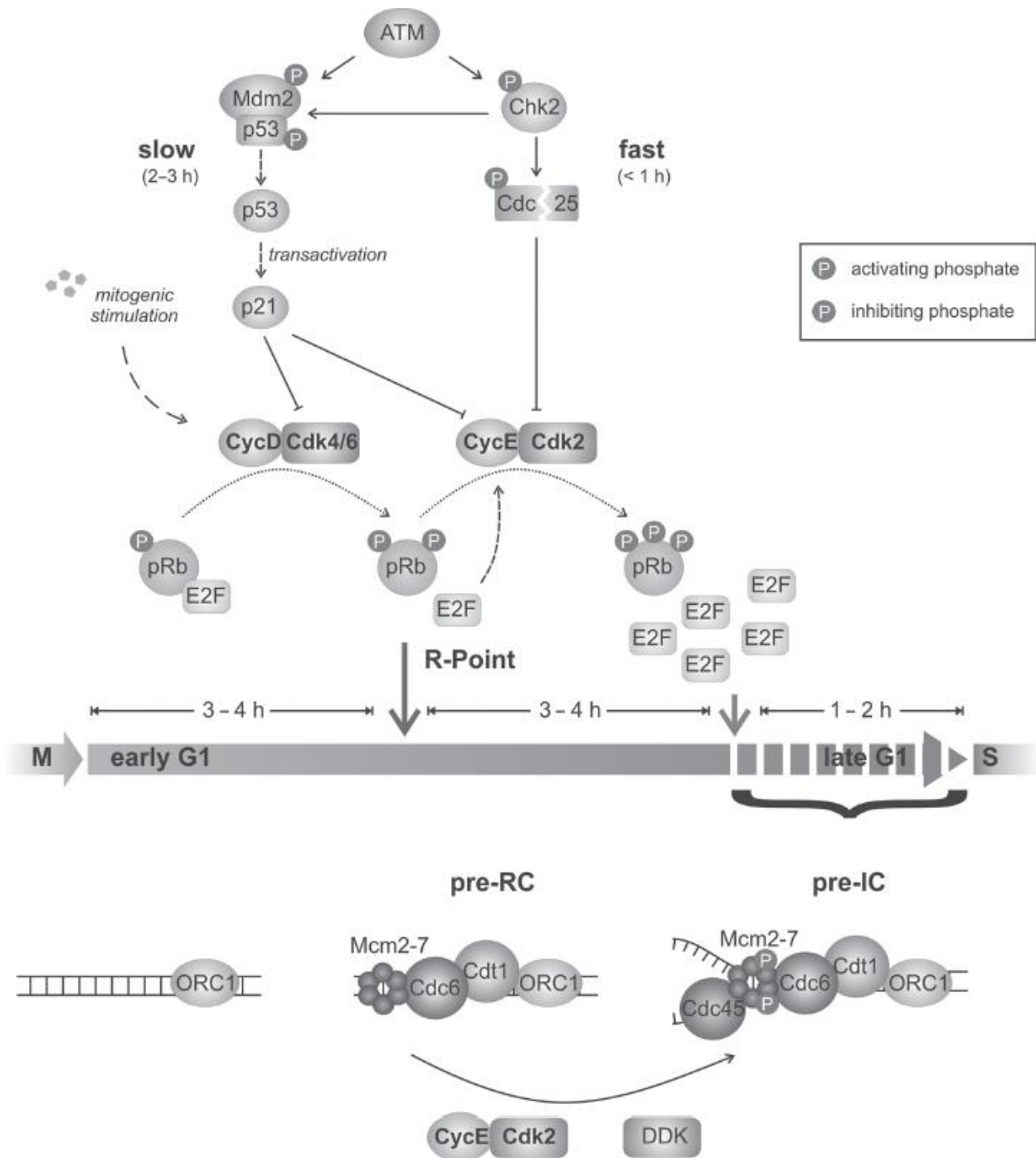
Figure 1.3. Schematic of the G1-S transition, including the key events that result in G1-S checkpoint induction. Reproduced from Deckbar et al. (2011) through open access permissions.

Cdc25A on S123, ultimately resulting in degradation of Cdc25A (Bartek and Lukas, 2007; Falck et al., 2001). Cdc25A is a critical phosphatase required to dephosphorylate and activate the kinase domains of Cdk2/4/6. Thus, in a transcription-independent manner, activated ATM can quickly inhibit the cell cycle progression feedback loop and slow down S-phase entry. A separate, transcription-dependent pathway depends on activation of ATM/Chk2 and stabilization of p53. p53 then transcriptionally activates many genes, including the potent Cdk inhibitor p21$^{CIP/Waf1}$. p21$^{CIP/Waf1}$ belongs to the CIP/KIP family of Cdk inhibitors, and has specificity for both CyclinD-Cdk4/6 and CyclinE-Cdk2 (reviewed in Sherr (1999)). In addition, p21$^{CIP/Waf1}$ has also been shown to cause degradation of pRb independent of Cdk inhibition (Broude et al., 2007). As this pathway of cell cycle inhibition requires transcription, it is necessarily slower, though it can be seen to be active within 2-3 hours post IR (Gadbois and Lehnert, 1997).

The G1-S checkpoint also features a point of no return, termed the restriction point, after which the checkpoint cannot be engaged. Up to 4-6 hours before S-phase, even very high levels of damage will only slow S-phase entry but not prevent it; cells beyond this point are committed to progress to S-phase (Deckbar et al., 2010). Because this timing appears to be after the time when p21 can be transcribed, it is hypothesized that these cells may have accumulated sufficient phosphorylated pRb such that inhibiting Cdk cannot inhibit cell cycle progression. However, given that p21 can modulate pRb, one might expect the point of no return to be closer in timing to the ability to 2-3 hours, not 4-6. The reason for this apparent discrepancy between timings is unclear and needs to be investigated.

The p53-dependent G1-S checkpoint is highly sensitive. It requires that the IRIF be maintained for the ~6 hours it takes to engage the checkpoint, but may be activated by only a single DSB (Di Leonardo et al., 1994; Yamauchi et al., 2008). Furthermore, checkpoint release is dose-

dependent, but counting γ-H2AX foci indicates that although cells have resolved most of the IRIF when they progress into S-phase, they can harbor a small number of breaks. When high doses are used, a small number of cells can escape arrest with high levels of damage, indicating that there may be an upper limit to how much damage the checkpoint can tolerate (Deckbar et al., 2010).

1.6.2. The Intra-S checkpoint

The S-phase checkpoint is intimately tied to the main cellular function during S-phase: replication of the genome. During this key process, the DNA duplex is denatured, and if a single-stranded break is present, a DSB can be formed when a replication fork reaches the break. In addition, replication is discontinuous on both the leading and lagging strands, and replication forks frequently stall or collapse even in unstressed cells. The kinase ATR, which is normally present at replication forks, has an integral role to begin replication each at each origin of replication exactly once, and to initiate repair mechanisms when a replication fork is distressed.

The existence of a checkpoint in S-phase has been known since at least the 1970s, though the specific mechanisms are only recently becoming clearer. Early work found that radiation and genotoxic drugs blocked incorporation of new DNA, and that caffeine greatly increased sensitivity to these treatments (Walters et al., 1974). Later work showed that this decrease in DNA incorporation was due to a block in new replication initiation sites (Larner et al., 1994; Painter, 1980). Because damaged or stalled replication forks are a potential source of chromosome instability, silencing the creation of new replication sites allows the damaged sites to be repaired rather than making even more damaged sites. Once the damaged sites have been resolved, it is safe to initiate new replication sites. Normal initiation of a replication origin requires
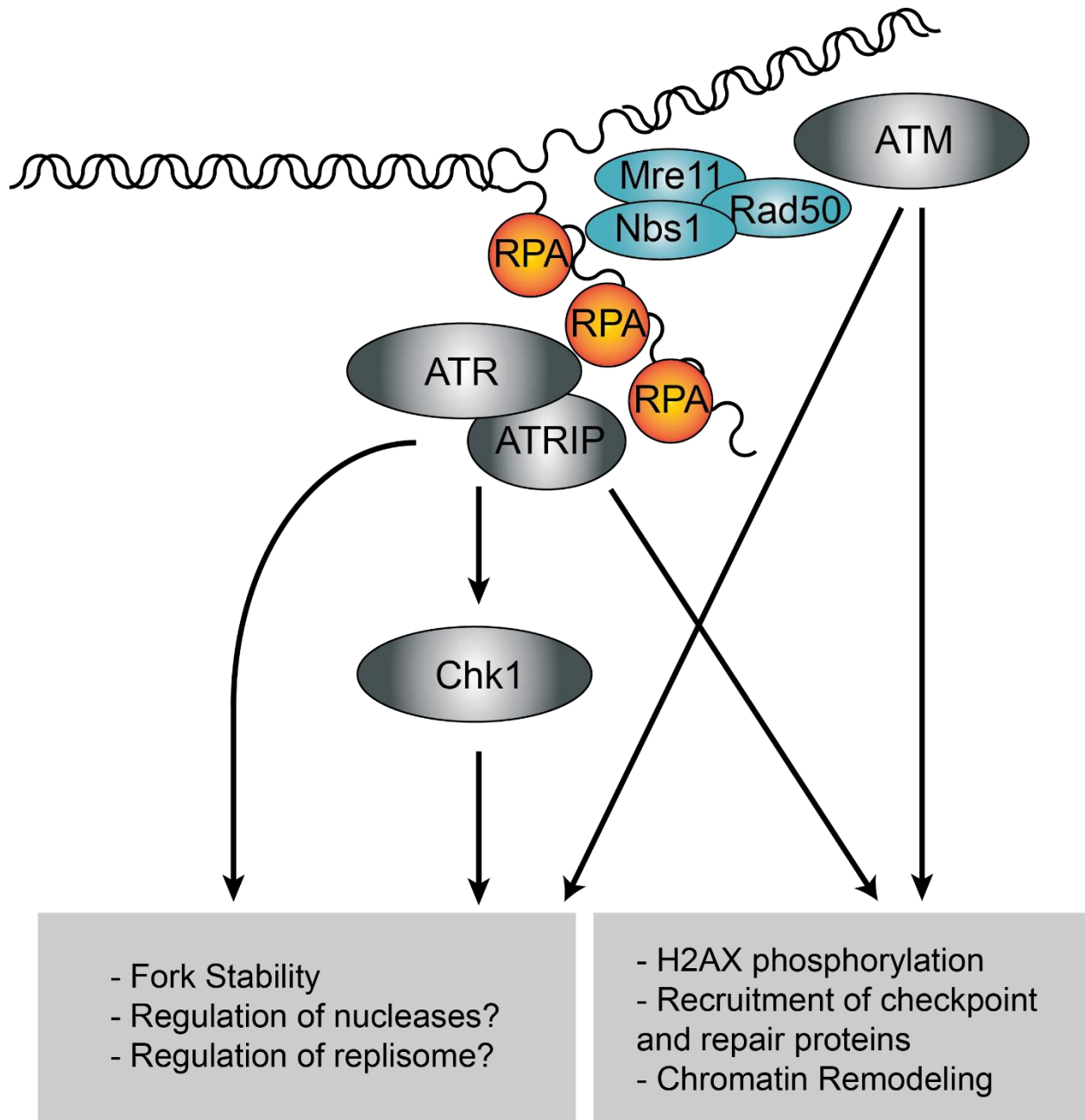
Figure 1.4. Schematic of Intra-S phase checkpoint. Though much is unknown about the precise intra-S mechanisms, it is clear that ATR/ATRIP and ATM, as well as Chk1 are able to cause the downstream effects that prevents replication origins from firing.

CyclinE/Cdk2, which in turn requires Cdc25A for dephosphorylation and activation of its Cdk activity.

The signaling events that initiate the intra-S checkpoint signal stem from ATM/ATR through two separate pathways to silence replication fork initiation. Activated Chk1 and Chk2 phosphorylate Cdc25A, causing its nuclear export and degradation (Falck et al., 2001). Furthermore, Chk1 has many other targets, and may be indirectly involved in preventing the loading of the MCM helicase to chromatin via preventing Cdc45 binding (Liu et al., 2006; Moyer et al., 2006). Alternatively, ATM directly phosphorylates the cohesin subunits Smc1 and Smc3 (Luo et al., 2008; Yazdi et al., 2002). Cohesin enhances recombinatorial DSB repair (Strom et al., 2007), possibly due to the cohesin correctly orienting the spatial proximity of the daughter strands. And though exactly how cohesin contributes to the intra-S checkpoint is unclear, cells deficient for Smc1-or Smc3 are have defects in the intra-S checkpoint, further emphasizing the importance of cohesin (Kim et al., 2002).

1.6.3. The G2-M checkpoint

The G2-M transition is driven in large part by the nuclear CyclinB1/CDK1 complex. Transcription of CyclinB1 is occurs only in the presence of CyclinA/CDK2, ensuring that CyclinB1 begins to be expressed in S phase and peaks in late G2 (reviewed in Fung and Poon (2005). During G2, the CyclinB1-CDK1 complex is held inactive by phosphorylation on T14 and Y15 on CDK1 in the kinase active site, maintained by Wee1 and Myt1 kinases (reviewed in Nigg (2001)). Under unstressed conditions, entry into M phase is thus induced by the Cdc25 phosphatases, which dephosphorylate the kinase active site and convert the inactive CyclinB1-CDK1 complex to an active state. Once active, CyclinB1-CDK1 complex phosphorylates Wee1
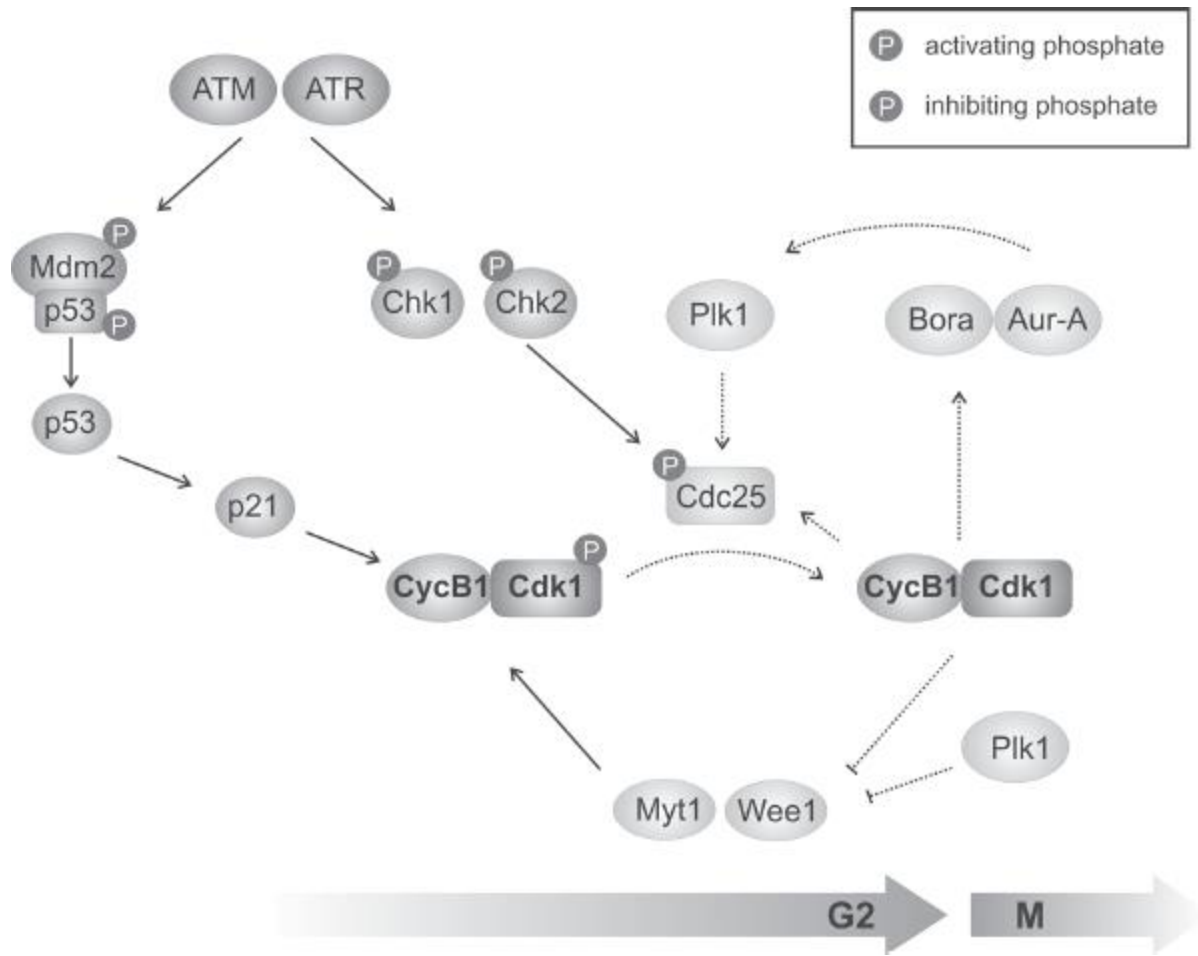
Figure 1.5. Schematic of the key signaling events surrounding the G2-M transition, including checkpoint activation via ATM/ATR through Chk1/Chk2. Reproduced from Deckbar et al. (2011) through open access permissions.

and Cdc25C on numerous sites, thereby closing a robust positive feedback loop whereby it simultaneously deactivates its inhibitor and activates its activator (reviewed in Lindqvist et al. (2009)). The eventual buildup of active CyclinB1-CDK1 complex causes wide-ranging effects that in a switch-like manner initiates early M phase.

Cells can respond to DNA damage and delay M phase initiation by breaking the feedback loops that ensure switch-like behavior. Activated Chk1 and Chk2 have both been reported to phosphorylate Cdc25C, most notably at S216, creating binding sites for 14-3-3 protein and resulting in nuclear export into the cytoplasm, physically preventing its ability to dephosphorylate nuclear Cdk1 (Chan et al., 2011). Additional p53-dependent pathways may also exist, though these remain relatively obscure (Bruno et al., 2006; Chan et al., 2000). In summary, activation of the upstream kinases ATM/ATR transmits a signal downstream through the intermediary kinases Chk1/Chk2 and p53 to halt the cell cycle and prevent the propagation of aberrant nuclear material.

Interestingly, while the G2-M checkpoint can be initiated by only a single DSB, maintenance of the G2-M checkpoint does not appear to be robust, in that it can be terminated before the completion of DSBR. G2-M checkpoint proficient tumor cells, as well as non-transformed cells, are able to enter mitosis despite the presence of 10 or more DSBs (Deckbar et al., 2007; Syljuasen et al., 2006). Careful analysis reveals that the threshold for checkpoint escape is not related to the initial number of breaks, but rather intrinsic to the cellular context (Lobrich and Jeggo, 2005). This process, known as checkpoint adaptation, is the subject of great interest and appears to involve Polo-like kinase (Plk1) and the inactivation of the Chk2 and Rad53 kinases (Leroy et al., 2003). Regardless of the exact mechanism, the G2-M checkpoint is best regarded as transient and insensitive, and can allow mitotic entry despite the presence of unrepaired breaks.

It is also important to note that once a cell has entered mitosis, the DNA damage response is largely silenced. While early events such as γ-H2AX foci formation and ATM phosphorylation on S1981 do occur, key molecules such as 53BP1 are excluded from chromatin (van Vugt et al., 2010). This process of mitotic inactivation seems to ensure that mitosis proceeds forward and prevents the creation of a tetraploid cell by aborting mitosis.

1.6.4. Apoptosis

The cell cycle checkpoints discussed above each has the net effect of slowing the cell cycle and allowing a stressed cell time to repair the genetic insult. This response is generally pro-survival and appropriate for spontaneous genomic damage and most environmental stresses, but sometimes it may not be sufficient. In the cases where the damage is too extensive, or persists and cannot be repaired, a normal cell will typically enter a sustained growth arrest (discussed below), while cancer cells will more often commit apoptosis (Barley et al., 1998).

Apoptosis is a conserved pathway that can be activated by a wide array of external and internal signals. As such, there are many paths to activation, but upstream signaling converges on two key somewhat redundant pathways: the extrinsic and the intrinsic. Both pathways can be activated by many different sensors, but regardless of the original apoptotic stimulus, the final result is always the same: a characteristic blebbing of the membrane, nuclear envelope condensation, nuclear fragmentation, and eventual lysis. The mitochondria of the cell are often but not always involved in releasing cytochrome c into the cytoplasm, where it binds Apoptotic protease activating factor 1 (Apaf-1), which cleaves procaspase-9, which in turn cleaves procaspase-3, amplifying the signal at each step and committing the cell to apoptosis (Li et al., 1997). The specific components of the apoptosis machinery that need to be activated are somewhat interchangeable depending on the

initiating stress and cellular context, as caspases are classified as either an initiator (caspases 8, 9, 10, and 2), or an effector (3, 6, 7). Regardless of how the caspase cleavage cascade is initiated, once begun, the cell is typically committed to complete apoptosis. Caspase-independent apoptosis has also been reported via an intracellular increase in calcium activating the protease calpain (Squìer et al., 1994).

The extrinsic pathway is activated by external cues, prototypically involving ligand-receptor interactions such as tumor necrosis factor (TNF) binding its receptor (TNFR). TNF binding TNFR in its extracellular domain sets off a chain reaction of intracellular protein interactions, cleavage events, and complex formation inside the cell, culminating in the activation of initiator caspase 8 and effector caspase 3 and 6 (reviewed in Chu (2013)).

The intrinsic pathway is activated by internal cues, including oxidative damage and persistent or overwhelming DNA damage. Intrinsic apoptosis can involve caspase-independent effectors such as apoptosis-inducing factor (AIF) and endonuclease G, and usually activates multiple caspases including 3, 6, 8, and 9. Intrinsic stress signaling converges on p53 as a critical decision point and results in p53 phosphorylation and stabilization. Activation of p53 results in a p21-dependent transcriptional repression of pro-survival genes such as BCL-2 (Akhtar et al., 2006), MCL-1 (Pietrzak and Puzianowska-Kuznicka, 2008), and survivin (Hoffman et al., 2002). On the other hand, p53's transcriptional target p21 opposes this by promoting survival. p21 has been demonstrated to inhibit apoptosis by forming complexes with procaspase-3 and preventing cleavage by caspase-9 (Sohn et al., 2006; Suzuki et al., 1999). However, a 15kD cleavage product of p21 does seem to be required for caspase-3 mediated apoptosis. Because p21 is required for p53-mediated repression of the aforementioned pro-survival genes, it is possible that the 15kD p21 cleavage product is required for this repression.

p53 is frequently mutated in cancer, and many of these mutations can affect p53's role in apoptosis/survival signaling. The majority of mutations in cancer result in gain-of-function properties, nuclear accumulation, longer half-life, and the ability to transcriptionally activate pro-survival genes not normally targeted by wild-type p53 (Deb et al., 1994; Frazier et al., 1998). Typically, cancers featuring gain-of-function mutated p53 expressed at high levels are highly resistant to apoptosis, and can be transiently reprogrammed by silencing p53 expression. An uncommon class of p53 misregulation results in nuclear exclusion and a novel inhibitory interaction with procaspase-3 (Frank et al., 2011). Finally, a minority of cancers have very low or no expression of p53, and are typically defective for cell cycle checkpoints and sensitive to apoptosis.

In summary, while p53 transcriptionally represses pro-survival genes, its downstream transcription target p21 is anti-apoptotic, though a cleavage product of p21 is pro-apoptotic. These conflicting signals are eventually integrated with others, possibly in a timing and cellular context dependent manner, that results in a decision of the cell eventually to either enter apoptosis or not. The relative expression levels of these and other molecules within the cell presumably explains why different cell lines have different sensitivities to genomic stress.

1.6.5. Senescence, growth arrest, and other phenotypes

While checkpoint activation and apoptosis have garnered most of the research interest for many years, we are now beginning to appreciate the complexities of other possible responses to genotoxic stress. These responses include permanent growth arrest and senescence, mitotic catastrophe, autophagy, and necrosis/necroptosis. Much less is known about these cellular states

than checkpoint activation and apoptosis, but in the interest of completion we will discuss them briefly here.

Most normal cells, when experiencing moderate DNA damage, do not commit apoptosis. Rather, if transient expression of p21 associated with checkpoint activation persists for a long enough time, cells can enter a permanent growth arrest known as stress-induced persistent senescence (SIPS). In SIPS, p21 gains an additional role of gene regulation, whereby it activates gene expression associated with cellular senescence, aging, and growth arrest (Barley et al., 1998; Chang et al., 2000; Devgan et al., 2005; Kitaura et al., 2000).

The role of p21 in cellular senescence has been elucidated in recent years. Cellular senescence is a distinct state of persistent growth arrest, marked by high expression of β-galactosidase, an enlarged and flattened "fried egg" morphology, and absolute lack of proliferation despite metabolic activity. SIPS should not be confused with senescence resulting from aging telomeres, termed replicative senescence. Cells undergoing SIPS can be kept alive in culture for months without proliferation, and display a remarkable resistance to apoptosis.

Because of the critical role of p53 and p21 in maintaining SIPS, it is observed mainly in cells containing wild-type p53. Most cancer lines carrying mutations in p53 are deficient in cell cycle checkpoints, as well as unable to efficiently activate SIPS. As a result, these cells either commit apoptosis, or ignore the DNA damage completely and attempt mitosis regardless of chromosomal damage. This latter class of cells often experience distressed mitotic events, termed mitotic catastrophe.

Mitotic catastrophe as a phenomenon is poorly defined, but the most common definition is the presence of multiple nuclei or aberrant nuclear structures termed micronuclei. Micronuclei result from aberrant chromosomal separation or chromosomal fragments that are not evenly distributed

50

upon cytokinesis, whereas multiple nuclei form upon a failed karyokinesis (Vakifahmetoglu et al., 2008). The signaling events that follow such abnormal structures remain unclear, but the possible cellular outcomes appear to include prolonged growth arrest and senescence as well as catastrophic mechanical failure of the cell membrane during future mitosis. Mitotic catastrophe has gained prominence recently because it has been shown that to result from treatment with chemotherapeutic drugs (Eom et al., 2005). While the doses used in this study were low, they may well represent a physiological local concentration of drug within a tumor. However, the specific downstream events involved in mitotic catastrophe remain obscure and the extent to which it causes cell death or senescence is unknown.

Autophagy is a confusingly paradoxical cellular phenotype that has been most extensively studied in response to DNA damage. Macroautophagy (simply known as autophagy) is a major pathway by which cells cannibalize intracellular components by fusing lysosomes with organelles to form a double-membrane autophagosome. Eventually, autophagosomes release fatty acids and amino acids for use elsewhere in the cell (Baehrecke, 2005; Klionsky, 2000). Autophagy is a normal function of unstressed cells, but can be massively upregulated in response to withdrawal of growth signals, oxidative stress, or DNA damage. It is easy to understand why scavenging fatty acids and amino acids in starvation conditions would be pro-survival, but it is harder to see why a cell undergoing DNA damage might need extra fatty acids or amino acids. Nonetheless, autophagy delays apoptotic death in response to DNA-damaging agent camptothecin (Abedin et al., 2007). Activated ATM is known to activate AMPK, which in turn inhibits mTOR, which inhibits autophagy in response to DNA damage (Alexander et al., 2010). However, p53-mediated autophagy accelerates apoptotic cell death, indicating that autophagy is not always pro-survival (Crighton et al., 2006). It has also been speculated that many of the stimuli used in the lab to create

DNA damage also inflict oxidative damage to lipids and protein, and that reactive oxygen species are generated at damaged DNA as a signaling molecule, explaining the need for spare amino acids and lipids. If this is the case, autophagy may well be a critical repair mechanism in the DDR. Indeed, the role of autophagy in determining cell fate is unclear and whether it is a net promoter of survival or death is unknown.

Necrosis is a chronically disregarded cellular response that has only recently begun to be appreciated in the context of DNA damage. Originally, necrosis was defined negatively as a "garbage pail" category: cells that could not be classified as undergoing apoptosis nor autophagic vacuolization were labeled necrotic and considered generally uninteresting. Necrosis is typically observed in response to hypoxia or mechanical damage, and in contrast to apoptosis does not feature an immunogenic display to stimulate cleanup of cellular debris. As such, necrosis as a whole was considered to be an uncoordinated, transcription-independent death mechanism. Recent evidence has shown that this simplistic view is incomplete, and that a subset of necrotic death can in fact be highly coordinated, involving production of reactive oxygen species (Goossens et al., 1996) and activation of receptor-interacting kinases 1 and 3 (RIP1/RIP3) (Cho et al., 2009) and tumor necrosis factor receptor 1 (TNFR) (Hitomi et al., 2008). The discovery that necrosis downstream of chemotherapeutic insult is coordinated has led to a renaming of the phenomenon as necroptosis to contrast with ischemic necrosis, and much work is in progress to elucidate the specific mechanisms involved.

Works Cited

Abedin, M.J., Wang, D., McDonnell, M.A., Lehmann, U., and Kelekar, A. (2007). Autophagy delays apoptotic death in breast cancer cells following DNA damage. Cell death and differentiation *14*, 500-510.

Akhtar, R.S., Geng, Y., Klocke, B.J., Latham, C.B., Villunger, A., Michalak, E.M., Strasser, A., Carroll, S.L., and Roth, K.A. (2006). BH3-only proapoptotic Bcl-2 family members Noxa and Puma mediate neural precursor cell death. The Journal of neuroscience : the official journal of the Society for Neuroscience *26*, 7257-7264.

Alexander, A., Cai, S.L., Kim, J., Nanez, A., Sahin, M., MacLean, K.H., Inoki, K., Guan, K.L., Shen, J., Person, M.D.*, et al.* (2010). ATM signals to TSC2 in the cytoplasm to regulate mTORC1 in response to ROS. Proceedings of the National Academy of Sciences of the United States of America *107*, 4153-4158.

Baehrecke, E.H. (2005). Autophagy: dual roles in life and death? Nature reviews Molecular cell biology *6*, 505-510.

Barley, R.D., Enns, L., Paterson, M.C., and Mirzayans, R. (1998). Aberrant p21WAF1-dependent growth arrest as the possible mechanism of abnormal resistance to ultraviolet light cytotoxicity in Li-Fraumeni syndrome fibroblast strains heterozygous for TP53 mutations. Oncogene *17*, 533-543.

Bartek, J., and Lukas, J. (2007). DNA damage checkpoints: from initiation to recovery or adaptation. Current opinion in cell biology *19*, 238-245.

Broude, E.V., Swift, M.E., Vivo, C., Chang, B.D., Davis, B.M., Kalurupalle, S., Blagosklonny, M.V., and Roninson, I.B. (2007). p21(Waf1/Cip1/Sdi1) mediates retinoblastoma protein degradation. Oncogene *26*, 6954-6958.

Bruno, T., De Nicola, F., Iezzi, S., Lecis, D., D'Angelo, C., Di Padova, M., Corbi, N., Dimiziani, L., Zannini, L., Jekimovs, C.*, et al.* (2006). Che-1 phosphorylation by ATM/ATR and Chk2 kinases activates p53 transcription and the G2/M checkpoint. Cancer cell *10*, 473-486.

Chan, P.M., Ng, Y.W., and Manser, E. (2011). A robust protocol to map binding sites of the 14-3-3 interactome: Cdc25C requires phosphorylation of both S216 and S263 to bind 14-3-3. Molecular & cellular proteomics : MCP *10*, M110 005157.

Chan, T.A., Hwang, P.M., Hermeking, H., Kinzler, K.W., and Vogelstein, B. (2000). Cooperative effects of genes controlling the G(2)/M checkpoint. Genes & development *14*, 1584-1588.

Chang, B.D., Watanabe, K., Broude, E.V., Fang, J., Poole, J.C., Kalinichenko, T.V., and Roninson, I.B. (2000). Effects of p21Waf1/Cip1/Sdi1 on cellular gene expression: implications for carcinogenesis, senescence, and age-related diseases. Proceedings of the National Academy of Sciences of the United States of America *97*, 4291-4296.

Cho, Y.S., Challa, S., Moquin, D., Genga, R., Ray, T.D., Guildford, M., and Chan, F.K. (2009). Phosphorylation-driven assembly of the RIP1-RIP3 complex regulates programmed necrosis and virus-induced inflammation. Cell *137*, 1112-1123.

Chu, W.M. (2013). Tumor necrosis factor. Cancer letters *328*, 222-225.

Coqueret, O. (2002). Linking cyclins to transcriptional control. Gene *299*, 35-55.

Crighton, D., Wilkinson, S., O'Prey, J., Syed, N., Smith, P., Harrison, P.R., Gasco, M., Garrone, O., Crook, T., and Ryan, K.M. (2006). DRAM, a p53-induced modulator of autophagy, is critical for apoptosis. Cell *126*, 121-134.

Deb, S.P., Muñoz, R.M., Brown, D.R., Subler, M.A., and Deb, S. (1994). Wild-type human p53 activates the human epidermal growth factor receptor promoter. Oncogene *9*, 1341-1349.

Deckbar, D., Birraux, J., Krempler, A., Tchouandong, L., Beucher, A., Walker, S., Stiff, T., Jeggo, P., and Lobrich, M. (2007). Chromosome breakage after G2 checkpoint release. The Journal of cell biology *176*, 749-755.

Deckbar, D., Jeggo, P.A., and Lobrich, M. (2011). Understanding the limitations of radiation-induced cell cycle checkpoints. Critical reviews in biochemistry and molecular biology *46*, 271-283.

Deckbar, D., Stiff, T., Koch, B., Reis, C., Lobrich, M., and Jeggo, P.A. (2010). The limitations of the G1-S checkpoint. Cancer Res *70*, 4412-4421.

Devgan, V., Mammucari, C., Millar, S.E., Brisken, C., and Dotto, G.P. (2005). p21WAF1/Cip1 is a negative transcriptional regulator of Wnt4 expression downstream of Notch1 activation. Genes & development *19*, 1485-1495.

Di Leonardo, A., Linke, S.P., Clarkin, K., and Wahl, G.M. (1994). DNA damage triggers a prolonged p53-dependent G1 arrest and long-term induction of Cip1 in normal human fibroblasts. Genes & development *8*, 2540-2551.

Eom, Y.W., Kim, M.A., Park, S.S., Goo, M.J., Kwon, H.J., Sohn, S., Kim, W.H., Yoon, G., and Choi, K.S. (2005). Two distinct modes of cell death induced by doxorubicin: apoptosis and cell death through mitotic catastrophe accompanied by senescence-like phenotype. Oncogene *24*, 4765-4777.

Falck, J., Mailand, N., Syljuåsen, R.G., Bartek, J., and Lukas, J. (2001). The ATM-Chk2-Cdc25A checkpoint pathway guards against radioresistant DNA synthesis. Nature *410*, 842-847.

Frank, A.K., Pietsch, E.C., Dumont, P., Tao, J., and Murphy, M.E. (2011). Wild-type and mutant p53 proteins interact with mitochondrial caspase-3. Cancer Biology & Therapy *11*, 740-745.

Frazier, M.W., He, X., Wang, J., Gu, Z., Cleveland, J.L., and Zambetti, G.P. (1998). Activation of c-myc gene expression by tumor-derived p53 mutants requires a discrete C-terminal domain. Molecular and cellular biology *18*, 3735-3743.

Fung, T.K., and Poon, R.Y. (2005). A roller coaster ride with the mitotic cyclins. Seminars in cell & developmental biology *16*, 335-342.

Gadbois, D.M., and Lehnert, B.E. (1997). Temporal position of G1 arrest in normal human fibroblasts after exposure to gamma-rays. Exp Cell Res *232*, 161-166.

Goossens, V., Grooten, J., and Fiers, W. (1996). The oxidative metabolism of glutamine. A modulator of reactive oxygen intermediate-mediated cytotoxicity of tumor necrosis factor in L929 fibrosarcoma cells. The Journal of biological chemistry *271*, 192-196.

Hitomi, J., Christofferson, D.E., Ng, A., Yao, J., Degterev, A., Xavier, R.J., and Yuan, J. (2008). Identification of a molecular signaling network that regulates a cellular necrotic cell death pathway. Cell *135*, 1311-1323.

Hoffman, W.H., Biade, S., Zilfou, J.T., Chen, J., and Murphy, M. (2002). Transcriptional repression of the anti-apoptotic survivin gene by wild type p53. The Journal of biological chemistry *277*, 3247-3257.

Kim, S.T., Xu, B., and Kastan, M.B. (2002). Involvement of the cohesin protein, Smc1, in Atm-dependent and independent responses to DNA damage. Genes & development *16*, 560-570.

Kitaura, H., Shinshi, M., Uchikoshi, Y., Ono, T., Iguchi-Ariga, S.M., and Ariga, H. (2000). Reciprocal regulation via protein-protein interaction between c-Myc and p21(cip1/waf1/sdi1) in DNA replication and transcription. The Journal of biological chemistry *275*, 10477-10483.

Klionsky, D.J. (2000). Autophagy as a Regulated Pathway of Cellular Degradation. Science *290*, 1717-1721.

Larner, J.M., Lee, H., and Hamlin, J.L. (1994). Radiation effects on DNA synthesis in a defined chromosomal replicon. Mol Cell Biol *14*, 1901-1908.

Leroy, C., Lee, S.E., Vaze, M.B., Ochsenbien, F., Guerois, R., Haber, J.E., and Marsolier-Kergoat, M.-C. (2003). PP2C Phosphatases Ptc2 and Ptc3 Are Required for DNA Checkpoint Inactivation after a Double-Strand Break. Molecular cell *11*, 827-835.

Li, P., Nijhawan, D., Budihardjo, I., Srinivasula, S.M., Ahmad, M., Alnemri, E.S., and Wang, X. (1997). Cytochrome c and dATP-dependent formation of Apaf-1/caspase-9 complex initiates an apoptotic protease cascade. Cell *91*, 479-489.

Lindqvist, A., Rodriguez-Bravo, V., and Medema, R.H. (2009). The decision to enter mitosis: feedback and redundancy in the mitotic entry network. The Journal of cell biology *185*, 193-202.

Liu, P., Barkley, L.R., Day, T., Bi, X., Slater, D.M., Alexandrow, M.G., Nasheuer, H.P., and Vaziri, C. (2006). The Chk1-mediated S-phase checkpoint targets initiation factor Cdc45 via a Cdc25A/Cdk2-independent mechanism. The Journal of biological chemistry *281*, 30631-30644.

Lobrich, M., and Jeggo, P.A. (2005). The two edges of the ATM sword: co-operation between repair and checkpoint functions. Radiotherapy and oncology : journal of the European Society for Therapeutic Radiology and Oncology *76*, 112-118.

Luo, H., Li, Y., Mu, J.J., Zhang, J., Tonaka, T., Hamamori, Y., Jung, S.Y., Wang, Y., and Qin, J. (2008). Regulation of intra-S phase checkpoint by ionizing radiation (IR)-dependent and IR-independent phosphorylation of SMC3. The Journal of biological chemistry *283*, 19176-19183.

Moyer, S.E., Lewis, P.W., and Botchan, M.R. (2006). Isolation of the Cdc45/Mcm2-7/GINS (CMG) complex, a candidate for the eukaryotic DNA replication fork helicase. Proceedings of the National Academy of Sciences of the United States of America *103*, 10236-10241.

Nigg, E.A. (2001). Mitotic kinases as regulators of cell division and its checkpoints. Nat Rev Mol Cell Biol *2*, 21-32.

Painter, R.B. (1980). Effect of caffeine on DNA synthesis in irradiated and unirradiated mammalian cells. J Mol Biol *143*, 289-301.

Pietrzak, M., and Puzianowska-Kuznicka, M. (2008). p53-dependent repression of the human MCL-1 gene encoding an anti-apoptotic member of the BCL-2 family: the role of Sp1 and of basic transcription factor binding sites in the MCL-1 promoter. Biological chemistry *389*, 383-393.

Sherr, C.J., Roberts, J. M. (1999). CDK inhibitors: positive and negative regulators of G1-phase progression. Genes & development *13*, 1501-1512.

Sohn, D., Essmann, F., Schulze-Osthoff, K., and Jänicke, R.U. (2006). p21 blocks irradiation-induced apoptosis downstream of mitochondria by inhibition of cyclin-dependent kinase-mediated caspase-9 activation. Cancer Res *66*, 11254-11262.

Squìer, M.K., Miller, A.C., Malkinson, A.M., and Cohen, J.J. (1994). Calpain activation in apoptosis. J Cell Physiol *159*, 229-237.

Strom, L., Karlsson, C., Lindroos, H.B., Wedahl, S., Katou, Y., Shirahige, K., and Sjogren, C. (2007). Postreplicative formation of cohesion is required for repair and induced by a single DNA break. Science *317*, 242-245.

Suzuki, A., Tsutomi, Y., Yamamoto, N., Shibutani, T., and Akahane, K. (1999). Mitochondrial regulation of cell death: mitochondria are essential for procaspase 3-p21 complex formation to resist Fas-mediated cell death. Molecular and cellular biology *19*, 3842-3847.

Syljuasen, R.G., Jensen, S., Bartek, J., and Lukas, J. (2006). Adaptation to the ionizing radiation-induced G2 checkpoint occurs in human cells and depends on checkpoint kinase 1 and Polo-like kinase 1 kinases. Cancer Res *66*, 10253-10257.

Vakifahmetoglu, H., Olsson, M., and Zhivotovsky, B. (2008). Death through a tragedy: mitotic catastrophe. Cell death and differentiation *15*, 1153-1162.

van Vugt, M.A., Gardino, A.K., Linding, R., Ostheimer, G.J., Reinhardt, H.C., Ong, S.E., Tan, C.S.M., H., Keezer, S.M., Li, J., Pawson, T.*, et al.* (2010). A mitotic phosphorylation feedback network connects Cdk1, Plk1, 53BP1, and Chk2 to inactivate the G(2)/M DNA damage checkpoint. PLoS Biol *8*.

Walters, R.A., Gurley, L.R., and Tobey, R.A. (1974). Effects of caffeine on radiation-induced phenomena associated with cell-cycle traverse of mammalian cells. Biophys J *14*, 99-118.

Yamauchi, M., Oka, Y., Yamamoto, M., Niimura, K., Uchida, M., Kodama, S., Watanabe, M., Sekine, I., Yamashita, S., and Suzuki, K. (2008). Growth of persistent foci of DNA damage checkpoint factors is essential for amplification of G1 checkpoint signaling. DNA repair *7*, 405-417.

Yazdi, P.T., Wang, Y., Zhao, S., Patel, N., Lee, E.Y., and Qin, J. (2002). SMC1 is a downstream effector in the ATM/NBS1 branch of the human S-phase checkpoint. Genes & development *16*, 571-582.

Part 2

Application of Lysate Microarray Technology

For High-Throughput Profiling and Drug Target Identification

In Liver-Stage Malaria Infection

2.1. Introduction

Parasites of the genus *Plasmodium* cause malaria, an ancient scourge that has shaped human genetics and history. Malaria continues to be a major cause of morbidity worldwide, affecting 150-300 million people annually, with 660,000 deaths (WHO, 2013). Efforts to produce a vaccine have been largely stymied, with the only Phase 3 trial to date recently reporting only a 16.8% efficacy over 4 years, declining with both time and increasing malaria exposure (Olotu et al., 2013). Furthermore, although increasing availability of treatment has decreased morbidity, evolution of resistance remains a recurring problem: chloroquinine was introduced in 1947 and resistance was documented as early as 1950, with widespread resistance obsoleting the drug by the 1980s. Artemisinin-resistant strains have been recently discovered (Kyaw et al., 2013), which if allowed to spread worldwide, will have devastating consequences as no other approved and effective treatments will be available for at least 3 years. The very credible threat of totally-resistant malaria, coupled with the general failure of vaccine efforts, has driven the need for new approaches toward a working prophylactic vaccine or treatment to crisis-level importance.

The liver stage of the infection presents an enticing target for prophylactic or palliative intervention. Immediately after transmission by the bite of an *Anopheles* mosquito, the parasite sporozoite travels through the bloodstream to the liver, where it infects hepatocytes and manipulates the host. The parasite then grows and replicates within the hepatocyte, evading host detection for a time, and eventually reenters the bloodstream as thousands of daughter merozoites that infect red blood cells and cause symptomatic malaria (Vaughan et al., 2008). *P. berghei*, which infects rodents, has been shown to actively inhibit apoptosis in the host hepatocyte both early (van de Sand et al., 2005) and late (Leirião et al., 2005). Although immunity does not typically result from *Plasmodium* infection (Tran et al., 2013), genetically

attenuated parasites that do not proceed past liver-stage have been shown to provoke long-term immunity (Doolan and Hoffman, 2000; Krzych et al., 2012). Indeed, preparations of both early- (Annoura et al., 2012) and late- (Butler et al., 2011) stage hepatocyte infection have been tried in rodent vaccine trials with varying success. Taken together, these insights suggest that *Plasmodium* blocks host apoptosis, and that restoring or promoting apoptosis in infected hepatocytes may be a fruitful approach for prophylactic vaccination.

Liver-stage malaria has historically been technically challenging, but reverse phase lysate microarray technology is perfectly positioned to interrogate the signaling events in infected cells. Isolating live parasite requires painstaking dissection of mosquito salivary glands by hand, which must then be used immediately, and while hepatocyte infection is an obligatory step in the *Plasmodium* lifecycle, very few hepatocytes are actually infected; as few as 0.1% both *in vivo* and *in vitro*. Producing sufficient cellular lysate for classical techniques such as immunoblotting is therefore impractical. Correspondingly, very little is known about the transcriptional, translational, and phosphorylation states of infected hepatocytes. Whereas lysate microarrays require extremely small amounts of lysate, we took advantage of the technique to interrogate the signaling changes that take place in the host cell upon infection and identified a key mechanism by which *Plasmodium* parasites modulate host apoptosis signaling.

This work was reproduced with modifications and additions from Kaushansky et al. (2013).

2.2. Results and Discussion

2.2.1. Development of a Lysate Microarray-based Platform for Profiling Infected Hepatocytes

The major technical challenge to studying liver-stage infection is the low infection rate and the technical difficulties in creating large amounts of parasite. In order to circumvent the problem, we chose a model system we had previous experience with. HepG2/CD81 hepatoma cells were ideal because are readily infected by *Plasmodium* and we have previously validated antibodies for use in that cell line (Luckert et al., 2012). We therefore assembled a list of antibodies, all of which have been demonstrated to pass stringent criteria for data quality. Specifically, we required that all antibodies used be highly specific for the listed antigen, producing only a single dominant band of the right size in immunoblotting, and that the changes in signal measured by microarray matched those observed in immunoblots. The antibodies we selected recognize proteins involved in diverse pathways including survival, apoptosis, proliferation, cell-cycle control, and autophagy.

It is important to note that while all the chosen antibodies have previously been validated for use in HepG2 cells, there may still be reasons why they might produce misleading data. We have previously shown in the lab that an antibody that produces a measurable, positive signal on lysate microarrays may actually not be measuring its target at all, but rather an off-target cross-reactive species, resulting in misleading data (Sevecka et al., 2011). Further compounding the off-target problem is the fact that the cross-reactive target is usually unknown, and that each antibody may have cross-reactivities that vary unpredictably according to cell line, treatment, and time point. Thus, we carefully constructed a list of candidate antibodies (Table 2.2), all previously validated for use in HepG2 cells after stimulation with growth factors such as HGF or

Wnt. The only way to fully validate the antibodies for use in malaria would have required prohibitive amounts of infected cells. As the lysate microarray technique is significantly more straightforward to use in medium throughput and consumes minimal sample, we decided to use a reverse screen approach and use all the pre-selected antibodies that we believed might work, keeping in mind the caveats and making sure to validate the ensuing results with multiple other techniques.

Given the potential technical problems mentioned above, we initially set out to test the experimental protocol to see if we could recapitulate known phenomenon. We were motivated by a report that HGF signaling was important for malaria infection (Carrolo et al., 2003), reasoning that HGF is a key growth factor in hepatocytes and that autocrine signaling might partially be responsible for the apoptosis defect. This is particularly intriguing considering that *Plasmodium* parasites are known to tunnel through, without apparently harming, hundreds of hepatocytes before finally selecting one to mature in. We hypothesized that Met signaling might prevent apoptosis in those cells that had been burrowed through, and acquired both Met$^-$ hepatocytes and Spect2$^-$ parasites deficient for this tunneling behavior (Ishino et al., 2005). We also hoped that we might be able to see the parasite-specific signaling above the background of uninfected cells, so we tested both unseparated samples and FACS sorted samples.

The total list of lysates collected for this proof-of-principle experiment is listed in Table 2.1. As the infection rate of *P. yoelli* is on the order of 0.1-0.3%, we considered that it may be necessary to separate out infected cells from uninfected cells. To do so, we selected a GFP-expressing *P. yoelli* strain (Tarun et al., 2006), which allowed us to use Fluorescence Activated Cell Sorting (FACS) to pull out the small number of infected cells. For the purposes of the sorted samples, we acquired 5000 cells for both negative and positive GFP staining, and lysed

Table 2.1 -- List of lysates used in pilot study to establish feasibility of lysate array analysis of *Plasmodium* infected HepG2 cells.			
Sample	Host	Description	time point
1	Wt HepG2	Mock treated Control	1 hour
2	wt HepG2	wt *P. falciperum*	1 hour
3	Met⁻ HepG2	spect2⁻ *P. yoelii*	1 hour
4	Met⁺ HepG2	spect2⁻ *P. berghei*	1 hour
5	wt HepG2	wt *P. falciparum*	24 hour
6	Met⁻ HepG2	wt *P. yoelii*	24 hour
7	Met⁺ HepG2	wt *P. berghei*	24 hour
8	wt HepG2	GFP *P. yoelii*, FACS sorted -	24 hour
9	wt HepG2	GFP *P. yoelii*, FACS sorted +	24 hour

Table 2.1. List of lysates used in pilot study to establish feasibility of lysate array analysis of *Plasmodium* infected HepG2 cells. Lysates were designed to test multiple hypotheses in one experiment: whether GFP sorting was necessary to measure host or parasite signaling, if non-traversing mutants could be used rather than GFP sorting, whether host Met signaling was affected by *Plasmodium* infection, and how necessary FACS sorting was for maximum contrast between infected and non-infected signaling.

them in 10 μL lysis buffer without filtering. All other lysates were collected from a single 10cm plate in 0.5 mL lysis buffer, and filtered according to established protocol. All lysates were then printed using an Aushon 2470 arrayer using 110 μm diameter pins at 350 μm spacing in duplicate. Arrays were then probed and quantified according to established protocol (Sevecka et al., 2011).

The data collected from this pilot experiment was very informative. Technical variation within replicate spots was very small: the average intra-sample coefficient of variation (c.v.) was 2.4%. These internal controls all gave us confidence that the malaria-infected experimental lysates were valid and interpretable. In some cases, we were also able to measure parasite protein without sorting, for example U154 in *P. berghei* (Figure 2.1, left). Most importantly, we were able to detect signal that varied significantly according to stimulus, indicating that at least

Antibody: U154 (parasite protein)   Antibody: p-Met (Y1349)

Lysate: 1 2 3 4 5 6 7 8 9   Lysate: 1 2 3 4 5 6 7 8 9

Antibody: β-actin   Antibody: β-actin
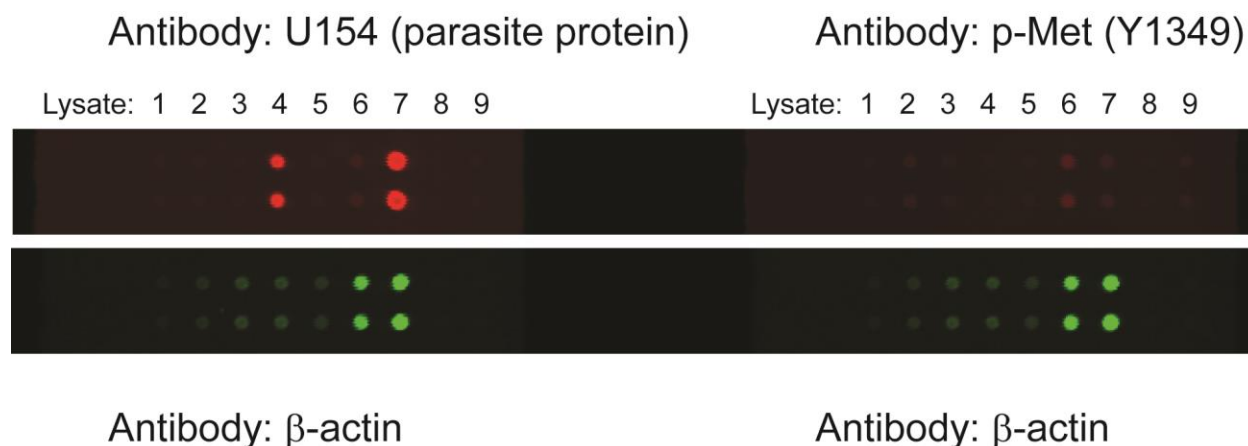
Figure 2.1. Representative example of lysate microarray data detecting changes in protein expression after *Plasmodium* infection. A representative example of lysate array raw images show a strong signal for U154 in *P. berghei* infected cells, as well as confirming no significant upregulation in phosphorylation on Met Y1349 in response to bulk infection with *Plasmodium.* At this scanning laser intensity, the sorted lysates (8-9) are not visible.

in some cases, our technique was working to detect changes in cellular signaling. We were able

to confirm that in bulk measurements, Met was not significantly higher in samples that had been

exposed to *Plasmodium,* regardless of Spect2 deletion and ability to tunnel (Figure 2.1, right).

We also noted that the signal for the GFP sorted sample was very low and could only be

observed when scanning laser intensity was increased to high power which increases background

fluorescence. This was due to the sample being too dilute. As a result, we concluded that 5,000

cells in 10 μL was too dilute, and estimated that 10,000 cells lysed in 3 μL would provide

sufficient protein concentration for detection. Despite the need for high laser power to analyze

the sorted samples, we found that Met was not significantly phosphorylated or upregulated in

response to *Plasmodium* tunneling or infection. Finally, we concluded that unsorted bulk

samples were insufficient to measure signaling in the minority of infected cells above the background of uninfected cells.

Armed with these data, we now proceeded to a more ambitious experiment to screen a panel of known cancer-associated signaling events surrounding apoptosis and survival in the context of *Plasmodium* infection.

2.2.2. Lysate Microarray-based Profiling of Host Signaling during *Plasmodium* infection

We grew HepG2 cells in 10-cm plates to about 50% confluence (5×10^6 cells), at which point 2×10^6 freshly isolated GFP-tagged *P. yoelli* were added to the culture. Infection was then allowed to proceed for 8 or 24 hours, at which point the cells were recovered and prepared for FACS. Typically, about 10,000 GFP-positive HepG2 cells could be collected from each plate; these were lysed in 3 μL of SDS lysis buffer. A corresponding number of GFP-negative HepG2 cells were analogously collected and lysed as a matched uninfected control. In addition, the following control lysates were also produced: unstimulated HepG2 cells, HepG2 cells stimulated with 25 ng/mL HGF for 10 minutes, and HepG2 cells stimulated 10 μM doxorubicin for 24 hours. The experiment was performed in triplicate to gain statistical significance and address reproducibility.

These lysates were then filtered and arrayed in quadruplicate on 60 separate nitrocellulose pads, followed by probing according to established protocol (Sevecka et al., 2011). The antibody list used was the same as that listed in Table 2.2. Included in each probing was also a primary antibody directed against β-actin to be used as an internal control against variation in total

Figure 2.2 (Next Page). Use of Lysate Microarrays to study Host Signaling in Liver-Stage Malaria Infection. (A) Schematic representing steps required to obtain microarray data from a HepG2 sample infected with *P. yoelii*-GFP liver stages. (B) Representative array images from 3 antibodies. (C) Graph representing overexpression ratio in host cells for 46 separate antibodies, plotted against the log p-value obtained. Each point represents a single antibody. Significant results that pass multiple hypothesis testing are shown in blue, nonsignficant results shown in red. Reproduced from Kaushansky et al. (2013) with permission.
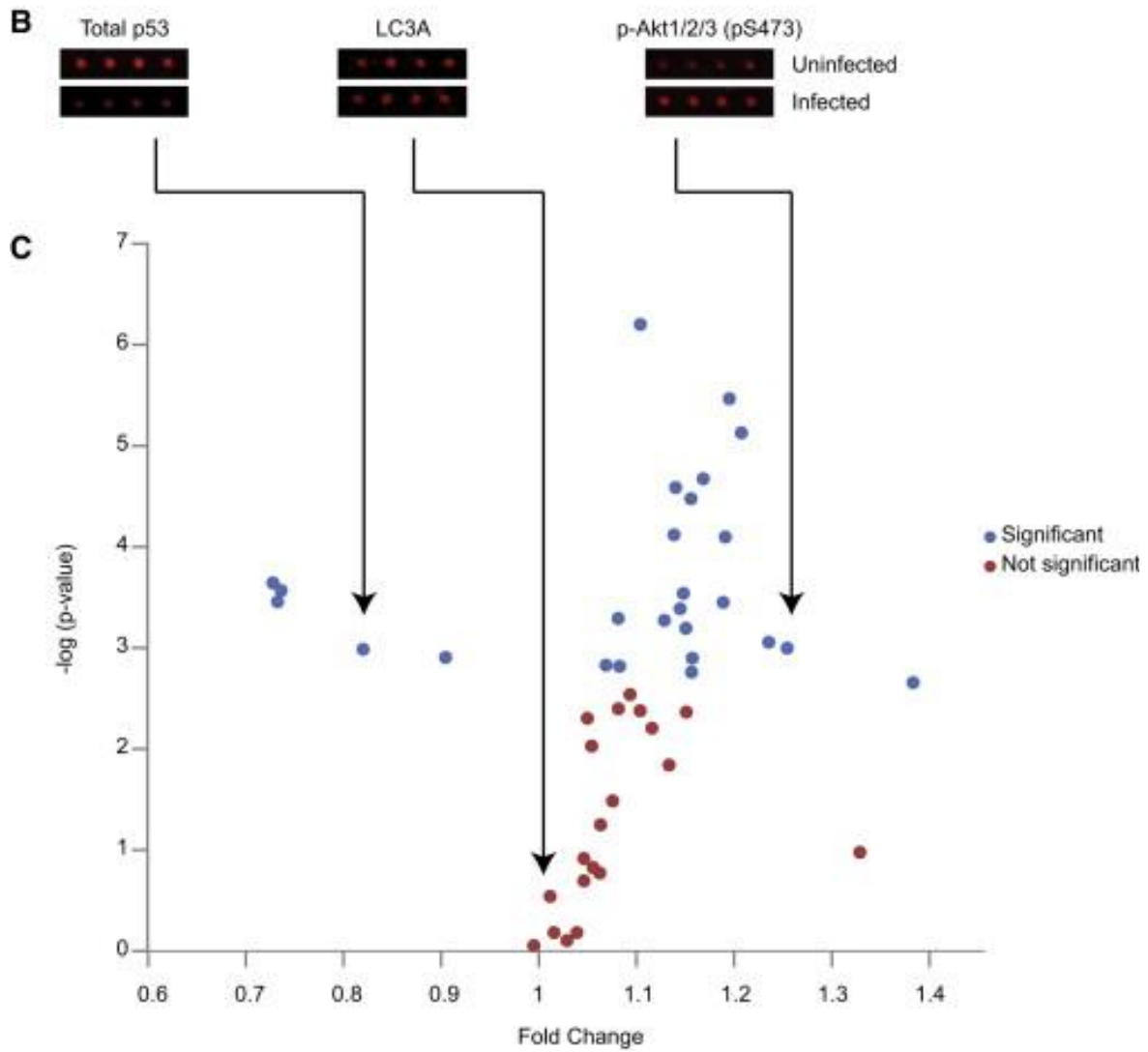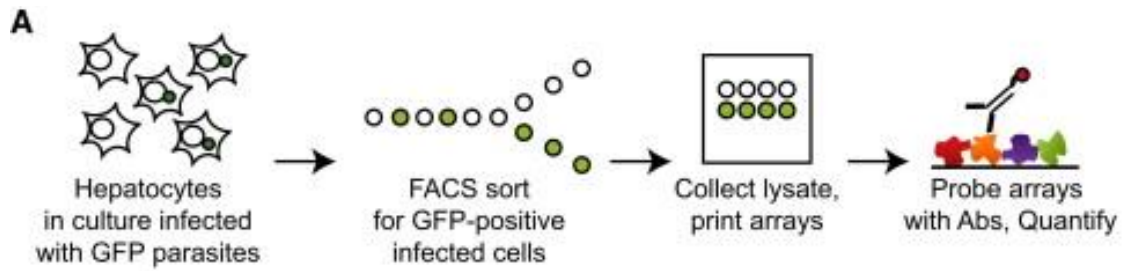
Figure 2.2 (Continued).

protein content. Commercially available secondary antibodies conjugated to near-IR fluorophores were used, after which the slides were washed, dried, and scanned. The slides were then scanned and quantified using MicroVigene by VigeneTech. A schematic of this experimental process is shown in Figure 2.2A. For each antibody, a ratio of upregulation post infection was calculated, as well as a p-value using Student's T-test followed by a Holm-Bonferroni multiple hypothesis test.

Visual inspection of the data indicated that many signaling pathways are perturbed in parasite-infected cells (Figure 2.2B-C, Table 2.3). While the absolute magnitudes for ratio of upregulation are often modest, they can nonetheless be significant as we have previously demonstrated (Sevecka et al., 2011). We were surprised by how many signals displayed a significant deviation from background after infection. Of the 46 antibodies used, we observed a significant upregulation in 22, significant downregulation in 5, and no significant change in 19. Full results are given in Table 2.3. The most striking results included increases in anti-apoptotic phosphorylation signaling in p-Bcl-2 (p=0.001) and p-Akt (p=0.0008 and p=0.000003 for 2 separate antibodies) and pro-survival phosphorylation signaling in mammalian target of rapamycin (mTor) (p=0.000008) and Retinoblastoma (Rb) (p=0.003). Further, we observed decreased phosphorylation in p53 at S15 (p=0.0004) and pro-apoptotic Bad (p=0.001and 0.0002 for 2 separate antibodies at S112 and S136, respectively).

These results, when taken as a group, seem to suggest a generally pro-survival network of signaling events that prevent the host from activating apoptosis in response to infection. In particular, malarial infection of hepatocytes causes cells to increase by 1000-fold in volume, which we would expect to greatly upregulate stress signaling through p53 phosphorylation on S15 (Astle et al., 2012). The observation that p53 S15 phosphorylation is actually lower than

baseline during infection strongly suggests active intervention by the parasite. The increases in activation in Akt and Bcl-2 coupled with the decrease in active Bad indicate a multifaceted, coordinated survival response. The increase in mTor signaling suggests protection against autophagy, which has been reported as a host mechanism to break down parasites in at least one other context (Luckhart et al., 2013). Activation of Rb suggests proliferative signaling which may stimulate synthesis of nucleotides and raw materials needed for parasite proliferation.

Given the results of our preliminary screen, we then sought to confirm the hits with secondary validation using immunoblotting. We first examined the Akt results, noting that both antibodies had been among the most robust in HepG2 and other cell lines (Luckert et al., 2012). Encouragingly, all Akt/mTor pathway antibodies showed significantly positive results (Figure 2.3C). We created sufficient lysate to perform immunoblotting and test these and other statistically significant hits. First, we addressed biological reproducibility and scalability of small magntiudes of upregulation (Figure 2.3A-B). We found that of the antibodies that detect total p53 used on lysate microarray, one (CST 9282) was reproducibly downregulated on immunoblots, therefore we conclude that p53 total protein is downregulated in response to infection. We also found that both Bad pS112 antibodies used in the screen produced reproducible signal on immunoblots, and that Bad phosphorylation was downregulated in response to infection.

We were particularly interested in the downregulation of p53, so we investigated it in more detail. We wanted to estimate the level to which p53 levels were lower after infection, but because the p53 levels in uninfected cells were close to the minimum detection limit in immunoblots, we were unable to directly interpolate with a dilution curve. Instead, we generated

Figure 2.3 (Next Page). Biological Reproducibility of Lysate Microarray Data, and Selected Subsets Broken Down by Signaling Pathway. (A and B) Data obtained from 2 biological replicates of infected and uninfected cells on protein lysate microarrays. Signal from antibodies that recognize total p53 (A) or Bad pS112 (B) are shown. (C) Graph representing the ratio of infected (GFP-positive) cells to uninfected (GFP-negative) cells for signals obtained, plotted against the log of the p-value obtained. Each point represents a single antibody of the Akt/mTor pathway. Only antibodies which demonstrate significant differences in signal between infected and uninfected cells are represented. (D) Graph representing the ratio of infected (GFP-positive) cells to uninfected (GFP-negative) cells for signals obtained, plotted against the log of the p-value obtained. Each point represents a single antibody against total or phosphorylated p53. Only antibodies which demonstrate significant differences in signal between infected and uninfected cells are represented. (E) Graph representing the ratio of infected (GFP-positive) cells to uninfected (GFP-negative) cells for signals obtained, plotted against the log of the p-value obtained. Each point represents a single antibody of the Bcl-2 family. Only antibodies which demonstrate significant differences in signal between infected and uninfected cells are represented. Reproduced from Kaushansky et al. (2013) with permission.
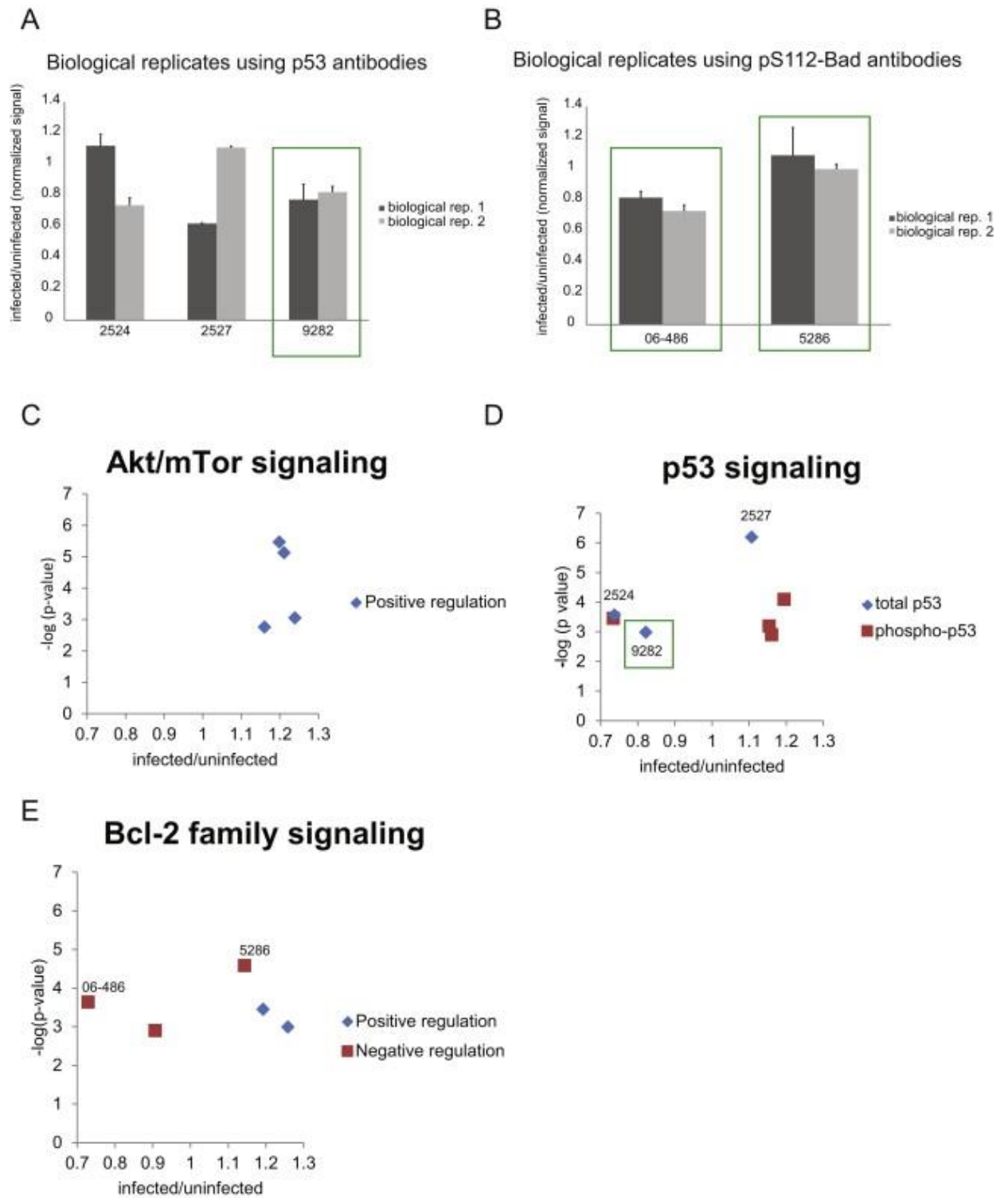
Figure 2.3 (Continued).

71

cellular lysates with varying p53 levels using multiple doses of Mdm2 inhibitor nutlin-3. We found that the signals obtained by lysate microarray and immunoblots were tightly linearly correlated, and using this relationship we estimate that a lysate overexpression ratio of 0.82 corresponds to a 68% decrease in p53 protein level (Figure 2.4B). It is also noteworthy that total levels of Mdm2, p53's cognate ubiquitin ligase, was observed to be significantly upregulated (p=0.005) in response to infection, suggesting a mechanism by which *Plasmodium* might regulate p53 levels.

We also investigated the apoptotic pathway because 2 of the 5 significantly downregulated signals were pro-apoptotic phosphorylated Bad, while the second highest significantly upregulated signal was its antagonist Bcl-2. Visual inspection of the Bcl-2 family subset of lysate microarray data indicated a strongly antiapoptotic signature (Figure 2.3E). Two of the three antibodies monitoring Bad phosphorylation (on S112 and S136 respectively) showed statistically significant differences after infection after Holm-Benferroni multiple hypothesis testing, while the other showed an increase in p-Bad (S112). To disentangle this discrepancy, and because p53 has been shown to regulate transcription of both Bcl-2 and Bad, we measured Bad and Bcl-2 transcript levels. Quantitative PCR revealed that Bad transcript levels were strongly downregulated after infection (p=0.0011) (Figure 2.4C), while Bcl-2 levels were strongly upregulated (p=0.05) (Figure 2.5D). We conclude from these data that *Plasmodium* infection causes downregulation of apoptosis in the host both by regulating transcription and post-translational modification.
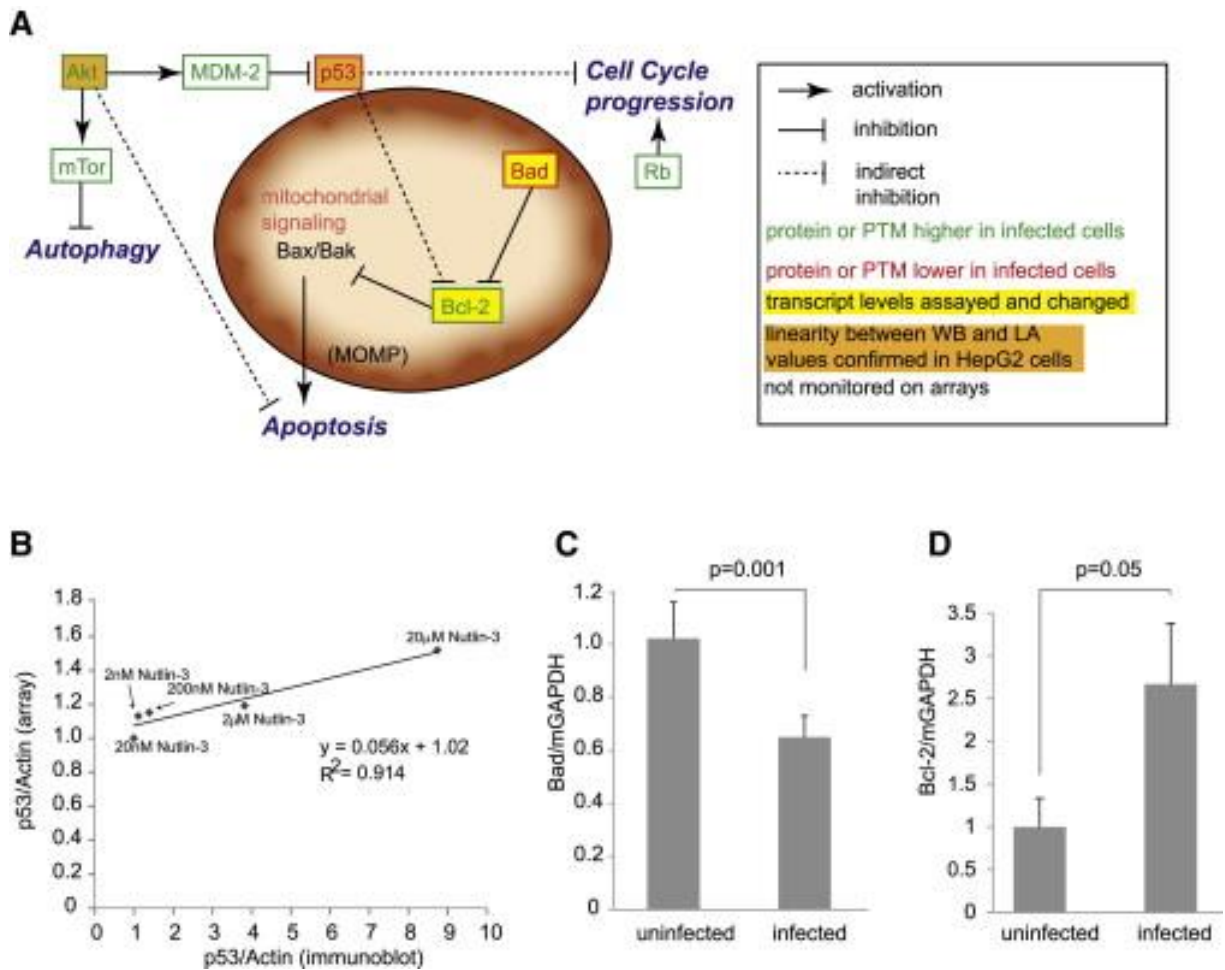
Figure 2.4. Key Host Signaling Pathways in *Plasmodium* Infected Hepatocytes and Linearity of Lysate Microarray Data. (A) Schematic showing the connectivity between host proteins significantly perturbed in liver-stage infected cells. Proteins for which total level or posttranslational modifications are increased in infected cells are shown in green, decreased levels in red. Select antibodies tested demonstrating a linear relationship between immunoblotting (western blotting [WB]) and lysate array (LA) are colored orange. Proteins for which transcripts where tested and changed are colored yellow. (B) Demonstration that total p53 antibody (#9282) produces a linear relationship for data obtained using western blotting and lysate array. Data were fit using a linear regression. (C) Quantitative PCR showing that transcript levels of Bad are decreased in infected hepatocytes. (D) Transcript levels of Bcl-2 are elevated in infected hepatocytes. Error bars represent SD of 3 biological replicates. Reproduced from Kaushansky et al. (2013) with permission.

Figure 2.5 (Next Page). Transgenic Mice and Pharmacological Perturbation Confirm a Critical Role for Host p53 in Liver-Stage Infection. (A) Mice with an additional copy of p53 (super-p53 mice) (n = 13), without p53 (p53 KO mice) (n = 7), or wild-type C57BL/6 mice (n = 20) were infected with 100,000 *P. yoelii* sporozoites. Liver-stage burden was monitored 42–44 hr after infection using quantitative reverse-transcription PCR. Parasite burden was significantly reduced in super-p53 mice (p = 0.004) and significantly elevated in p53 KO mice (p = 0.04). (B–D) p53 levels increase in response to 48 hr Nutlin-3 treatment, as demonstrated by western blot using an anti-p53 antibody (B). Nutlin-3 treatment (20 μM) 24 hr before and during infection (pre and post) dramatically reduces liver-stage burden of *P. yoelii* (C, middle) and *P. berghei* (D, middle). When treatment is applied beginning at time of infection and continuing until 24 hr after infection (post), liver-stage burden is also reduced, albeit less substantially for both *P. yoelii* (C, right) and *P. berghei* parasites (D, right). All liver stages were quantified 24 hr post infection in HepG2 cells. Error bars represent SD between 3 biological replicates. (E) To monitor the effects of Nutlin-3 on *P. yoelii* (Py) sporozoite infection of HepG2 cells, cells were trypsinized 90 min post infection, fixed, stained with an antibody to CSP, and subjected to flow cytometric analysis. Wells that were not infected with sporozoites were used as a control. Error bars represent SD of 3 biological replicates. (F and G) Nutlin-3 treatment dramatically reduces liver-stage burden in mice. A total of 50 mg/kg Nutlin-3 was administered once daily for 2 days to BALB/cJ mice. At the time of the last administration of Nutlin-3, mice were infected with 50,000 *P. yoelii* sporozoites. Livers were removed at 24 hr (F) or 44 hr (G) post infection, and parasite 18S ribosomal RNA was assessed by quantitative real-time PCR. Signal was normalized to mouse GAPDH. For in vivo experiments, the mean is represented by a horizontal line, and the level of Py18S/GAPDH is shown for each individual mouse. Reproduced from Kaushansky et al. (2013) with permission.
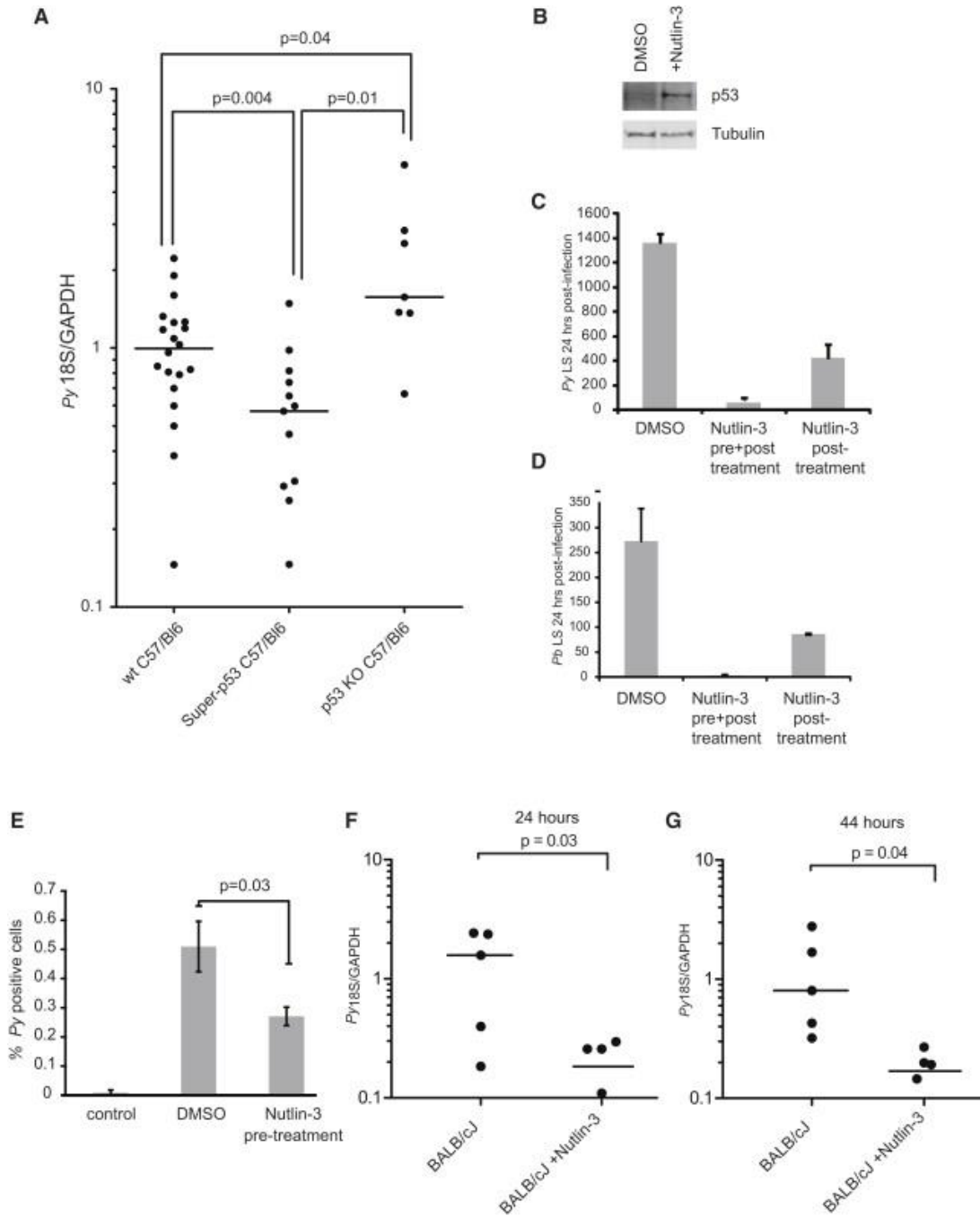
Figure 2.5 (Continued).

2.2.3. Investigation of *Plasmodium* modulation of p53 in mouse liver

Having established that *Plasmodium* infection in cell culture affects p53 and apoptotic signaling, we then investigated their effects in a host liver. To do this, we used two strains of transgenic mice: a "super-p53 mice" that carries an additional genomic copy of p53 under its endogenous promoter (García-Cao et al., 2002), and mice that lack p53 entirely ("p53 KO mice") (Jacks et al., 1994). Super-53 mice overexpress p53 at approximately 2-fold above C57BL/6 controls. We injected mice from all three strains and compared their susceptibilities to liver-stage infection (Figure 2.5A). We found that p53 status was a strong determinant of liver-stage burden: the KO mice carried a significantly higher parasite burden than wt mice, which in turn carried a significantly higher parasite burden than super-p53 mice. This is consistent with our lysate microarray findings that liver-stage modulation of p53 may be required for the parasite life cycle.

Having established that a transgenic increase in background p53 expression is correlated with decreased susceptibility to malaria parasite, we next asked if pharmacological intervention could increase host defenses by increasing p53 levels. Nutlin-3 is a drug under clinical development for multiple cancer indications that increases intracellular p53 levels by inhibiting the p53-Mdm2 interaction (Brown et al., 2009; Wang et al., 2011). Inhibition of the p53-Mdm2 interaction prevents p53 ubiquitinylation and degradation, increasing its intracellular levels. Nutlin-3 thus acts on cancer cells by increasing p53 levels and causing growth arrest and apoptosis, and is highly selective for tumor cells *in vivo* (Vassilev et al., 2004). Treating HepG2 cells with 20 μM Nutlin-3 for 24 hours efficiently increased background levels of p53 (Figure 2.5B). Compared with untreated controls, HepG2 cells that were concomitantly treated with 20 μM Nutlin-3 for 24 hours at time of infection had greatly reduced parasite burden at 24 hours

post infection. This resistance was further enhanced if the cells were pre-treated with 20 µM Nutlin-3 for 24 hours in addition to cotreatment during the infection. This resistance phenotype was observed after infection with both *P. yoelli* and *P. berghei* (Figure 2.5C-D). We also wondered if increased intracellular levels of p53 increased resistance to infection, or if those cells that were infected were able to commit apoptosis. By observing Nutlin-3 pretreated cells at an early time point after infection (90 min), we found that significantly fewer host cells were infected (p=0.03) (Figure 2.5E). In order to extend our findings in cell cultures to whole organisms, we pretreated BALB/cJ mice once daily for 2 days with 50mg/kg Nutlin-3, then infected each mouse with 5×10^4 *P. yoelli*. The mice were sacrificed at 24 or 44 hours, and at both time points the liver-stage burden was significantly lower in the Nutlin-3 treated group.

The data presented in this section, taken together, show that increased intracellular p53 levels render host cells more resistant to *Plasmodium* infection, and that treatment of both cells and mice with Nutlin-3 can greatly reduce parasite burden post-infection.

2.3.Conclusions

In the Western world, infectious diseases of poor sanitation or of the tropics are sometimes ignored because they are not endemic in wealthy countries. Malaria is one such disease that currently critically endangers millions in tropical regions, but if global climate change continues at present rates, may eventually become endemic in the United States (Rogers and Randolph, 2000). Given the current threat of malarial drug resistance forcing a return to a pre-antimicrobial era, we must redouble our efforts to find novel treatments for malaria.

We performed a reverse screen for host proteins that were altered in liver-stage malarial infection. Our screen focused on known apoptotic and related cancer pathways, and we were able to identify several pathways that appeared to be significantly modulated by *Plasmodium* infection. Notably, Bcl-2/Bad signaling was modified in such a way as to inhibit apoptosis, Akt/mTor were activated to increase survival signaling and prevent autophagy, and p53 levels were decreased to prevent apoptotic and stress signaling. We selected the p53 pathway for deeper inspection, but we suspect potentially fruitful avenues of attack exist in the apoptosis and Akt pathways, as both have previously been implicated in liver-stage infection (Leirião et al., 2005; van de Sand et al., 2005). This outside confirmation of our findings gives us confidence in our results and also suggests that our approach could be broadened to other pathways in a more global search for other changes that the parasite makes in host signaling.

The p53 pathway has been extensively studied in the context of cancer signaling, but very little is known about its role in malarial infection. We demonstrate that p53 is specifically targeted by the parasite for downregulation, and that this repression is critical for optimal parasite proliferation. By using a transgenic mouse overexpressing p53 or pharmacologically stimulating p53 buildup using Nutlin-3, we were able to show that counteracting this repression

significantly and dramatically increases the host's defenses against infection and parasite proliferation. It is unknown at this time if there is any connection to p53's role in the cell cycle or if this is strictly due to p53's roles in stress response and apoptosis. We did not address which functions of p53 are required for malarial repression, for example, if transcriptional activity is required. However, because infection and parasite proliferation are temporally separate steps in the parasite liver stage, we speculate that p53 likely interferes with the parasite life cycle at multiple stages.

Our work is unique because it identifies a host signaling molecule that, in cell culture and in mice, can be drugged to great effect in reducing liver-stage parasite burden. Not only do we expect this treatment to have a palliative effect on the patient's health, this approach has great potential as a prophylactic treatment, an especially exciting prospect considering the recent disappointing results in vaccine trials (Olotu et al., 2013). Given that genetically attenuated parasites that do not proceed past liver-stage have been shown to provoke long-term immunity (Doolan and Hoffman, 2000; Krzych et al., 2012), we feel if Nutlin-3 may represent a bona fide vaccine in regions of the world where malaria is endemic. That possibility alone should be reason for excitement in the search for host-targeted malaria drugs.

Finally, to our knowledge, this work represents the first published application of lysate microarray technology to infectious disease. Liver-stage malaria is a particularly difficult problem because of its low infectivity rate coupled with the need to freshly prepare parasite from mosquito salivary glands. By exploiting a FACS-based technique combined with a GFP-tagged parasite, we were able to separate the infected population from the much more numerous uninfected background, and were thus able to obtain enough biological sample to perform lysate

microarrays. We hope that our example will inspire future use of the technology to explore other infectious diseases that are also critically in need of host-targeted antibiotic discovery.

2.4. Tables

Table 2.2 – Full list of antibodies used in preliminary screen for use in *Plasmodium* lysates			
Protein of Interest	**Product #**	**Species**	**Company**
HSP70	sc-4872	M	Santa Cruz
U154		R	Custom
CSP Py		M	Custom
MET	sc-10	R	Santa Cruz
p-MET (Y1349)	3133	R	Cell Signaling
p-Akt1/2/3 (S473)	9271	R	Cell Signaling
p-Akt1/2/3 (S473)	4058P	R	Cell Signaling
p-mTOR (S2448)	2971	R	Cell Signaling
p-mTOR (S2481)	2974	R	Cell Signaling
p-p90RSK (S380)	9341S	R	Cell Signaling
p-NF-κB p65 (S536)	3033	R	Cell Signaling
p-NF-κB p105 (S933)	4806	R	Cell Signaling
p53	2524	M	Cell Signaling
p53	2527	R	Cell Signaling
p53	9282	R	Cell Signaling
p-p53 (pS6)	9285	R	Cell Signaling
p-p53 (pS9)	9288	R	Cell Signaling
p-p53 (S15)	9284	R	Cell Signaling
p-p53 (S15)	9286	M	Cell Signaling
p-p53 (pS20)	9287	R	Cell Signaling
p-p53 (pS37)	9289	R	Cell Signaling
p-p53 (S46)	2521	R	Cell Signaling
p-p53 (T81)	2676	R	Cell Signaling
p-p53 (S392)	9281	R	Cell Signaling
p-MDM2 (S166)	3521	R	Cell Signaling
p-cdc2 (Y15)	9111	R	Cell Signaling

Table 2.2. List of antibodies used in pilot experiment to test validity of lysate microarray approach to measure signaling differences that result from *Plasmodium* infection. All antibodies except for those in red were previously validated for use in HepG2 cells. Antibodies in red were not previously validated antibodies targeted against parasite proteins, generously provided by the Kappe lab. (Continued on next page.)

Table 2.2 – Full list of antibodies used in preliminary screen for use in *Plasmodium* lysates (Continued)			
Protein of Interest	**Product #**	**Species**	**Company**
p-cdc2 (Y15)	4539	R	Cell Signaling
p-Rb (S795)	9301	R	Cell Signaling
p-Rb (S807/S811)	9308	R	Cell Signaling
Cleaved Caspase 3 (D175)	9661	R	Cell Signaling
Cleaved Caspase 3 (D175)	9664	R	Cell Signaling
Cleaved PARP (Asp214)	9541	R	Cell Signaling
p-BCL-2 (T56)	2875	R	Cell Signaling
p-BCL-2 (S70)	2827	R	Cell Signaling
p-BAD (S112)	5284	R	Cell Signaling
CSP pb		M	Custom
p-BAD (S112)	06-853	R	Upstate
p-BAD (S136)	5286	R	Cell Signaling
p-c-Cbl (Y774)	3555	R	Cell Signaling
p-BAD (S136)	06-846	R	Upstate
FLIP	3210	R	Cell Signaling
Fas	4233	R	Cell Signaling
FADD	2782	R	Cell Signaling
p-glycogen synthase (S641)	3891	R	Cell Signaling
p-c-Cbl (Y731)	3554	R	Cell Signaling
Beclin-1	3495	R	Cell Signaling
LC3A	4599	R	Cell Signaling
LC3B	3868	R	Cell Signaling
Atg5	8540	R	Cell Signaling
Atg12	4180	R	Cell Signaling
Atg7	2631	R	Cell Signaling
Atg3	3415	R	Cell Signaling

Table 2.2. (Continued) List of antibodies used in pilot experiment to test validity of lysate microarray approach to measure signaling differences that result from *Plasmodium* infection. All antibodies except for those in red were previously validated for use in HepG2 cells. Antibodies in red were not previously validated antibodies targeted against parasite proteins, generously provided by the Kappe lab.

Table 2.3 – Full list of results from Lysate microarray Profiling of Host Signaling during *Plasmodium* infection						
Protein of Interest	**product #**	**Upregulation**	**Std**	**T-Test**	**H-B value**	**H-B pass?**
Significantly Upregulated, passes Holm Benferroni						
p-Rb (S807/S811)	9308	1.39	0.15	2.21E-03	2.38E-03	yes
p-BCL-2 (S70)	2827	1.26	0.05	1.01E-03	1.79E-03	yes
p-Akt1/2/3 (S473)	9271	1.24	0.06	8.85E-04	1.72E-03	yes
p-mTOR (S2448)	2971	1.21	0.03	7.45E-06	1.14E-03	yes
p-Akt1/2/3 (S473)	4058P	1.20	0.03	3.43E-06	1.11E-03	yes
p-p53 (pS37)	9289	1.19	0.04	8.01E-05	1.28E-03	yes
p-BCL-2 (T56)	2875	1.19	0.03	3.55E-04	1.47E-03	yes
Atg7	2631	1.17	0.02	2.13E-05	1.16E-03	yes
p-p53 (pS9)	9288	1.16	0.05	1.27E-03	2.00E-03	yes
p-mTOR (S2481)	2974	1.16	0.06	1.75E-03	2.27E-03	yes
p-cdc2 (Y15)	9111	1.16	0.03	3.36E-05	1.22E-03	yes
p-p53 (S392)	9281	1.15	0.03	6.42E-04	1.67E-03	yes
Atg3	3415	1.15	0.03	2.91E-04	1.39E-03	yes
p-c-Cbl (Y774)	3555	1.15	0.03	4.12E-04	1.52E-03	yes
Cleaved Caspase 3 (D175)	9661	1.14	0.03	2.60E-05	1.19E-03	yes
p-BAD (S112)	5284	1.14	0.03	7.64E-05	1.25E-03	yes
p-cdc2 (Y15)	4539	1.13	0.04	5.36E-04	1.61E-03	yes
p53	2527	1.11	0.01	6.32E-07	1.09E-03	yes
FADD	2782	1.09	0.02	1.53E-03	2.17E-03	yes
p-NF-κB p65 (S536)	3033P	1.08	0.02	5.14E-04	1.56E-03	yes
p-GYS2 (S641)	3891	1.07	0.02	1.49E-03	2.08E-03	yes

Table 2.3. Protein microarrays were printed using whole cell extracts from FACS sorted infected and uninfected HepG2 cells, and probed using antibodies targeted to signaling molecules in the host cell. Quantified fluorescent signal was calculated as a ratio of the signals from infected to uninfected cells, normalized for actin for spotting variation. Significance was calculated by t-test and the Holm-Benferroni method for multiple hypothesis testing using the overexpression ratio and propagated error. Data shown is representative of three independent experiments.

Table 2.3 – Full list of results from Lysate microarray Profiling of Host Signaling during *Plasmodium* infection (Continued)						
Protein of Interest	product #	Upregulation	Std	T-Test	H-B value	H-B pass?
Significantly Downregulated, passes Holm Benferroni						
p-BAD (S112)	06-853	0.91	0.03	1.25E-03	1.92E-03	yes
p53	9282	0.82	0.04	1.04E-03	1.85E-03	yes
p53	2524	0.74	0.05	2.72E-04	1.35E-03	yes
p-p53 (S15)	9286	0.73	0.09	3.51E-04	1.43E-03	yes
p-BAD (S136)	06-846	0.73	0.04	2.28E-04	1.32E-03	yes
Non-statistically significant data and/or data does not pass Holm Benferroni						
p-p53 (S15)	9284	1.33	0.40	1.06E-01	5.00E-03	no
Atg12	4180	1.15	0.04	4.33E-03	2.94E-03	no
p-p90RSK (S380)	9341S	1.14	0.07	1.45E-02	3.85E-03	no
Fas	4233	1.12	0.06	6.27E-03	3.33E-03	no
Cleaved Caspase 3 (D175)	9664	1.11	0.03	4.20E-03	2.78E-03	no
p-p53 (T81)	2676	1.10	0.03	2.90E-03	2.50E-03	no
p-p53 (S46)	2521	1.08	0.03	4.03E-03	2.63E-03	no
Beclin-1	3495	1.08	0.05	3.28E-02	4.17E-03	no
p-c-Cbl (Y731)	3554	1.07	0.05	5.66E-02	4.55E-03	no
Atg5	8540	1.07	0.08	1.70E-01	7.14E-03	no
p-NF-κB p105 (S933)	4806P	1.06	0.06	1.50E-01	6.25E-03	no
Cleaved PARP (Asp214)	9541	1.06	0.02	9.39E-03	3.57E-03	no
p-MDM2 (S166)	3521	1.05	0.02	5.00E-03	3.13E-03	no
p-p53 (pS6)	9285	1.05	0.05	1.22E-01	5.56E-03	no
FLIP	3210	1.05	0.06	2.03E-01	8.33E-03	no
p-Rb (S795)	9301	1.04	0.17	6.60E-01	1.67E-02	no
p-p53 (pS20)	9287	1.03	0.23	7.90E-01	2.50E-02	no
LC3B	3868	1.02	0.08	6.59E-01	1.25E-02	no
LC3A	4599	1.01	0.03	2.89E-01	1.00E-02	no
p-BAD (S136)	5286	1.00	0.03	8.87E-01	5.00E-02	no

Table 2.3. (Continued) Protein microarrays were printed using whole cell extracts from FACS sorted infected and uninfected HepG2 cells, and probed using antibodies targeted to signaling molecules in the host cell. Quantified fluorescent signal was calculated as a ratio of the signals from infected to uninfected cells, normalized for actin for spotting variation. Significance was calculated by t-test and the Holm-Benferroni method for multiple hypothesis testing using the overexpression ratio and propagated error. Data shown is representative of three independent experiments.

2.5. Experimental Methods

Antibody Reagents

Pan and phospho-specific antibodies for signaling proteins were purchased from Abcam (Cambridge, MA), BD Biosciences (San Jose, CA), Cell Signaling Technology (Beverly, MA), Santa Cruz Biotechnology (Santa Cruz, CA), and Upstate (Charlotteville, VA). Mouse monoclonal anti-β-actin antibody (clone AC-15) was purchased from Sigma-Aldrich (Saint Louis, MO), rabbit monoclonal anti-β-actin antibody was catalog # 4970 (Cell Signaling Technology (Beverly, MA)). Secondary detection antibodies were purchased from Li-Cor Biosciences (Lincoln, NE).

Cell Culture

HepG2 cells used in this study were a generous gift from INSERM-TRANSFERT and maintained in DMEM media (See Appendix A) and split 1-2 times weekly. Where indicated, Nutlin-3 was used at 20 μM in DMSO.

Mosquito Rearing and Sporozoite Production

For *P. berghei* and *P. yoelli* sporozoite production, female Swiss- Swiss Webster (SW) mice (Harlan (Indianapolis, IN)) were injected with blood stage P. yoelii (17XNL) or P. berghei (ANKA) parasites to begin the growth cycle. Animal handling was conducted according to Institutional Animal Care and Use Committee-approved protocols. We used infected mice to feed female *A. stephensi* mosquitoes after gametocyte exflagellation was observed. For all *P. yoelii* experiments we isolated salivary gland sporozoites according to standard procedures at days 14 or 15 post blood meal. We isolated *P. berghei* sporozoites 20 days post-infection. For

each experiment, salivary glands were isolated in parallel in order to ensure sporozoites were extracted from salivary glands under the same conditions.

Isolation of PyGFP-Infected HepG2 Cells

Cells were grown as described above. 5×10^6 cells were infected with 2×10^6 *P. yoelli* transgenic GFP-expressing parasites (Tarun et al., 2006). Cells were detached with 0.25% Trypsin-EDTA and resuspended in DMEM complete media with 5 mM EDTA. Cells were passed through a cell strainer to prepare for FACS. Flow cytometric analysis and cell sorting of PyGFP-infected hepatocytes were carried out using a Cytopeia Influx Cell Sorter using the Spigot Operating Software Version 5.0.3.1 (Cytopeia).

Microarray Fabrication

Cells were lysed in 2% SDS lysis buffer (see Appendix A) and stored at -80°C and were not filtered, unlike previous experiments. Custom arrays were printed in-house using an Aushon 2470 arrayer (Aushon Biosystems (Billerica, MA)) on 16-pad nitrocellulose-coated glass slides (Grace Biolabs (Bend, OR)). Lysates were printed at 333 μm spacing using steel solid 110 μm pins, with an average feature diameter of 170 μm.

For the initial screen, lysates were printed in technical duplicates, and for the later experiment, lysates were printed in quadruplicate technical replicates. Slides were stored in a dry, dark, room temperature environment until probing. Probing was according to previous protocol (Sevecka et al., 2011).

Analysis of Microarray Data

Signal intensities from target proteins were normalized using the β-actin signal intensities from the same spot to normalize for spotting variation. Data from quadruplicate spots were averaged, and the ratio of signal from GFP-positive samples to GFP-negative samples computed for each target protein. For each antibody specific to a hepatocyte protein measured, we calculated a value according to Equation 2.1.

$$x = \frac{\text{signal(i)}/\beta\text{-actin(i)}}{\text{signal(u)}/\beta\text{-actin(u)}}$$

Equation 2.1. Calculation for upregulation of signaling after malaria infection. "Signal" refers to fluorescence measured from experimental antibody, "β-actin" refers to fluorescence measured from β-actin antibody, "i" refers to infected samples, "u" refers to uninfected samples. Statistical significance was calculated using a 2-tailed t-test with the standard error against a ratio of 1 (unchanged after infection).

Quantification of Liver Stages by FACS

Cells were cultured as described above. A total of 2×10^5 HepG2 cells were plated in each well of a 24-well plate and infected with 5×10^4 *P. yoelii* sporozoites. Cells were treated with or without Nutlin-3 as described above. At the desired time point, cells were harvested and stained as described previously by (Luckert et al., 2012). All experimental conditions were tested in biological triplicate. All data are representative of three independent experiments.

***In Vivo* Nutlin-3 Experiments**

A total of 26 BALB/cJ mice (Jackson Lab (Bar Harbor, ME)) were treated with either vehicle control or 50 mg/kg of Nutlin-3 once daily for 2 days. On the second day of treatment, mice were injected with 5×10^4 P. yoelii sporozoites. Livers were excised from mice at either 24

or 44 hr after infection. Animal handling was conducted according to Institutional Animal Care and Use Committee-approved protocols.

Super p53 and p53 KO Experiments

A total of 20 male C57BL/6 (Jackson), 13 C57BL/6-super-p53, and 7 C57BL/6-p53-KO (Jackson Lab (Bar Harbor, ME)) mice were injected with 105 P. yoelii-GFP-luciferase sporozoites. At 42–44 hr post-infection, livers were excised from mice and lysed with TRIzol reagent (Invitrogen (Carlsbad, CA)). Animal handling was conducted according to Institutional Animal Care and Use Committee-approved protocols.

Quantification of Liver Burden by Real-Time qRT-PCR

Total RNA was extracted using TRIzol reagent (Invitrogen (Carlsbad, CA)). cDNA synthesis and qRT-PCR was performed using the Super Script III Platinum two-step qRT-PCR kit according to the manufacturer's instructions. All PCR amplification cycles were performed at 95°C for 30 s for DNA denaturation, and 60°C for 4 min for primer annealing and DNA strands extension. Parasite ribosomal 18S RNA was amplified using primers with sequences: 5'GGGGATTGGTTTTGACGTTTTTGCG3' and 5'AAGCATTAAATAAAGCGAATACATCCTTAT3'. Mouse GAPDH was amplified using sequences 5'CCTCAACTACATGGTTTACAT3' and 5'GCTCCTGGAAGATGGTGATG3'.

Works Cited

Annoura, T., Ploemen, I.H., van Schaijk, B.C., Sajid, M., Vos, M.W., van Gemert, G.J., Chevalley-Maurel, S., Franke-Fayard, B.M., Hermsen, C.C., Gego, A.*, et al.* (2012). Assessing the adequacy of attenuation of genetically modified malaria parasite vaccine candidates. Vaccine *30*, 2662-2670.

Astle, M.V., Hannan, K.M., Ng, P.Y., Lee, R.S., George, A.J., Hsu, A.K., Haupt, Y., Hannan, R.D., and Pearson, R.B. (2012). AKT induces senescence in human cells via mTORC1 and p53 in the absence of DNA damage: implications for targeting mTOR during malignancy. Oncogene *31*, 1949-1962.

Brown, C.J., Lain, S., Verma, C.S., Fersht, A.R., and Lane, D.P. (2009). Awakening guardian angels: drugging the p53 pathway. Nature reviews Cancer *9*, 862-873.

Butler, N.S., Schmidt, N.W., Vaughan, A.M., Aly, A.S., Kappe, S.H., and Harty, J.T. (2011). Superior antimalarial immunity after vaccination with late liver stage-arresting genetically attenuated parasites. Cell host & microbe *9*, 451-462.

Carrolo, M., Giordano, S., Cabrita-Santos, L., Corso, S., Vigario, A.M., Silva, S., Leiriao, P., Carapau, D., Armas-Portela, R., Comoglio, P.M.*, et al.* (2003). Hepatocyte growth factor and its receptor are required for malaria infection. Nature medicine *9*, 1363-1369.

Doolan, D.L., and Hoffman, S.L. (2000). The complexity of protective immunity against liver-stage malaria. J Immunol *165*, 1453-1462.

García-Cao, I., García-Cao, M., Martín-Caballero, J., Criado, L.M., Klatt, P., Flores, J.M., Weill, J.C., Blasco, M.A., and Serrano, M. (2002). "Super p53" mice exhibit enhanced DNA damage response, are tumor resistant and age normally. EMBO J *21*, 6225-6235.

Ishino, T., Chinzei, Y., and Yuda, M. (2005). A Plasmodium sporozoite protein with a membrane attack complex domain is required for breaching the liver sinusoidal cell layer prior to hepatocyte infection. Cellular microbiology *7*, 199-208.

Jacks, T., Remington, L., Williams, B.O., Schmitt, E.M., Halachmi, S., Bronson, R.T., and Weinberg, R.A. (1994). Tumor spectrum analysis in p53-mutant mice. Curr Biol *4*, 1-7.

Kaushansky, A., Ye, A.S., Austin, L.S., Mikolajczak, S.A., Vaughan, A.M., Camargo, N., Metzger, P.G., Douglass, A.N., Macbeath, G., and Kappe, S.H. (2013). Suppression of Host p53 Is Critical for Plasmodium Liver-Stage Infection. Cell reports.

Krzych, U., Dalai, S., Zarling, S., and Pichugin, A. (2012). Memory CD8 T cells specific for plasmodia liver-stage antigens maintain protracted protection against malaria. Frontiers in immunology *3*, 370.

Kyaw, M.P., Nyunt, M.H., Chit, K., Aye, M.M., Aye, K.H., Lindegardh, N., Tarning, J., Imwong, M., Jacob, C.G., Rasmussen, C.*, et al.* (2013). Reduced Susceptibility of Plasmodium falciparum to Artesunate in Southern Myanmar. PloS one *8*, e57689.

Leirião, P., Albuquerque, S.S., Corso, S., van Gemert, G.J., Sauerwein, R.W., Rodriguez, A., Giordano, S., and Mota, M.M. (2005). HGF/MET signalling protects Plasmodium-infected host cells from apoptosis. Cell Microbiol *7*, 603-609.

Luckert, K., Gujral, T.S., Chan, M., Sevecka, M., Joos, T.O., Sorger, P.K., Macbeath, G., and Potz, O. (2012). A dual array-based approach to assess the abundance and posttranslational modification state of signaling proteins. Science signaling *5*, pl1.

Luckhart, S., Giulivi, C., Drexler, A.L., Antonova-Koch, Y., Sakaguchi, D., Napoli, E., Wong, S., Price, M.S., Eigenheer, R., Phinney, B.S.*, et al.* (2013). Sustained activation of Akt elicits mitochondrial dysfunction to block Plasmodium falciparum infection in the mosquito host. PLoS pathogens *9*, e1003180.

Olotu, A., Fegan, G., Wambua, J., Nyangweso, G., Awuondo, K.O., Leach, A., Lievens, M., Leboulleux, D., Njuguna, P., Peshu, N.*, et al.* (2013). Four-year efficacy of RTS,S/AS01E and its interaction with malaria exposure. The New England journal of medicine *368*, 1111-1120.

Rogers, D.J., and Randolph, S.E. (2000). The global spread of malaria in a future, warmer world. Science *289*, 1763-1766.

Sevecka, M., Wolf-Yadlin, A., and G., M. (2011). Lysate microarrays enable high-throughput, quantitative investigations of cellular signaling. Mol Cell Proteomics *10*.

Tarun, A.S., Baer, K., Dumpit, R.F., Gray, S., Lejarcegui, N., Frevert, U., and Kappe, S.H. (2006). Quantitative isolation and in vivo imaging of malaria parasite liver stages. International journal for parasitology *36*, 1283-1293.

Tran, T.M., Li, S., Doumbo, S., Doumtabe, D., Huang, C.Y., Dia, S., Bathily, A., Sangala, J., Kone, Y., Traore, A.*, et al.* (2013). An Intensive Longitudinal Cohort Study of Malian Children and Adults Reveals No Evidence of Acquired Immunity to Plasmodium falciparum Infection. Clin Infect Dis.

van de Sand, C., Horstmann, S., Schmidt, A., Sturm, A., Bolte, S., Krueger, A., Lutgehetmann, M., Pollok, J.M., Libert, C., and Heussler, V.T. (2005). The liver stage of Plasmodium berghei inhibits host cell apoptosis. Molecular microbiology *58*, 731-742.

Vassilev, L.T., Vu, B.T., Graves, B., Carvajal, D., Podlaski, F., Filipovic, Z., Kong, N., Kammlott, U., Lukacs, C., Klein, C.*, et al.* (2004). In vivo activation of the p53 pathway by small-molecule antagonists of MDM2. Science *303*, 844-848.

Vaughan, A.M., Aly, A.S., and Kappe, S.H. (2008). Malaria parasite pre-erythrocytic stage infection: gliding and hiding. Cell host & microbe *4*, 209-218.

Wang, J., Zheng, T., Chen, X., Song, X., Meng, X., Bhatta, N., Pan, S., Jiang, H., and Liu, L. (2011). MDM2 antagonist can inhibit tumor growth in hepatocellular carcinoma with different types of p53 in vitro. Journal of gastroenterology and hepatology *26*, 371-377.

WHO (2013). Malaria Fact Sheet (WHO).

Part 3

Application of Lysate Microarray Technology

For High-Throughput Profiling Of Apoptotic Signaling Networks

3.1. Introduction

Cancer has probably been the most highly studied biological phenomenon in the last 30 years. Much has been learned from studying the myriad biological pathways that promote tumor growth, lending insight into normal as well as diseased metabolism, signaling, and genetics. However, despite the hundreds of billions of dollars and millions of hours spent on research, there are relatively few truly successful treatment options. Our ever-desperate search for the cure for cancer has not been without bright spots, however: we do have a regimen of standard treatments for cancer that includes a large number of chemotherapeutic drugs.

Chemotherapy drugs come in many types, but one of the major classes of chemotherapeutic drugs, like radiation treatment, functions by causing DNA damage indiscriminately in both cancer and normal cells (Lichter and Lawrence, 1995). Much of the machinery involved in the DNA Damage Response (DDR) pathway has become more clearly defined in the last 20 years, and we now know it is intimately tied to cell cycle, damage repair, and cell death (Harper and Elledge, 2007). Indeed, the DDR represents a primary nexus of pro-survival and pro-death signaling that controls cellular fate in large part. Complicating matters, however, are cross-talk interactions with other signaling networks, especially aberrant pro-survival and anti-death signaling in cancer cells.

Even simple networks can lead to highly nonlinear and complex behavior, and our ability to predict network behavior vastly decreases with increasing network complexity. In the case of the DDR, the complexity of the known network is already well beyond our ability to reliably predict cell fate behavior. Our efforts here attempt to understand how in part how multiple input signals are interpreted by the cell, and especially to understand how networks can be "rewired" after drug inhibition (Sachs et al., 2005). We also seek to understand the interplay between growth factor signaling and genotoxic chemotherapy.

92

Breast cancer is the most common cancer worldwide, accounting for 22.9% (excluding non-melanoma skin cancers) of cancers in women in 2008 (IARC, 2008). Many breast cancers have aberrant hormonal and/or growth factor signaling as key drivers of tumor growth, and these pathways often present resistance to treatment (Hanahan and Weinberg, 2000, 2011). Sub-classification of breast cancers by their specific molecular drivers has allowed stratification of targeted therapy and improved patient outcomes dramatically (Schechter et al., 1984; Slamon et al., 1987). Despite these advances, there remains a "garbage pail" classification of so-called triple-negative breast cancers (TNBC), which are those breast cancers that do not express estrogen receptor (ER) or progesterone receptor (PR), nor have an amplification in Her2 oncogene (Perou et al., 2000). Patients with TNBCs tend to respond initially to genotoxic chemotherapy, but also have a worse prognosis and shorter relapse-free survival than patients with other types of breast cancer (Dent et al., 2007). TNBC patients do tend to do well if chemotherapy is successful, but when complete pathologic response is not achieved, prognosis tends to be poor (Abeloff et al., 2008). Hence, there is little room for error in TNBC, and strategies should be developed to enhance the likelihood of success of the initial round of genotoxic chemotherapy.

We were therefore motivated to explore possible drug combinations that might sensitize otherwise recalcitrant TNBC cells to respond more strongly to a dose of chemotherapy. We utilize a systems biology approach of deep pathway analysis utilizing lysate microarrays among other techniques to observe signaling events downstream of drug treatment. Furthermore, we report a critical timing where Epidermal Growth Factor Receptor (EGFR) inhibitors can act as a sensitizer for apoptosis when given in advance of traditional DNA damaging chemotherapy in a subclass of TNBC. We investigate the intracellular signaling that results from inhibition and find that during pretreatment, TNBC cells actively rewire intracellular networks, relieving inhibition on normally

suppressed apoptotic pathways. We believe this discovery has clinical implications and hint at generalizable principles of network behavior.

This work was reproduced with modifications and additions from Lee et al. (2012).

3.2. Results and Discussion

3.2.1. Preliminary Screen for Evidence of Drug Synergy

Signaling pathways are dynamic and can be functionally rewired by exposure to drugs and ligands (Janes et al., 2005; Janes et al., 2008). Furthermore, rewiring is a time-dependent process and cells may take some time to transition between stable states. Therefore, if a TNBC cell is initially recalcitrant to chemotherapy in the absence of treatment, we reasoned that by altering basal signaling by applying an inhibitor, it may be possible to find either a steady state or transition state where the TNBC becomes sensitized to chemotherapy. To this end, we assembled a panel of clinically important genotoxic chemotherapy agents and inhibitors against important oncogenic signaling pathways, and three representative TNBC cell lines, then systematically explored timing combinations to assess for synergy. The drugs selected are clinically useful in other cancers, but have been tried unsuccessfully in TNBC, individually or in combination therapy (Bosch et al., 2010; Winer and Mayer, 2007). For example, EGFR inhibitors in combination with cisplatin had nearly no effect in cell culture (Corkery et al., 2009), while cetuximab addition to patients undergoing carboplatin did not improve outcome (Carey et al., 2012). Despite these failures in and out of the clinic, combinations of drug, dose, and especially timing have not been exhaustively tried. Given the recent advances in understanding network rewiring, we expect that a search for combination therapies should exhaustively explore the possible combinations of all variables for synergies. In this spirit, we performed the systematic screen of stimulus combinations shown in Figure 3.1A.

We selected three cell lines initially as representative of the main classes of breast cancer: hormone sensitive (MCF7), Her2 overexpressing (MDA-MB-453), and triple-negative (BT-20) (Neve et al., 2006). Measuring apoptosis as a readout, we identified a previously unknown
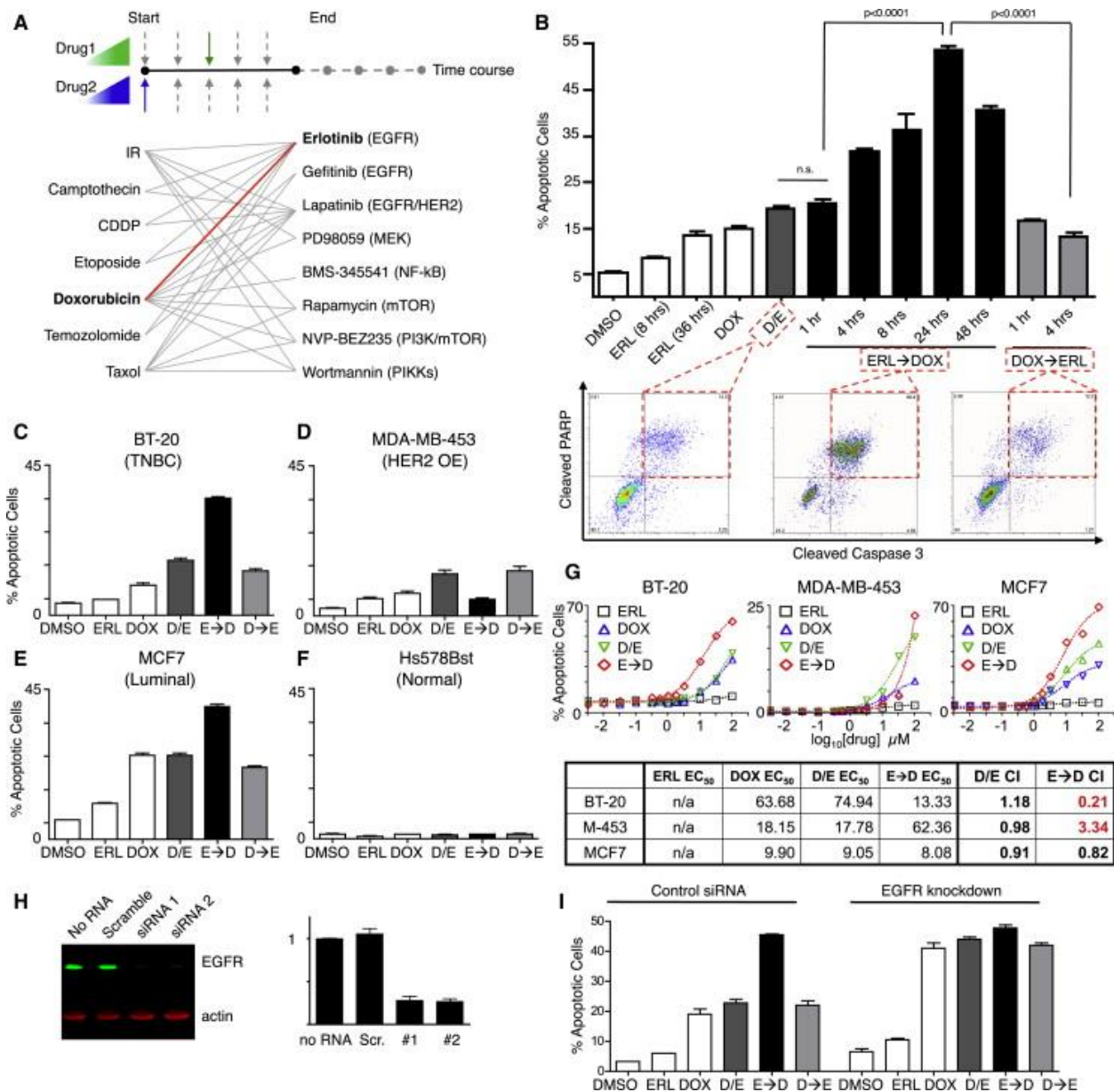
Figure 3.1. A Screen for Novel Combination Treatment Reveals Dosing Schedule-Dependent Efficacy for Killing TNBC Cells. (A) Schematic of combinations tested. Seven genotoxic drugs and eight targeted signaling inhibitors were tested in pair-wise combinations, varying dose, order of presentation, dose duration, and dosing schedule. (B) Apoptosis in BT-20 cells. Cleaved-caspase 3/cleaved-PARP double-positive cells were quantified using flow cytometry (bottom). In cells treated with DMSO, erlotinib (ERL), or doxorubicin (DOX), apoptosis measurements were performed 8 hr after drug exposure or at the indicated times. D/E, ERL→DOX, and

(Figure 3.1 Continued.) DOX→ERL refer to DOX and ERL added at the same time, ERL given at the indicated times before DOX, and DOX given at the indicated times before ERL, respectively. For each, apoptotic measurements were made 8 hr after the addition of DOX. Erlotinib and doxorubicin were used at 10 μM. Mean values ±SD of three independent experiments, each performed in duplicate, are shown (top). (C–F) Apoptosis in different subtypes of breast cancer. Apoptosis was measured as in (B). (D and E) D/E, E→D, and D→E refer to DOX and ERL added at the same time, ERL given 24 hr before DOX, and DOX given 4 hr before ERL, respectively. Data are mean values ±SD of three independent experiments. (G) Dose-response profiles of erlotinib/doxorubicin drug combinations. Apoptosis was measured as in (B). Drugs were added at a 1:1 ratio, and combination index (CI) was calculated according to the Chou-Talalay method. (H) Knockdown of EGFR in BT-20 cells measured 48 hr after addition of the indicated siRNA by immunoblotting (left). EGFR expression relative to ''no RNA'' control is quantified on right. (I) Apoptosis in BT-20 cells ± EGFR knockdown measured as in (B). Scrambled RNAi shown as control. Data shown are the mean ±SD of both siRNAs, each performed in biological duplicate. Reproduced with permission from Lee et al. (2012).

combination of erlotinib and doxorubicin that is highly efficacious and specific for killing BT-20

TNBC cells (Figure 3.1B-E). Erlotinib alone, doxorubicin alone, nor erlotinib/doxorubicin

cotreatment could initiate apoptosis in TNBC cells, in agreement with the published literature.

However, closer inspection revealed that when erlotinib was given at least 4 hours before

doxorubicin, apoptosis was greatly enhanced, with a peak at up to 500% when given 24 hours

before (Figure 3B). The order was critical; when the order was reversed, with doxorubicin given

before erlotinib, apoptosis levels were comparable to either drug given alone or cotreatment. In

order to quantify the level of synergy of the time staggered erlotinib-doxorubicin treatment versus

cotreatment, we used the Chou-Talalay method to calculate a combination index across all cell

types (Figure 3.1G) (Chou and Talalay, 1984). Emphasizing the need for proper matching of

cancer type and treatment regimen, we found that the erlotinib-doxorubicin timing was highly

synergistic for killing BT-20 TNBC cells, highly antagonistic in Her2 overexpressing MB-453

cells, and additive in hormone-sensitive MCF7 cells. All drug combinations tested had little effect on the control line Hs578Bst derived from peripheral breast tissue (Figure 3.1F).

Kinase inhibitors tend to begin their effects within minutes, and erlotinib is no exception. Because the sensitization effect of the E-D timing effect manifests on the time scale of 4 hours, we were wary that it may be due to an off-target or nonspecific effect of erlotinib. To test that the sensitization phenotype is indeed specific to EGFR, we used two small interfering RNAs (siRNAs) directed against EGFR to knock down EGFR (Figure 3.1H). Not only did this treatment increase apoptosis following knockdown in the doxorubicin only treatment to similar levels to the time-staggered treatment without knockdown, there was no further increase when erlotinib was also applied (Figure 3.1I). This result, combined with the fact that other EGFR inhibitors (gefitinib, lapatinib) also display similar timing-sensitization effects with doxorubicin and camptothecin, gives us confidence that 1) the sensitization effect is a specific result of EGFR inhibition, not an off-target effect of erlotinib, 2) the genotoxic effect being amplified is not specific to doxorubicin but may be generalizable, and 3) the sensitization effect is not due to transient acute EGFR inhibition, but rather is due to longer-term effects of chronic inhibition.

3.2.2. Lysate Microarray Antibody Validation Screen for Breast Cancer Panel

We wanted to understand the molecular events that stem from, and effect the differential survival/death phenotype we had observed. Because we wanted to collect signaling information from as many nodes in as many signaling networks as possible, we performed a reverse screen of antibodies tested against lysates from all three cell lines. We designed a set of control conditions, selected such that every node monitored by an antibody is activated in at least one condition. In total, this was a list of 30 control lysates for each cell line. Also included were serial 2-fold dilutions for 5 of these lysates for BT-20 only, for a total of 128 total samples, including all

98

controls. A full list of these lysates is included in Table 3.1. All samples were collected according to established protocol (Sevecka et al., 2011) with modifications to collect apoptotic cells (See Methods Section). These samples were then printed in duplicate onto nitrocellulose-coated glass slides using an Aushon 2470 arrayer and probed with the collection of all available antibodies in the MacBeath and Yaffe labs. In total, this collection numbered 483 antibodies, for a total of 123,648 measurements. Probing was carried out as previously described, with each array being exposed to a unique primary antibody and a standardization antibody (Sevecka et al., 2011). Image quantification was performed using Array-Pro by MediaCybernetics and data analysis was performed in Matlab.

Our selection criteria for passing the screen were stringent: significant signal ($p<0.05$) over background of at least 2-fold or 1/2-fold in at least 1 control lysate. We considered each cell line uniquely, and a particular antibody could be counted as a hit for any or all of the cell lines. Of the 483 antibodies tested, 49 were found to have positive signal in at least one cell line. These were then subjected to further standardization by immunoblotting. Of the 49, 24 were verified by immunoblotting to produce a single band of the expected size in all three cell lines, with high linearity with the screening result (Table 3.2). These antibodies were considered validated for use in lysate microarrays for the purposes of our next experiment.

3.2.3. Gathering a Dataset for Network Analysis of Erlotinib-Doxorubicin Drug Interaction

In order to understand the effects on signaling downstream of treatment with chronic erlotinib treatment, we created a collection of lysates spanning a long time course beginning at time of erlotinib treatment. Because differences in signaling most likely explain the differences in cell

A

Antibody: p-S6 (S240/244)

Antibody: β-actin

B

Technical
Replicates

Dilution Series

Biological
Replicates
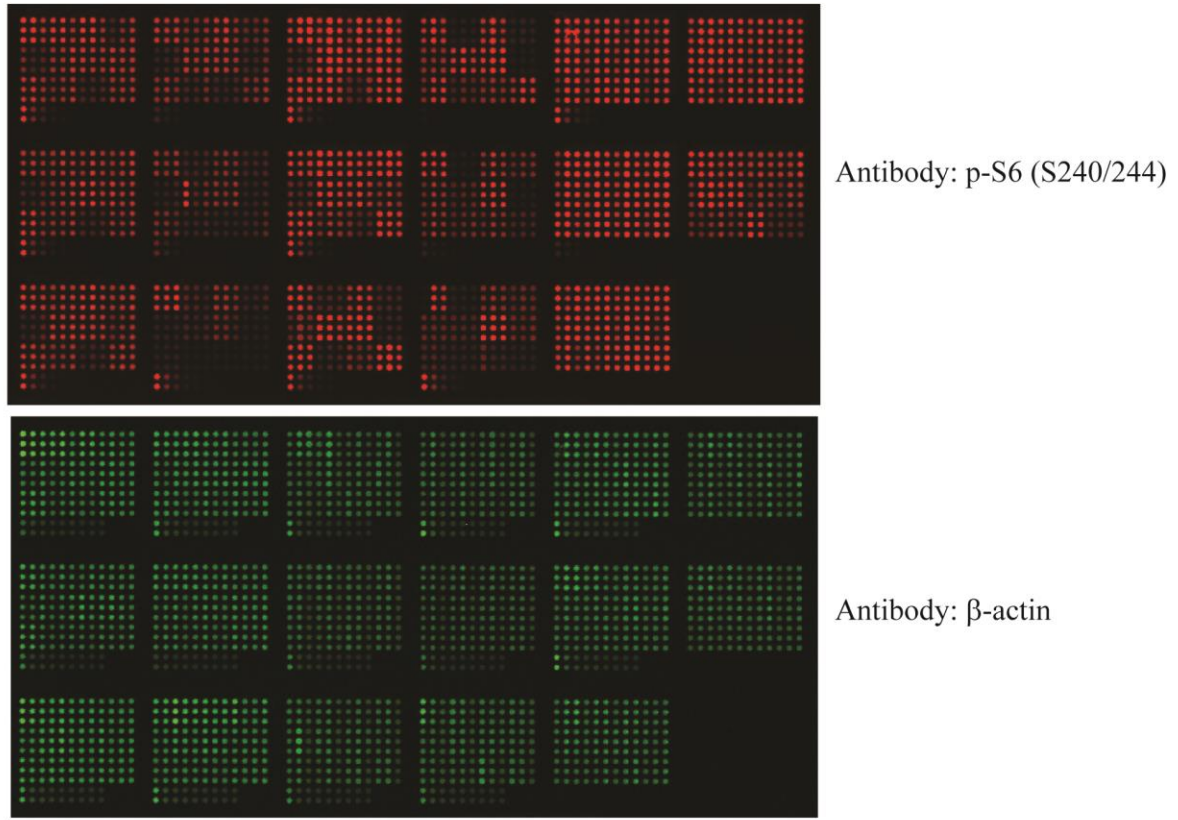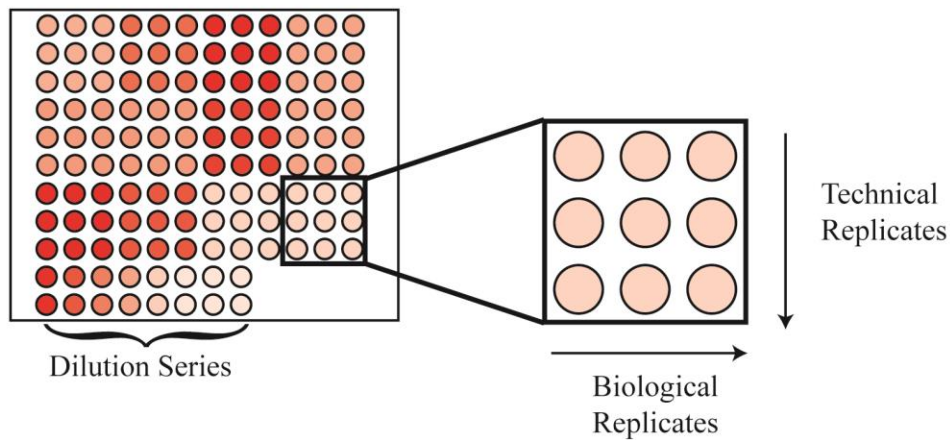
Figure 3.2. Lysate microarrays were used to monitor intracellular signaling after erlotinib-doxorubicin treatment. (A) Each microarray of 2348 spots was simultaneously probed with a single primary antibody and a normalization antibody against β-actin. The microarray shown here was probed with an antibody against p-S6 (S240/244). Significant variation was observed in p-S6 upon erlotinib/doxorubicin treatment. (B) Lysates were printed as 17

(Figure 3.2 Continued.) subarrays, each containing 12 unique combinations of cell line, drug treatment, and time point, with biological replicates on the X-axis and technical replicates on the Y-axis. Technical variation was extremely small (c.v. = 2.1%), while biological variation was larger (c.v. = 12%).

fate observed between the cell lines, it was critical we included all three cell lines in our analysis. For each cell line, we created 6 lysates at each time point: erlotinib alone, doxorubicin alone, erlotinib/doxorubicin combination treatment, erlotinib 24 hour time-staggered before doxorubicin, doxorubicin 24 hour time-staggered before erlotinib, and a mock treated control. We grew each cell line in 10 cm plates to 60% confluence, at which point treatment was administered. In cases of time-staggered treatment, the time course began when the second drug was administered 24 hours later. Lysates were collected in biological triplicate at 12 time points ranging from 5 minutes to 24 hours post treatment, a total of 612 lysates. All lysates were created and processed according to established protocol (Sevecka et al., 2011), with modification to collect apoptotic cells (see Methods Section).

These lysates were printed in technical triplicate on nitrocellulose-coated slides along with dilution curves, control lysates, and control spots, totaling 2376 spots per microarray. The slides were probed with the set of 24 pre-validated antibodies for a total of 57,024 unique measurements, and quantified using ArrayPro by MediaCybernetics. Analysis was performed in Matlab. A representative scan of an array is shown in Figure 3.2A, along with an explanation of the subarray printing strategy in Figure 3.2B.

Visual inspection showed that every node measured by lysate microarray gave significant variation in at least some experimental conditions. Spotting was consistent and technical variation was low: the average c.v. for between technical spots was 2.1%. Biological variation was by comparison much higher at 12%, though this is in line with our previous experience with biological

replicates. All data were normalized as previously described using dilution curves as standards fit to sigmoidal curves (See Methods Section).

Because our set of pre-validated antibodies was heavily biased towards measuring growth factor and stress signaling and relatively light on DNA damage and apoptotic pathways, we supplemented the lysate microarray signaling dataset with immunoblotting at key nodes such as p53. We were motivated by gene expression microarrays to monitor additional genes (Bcl2-interacting mediator of cell death (BIM), BH-3 interacting domain (BID), caspase-8, 4E-BP1, S6K, Stat3, DUSP6, and inhibitor of kappa B (IKB). This process was far more expensive, labor intensive, and time consuming, but did have the advantages of being relatively reliable and less stringent on antibody specificity. In all, 35 signaling nodes were monitored by lysate microarray or immunoblotting. A schematic of important signaling nodes in growth factor signaling, DNA damage signaling, and death signaling is presented in Figure 3.3, with those monitored by lysate microarray or immunoblotting highlighted in white. In total, this dataset comprised over 45,000 individual measurements.

Concomitant with the collection of this signaling dataset, we also wanted to know what cell fate cells resulted from each condition. To this end, we collected phenotypic data by several methods: luminescent proliferation assays, flow cytometry, and automated microscopy. Phenotypes monitored included cell-cycle arrest/proliferation, apoptotic and non-apoptotic cell death, and autophagy, measured in biological triplicate at 6 time points. In total, over 2,000 phenotypic data points were collected. A summary of the data is presented in Figure 3.4.
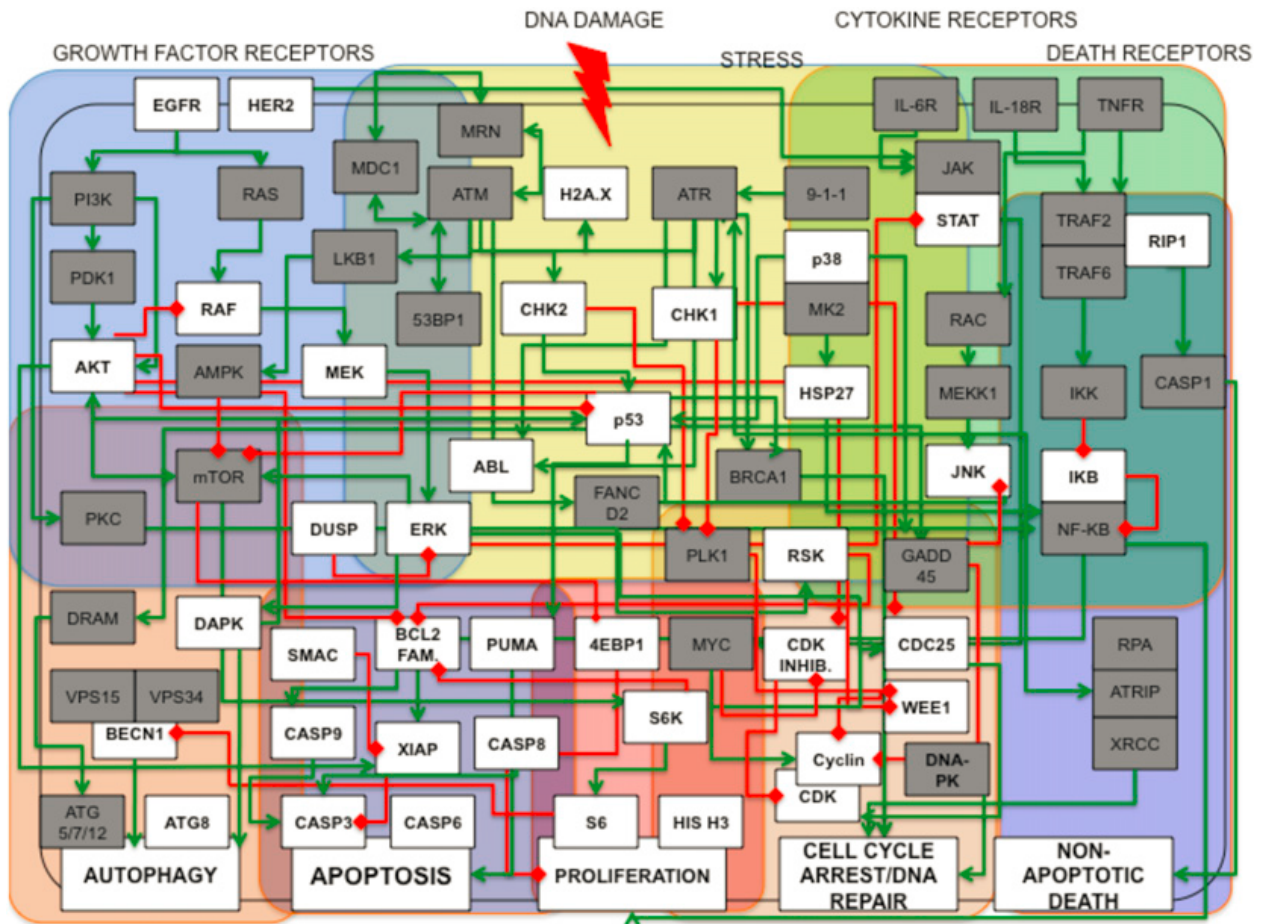
Figure 3.3. Detailed pathway diagram of the EGFR pathway, DNA Damage pathway, and associated stress signaling pathways. Proteins marked in white whose activity or total levels were monitored by either immunoblotting or lysate microarray. Reproduced with permission from Lee et al. (2012).
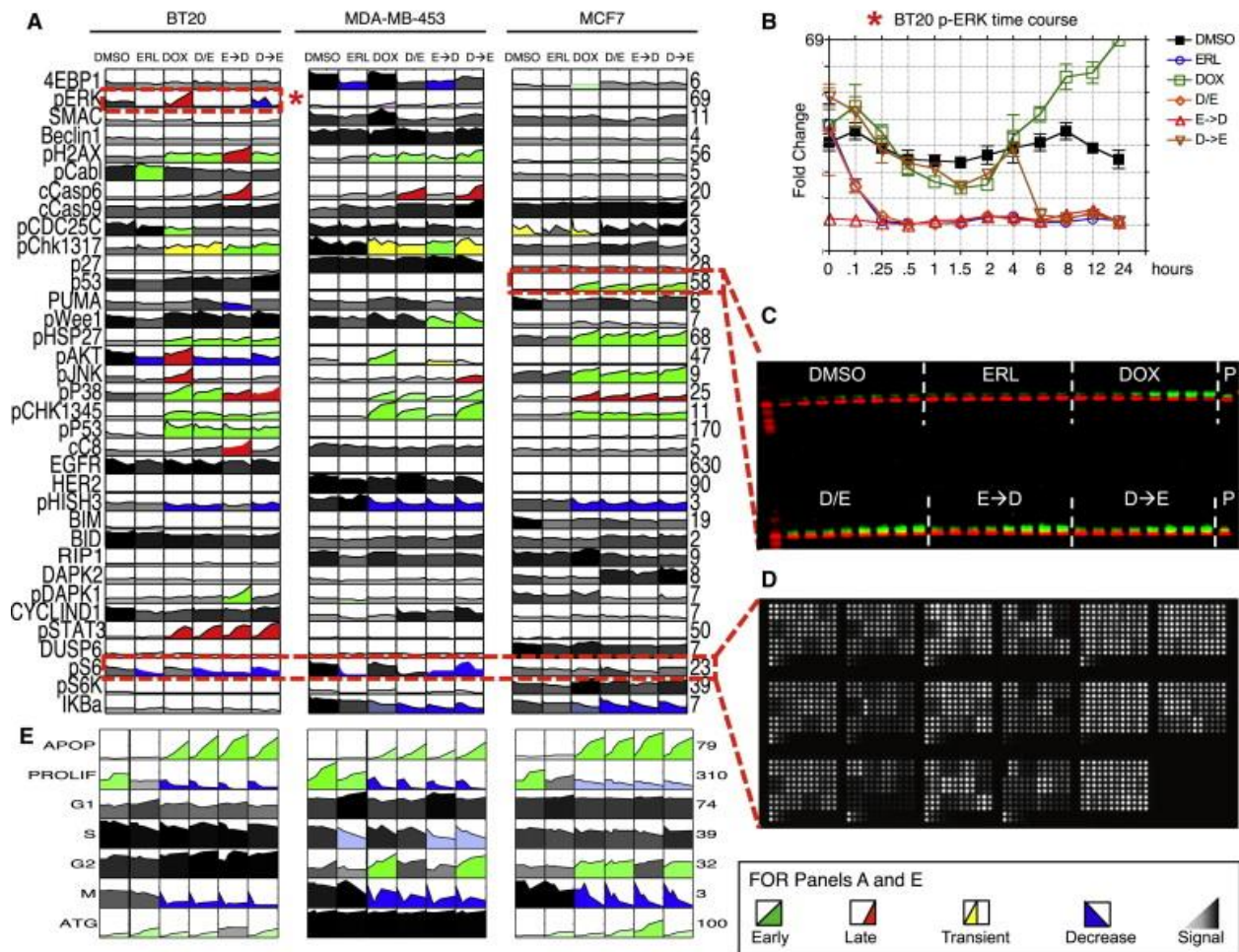
Figure 3.4. A Systems-Level Signal-Response Data Set Collected Using a Variety of High-Throughput Techniques (A–D) (A) The complete signaling data set for three different breast cancer subtypes following combined EGFR inhibition and genotoxic chemotherapy treatments. Each box represents an 8 or 12 point time course of biological triplicate experiments. Time course plots are colored by response profile, with early sustained increases in signal colored green, late sustained increases colored red, and transient increases colored yellow. Decreases in signal are colored blue. Signals that are not significantly changed by treatment are shaded gray to black with darkness reflecting signal strength. Numbers to the right of each plot report fold change across all conditions and/or cells. (B) Sample detailed signaling time course from (A), highlighted by dashed box and asterisk, showing p-ERK activation in BT-20 cells. Mean values ±SD of three experiments are shown. (C) Forty-eight-sample western blots analyzed using two-color infrared detection. Each gel contained an antibody-specific positive control (P) for blot-to-blot normalization. The example shown is one of three gels for

(Figure 3.4 Continued.) total p53 in MCF7 cells (p53 in green; β-actin in red). (D) Reverse-phase protein lysate microarrays were used to analyze targets of interest when array-compatible antibodies were available. The slide shown contains ~2,500 lysate spots (experimental and technical triplicates of all of our experimental samples, and control samples used for antibody calibration), probed for phospho-S6. (E) The complete cellular response data set, colored as in (A). Reproduced with permission from Lee et al. (2012).

3.2.4. Statistical Analysis of Signaling and Phenotype Dataset

We wanted to build a model to relate signaling data to phenotypes to identify signaling events that correlate with the observed phenotypes. We started with principal component analysis (PCA) and partial least-squares regression (PLSR) models, in order to identify covariance between signals and to identify covariance between signals and cellular phenotype, respectively (Janes and Yaffe, 2006). Both techniques produce vectors of weights corresponding to the levels of specific signaling proteins. Reducing these vectors to principal components allows iterative creation of multiple PCA or PLS dimensions, each capturing the maximum covariation not already captured by a previous vector. This iterative process is repeated until the data captured in an additional dimension is comparable to the remaining experimental noise.

After PCA, we projected the loadings of each signaling measurement along the first 2 principal components (Figure 3.5A). We found that measurements made in MB-453 cells projected negatively in Principal Component 1 (PC1), while measurements from BT-20 cells projected positively in PC1 and MCF7 were mostly close to 0 in PC1. PC1 thus separated largely based on cell type. On the other hand, PC2 separated by treatment type, with control and erlotinib-only treated cells projected negatively, doxorubicin-only and doxorubicin-erlotinib staggered close to 0, and cotreatment and erlotinib-doxorubicin staggered projected positively. These results suggest that while signaling is significantly different between the cell lines (PC1), all cell lines tested
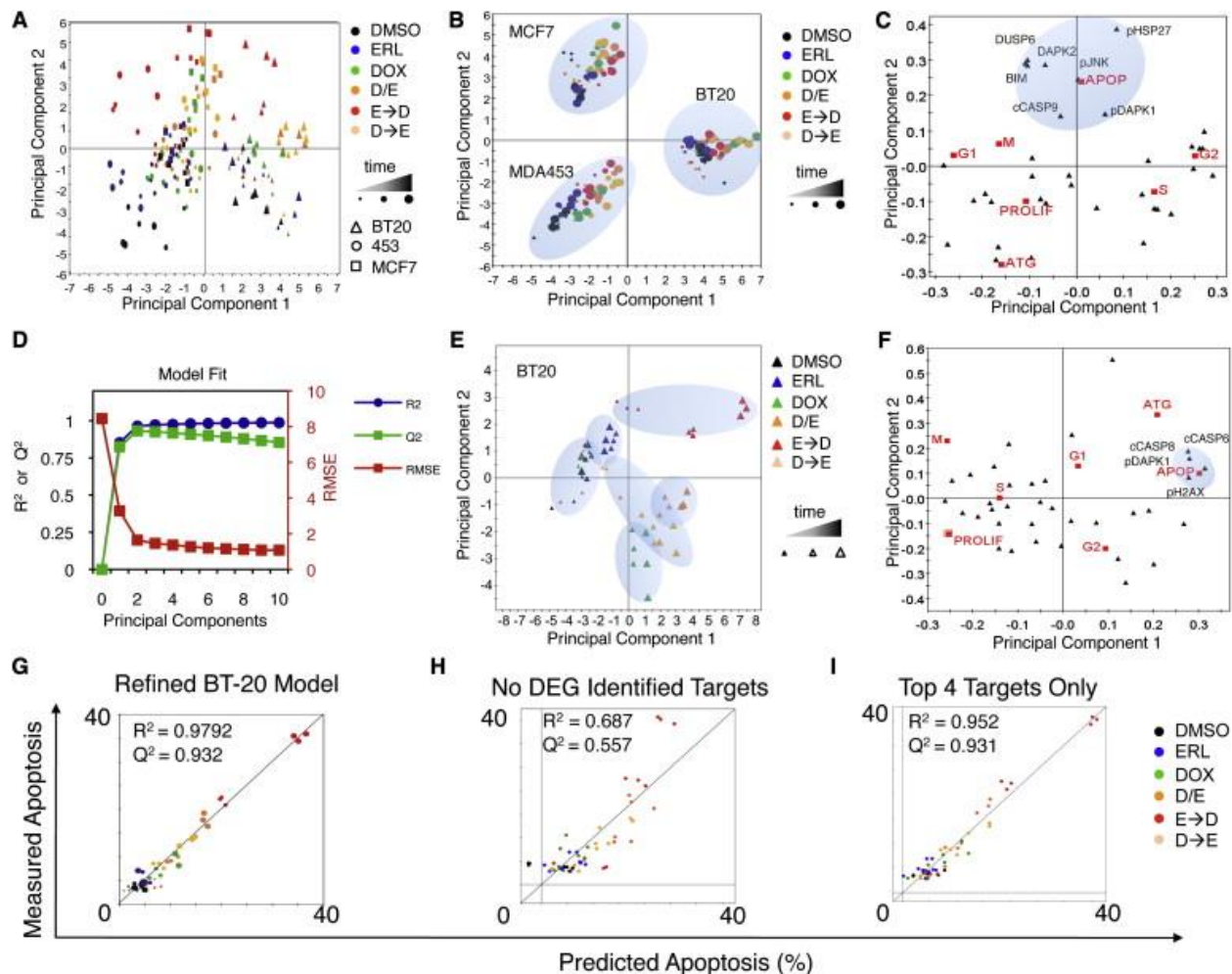
Figure 3.5. A PLS Model Accurately Predicts Phenotypic Responses from Time-Resolved Molecular Signals. (A) Principal components analysis of covariation between signals. Scores plot represents an aggregate measure of the signaling response for each cell type under each treatment condition at a specified time, as indicated by the colors and symbols in the legend. (B and C) Scores and loadings for a PLS model. (B) Scores calculated and plotted as in (A), except the principal components now reflect covariation between signals and responses. (C) PLS loadings plotted for specific signals and responses projected into principal component space. (D–I) BT-20 cell line-specific model calibration. (D) R^2, Q^2, and RMSE for BT-20 models built with increasing numbers of principal components. (E and F) Scores and loadings plots, respectively, for a two-component model of BT-20 cells. (G–I) Apoptosis as measured by flow cytometry or as predicted by our model using jack-knife cross-validation. R^2 reports model fit, and Q^2 reports model prediction accuracy. (G) Final refined model of

respond generally with similar mechanisms when challenged with erlotinib and doxorubicin (PC2). PLSR analysis signaling to downstream phenotypes was similar, though cell-type differences were now explained between PC1 and PC2, and stimulus-dependent differences captured in PC3, though PC3 did not capture statistically significant variation (Figure 3.5B). Because our statistical analysis was able to separate by both cell line and stimulus, we were confident that the dataset also included information that could explain the differences between cell lines and stimulus conditions.

To this end, and with focused interest in the differences between the cell lines, we built models for each cell line in isolation. We paid particular attention to the PLS model for the TNBC line BT-20, and we found that 97% of the variance linking signals to responses could be explained by two principal components, with additional components actually decreasing model fitness (Figure 3.5D). As a result, we focused on PC1 and PC2 and explored the individual projections of signaling measurements and phenotypic outcomes. Plotting the loading vectors (signals and phenotypic outcomes) by their weightings in PC1 and PC2 revealed a clear cluster of signals highly correlated with apoptosis projected positively in PC2, while proliferation was projected negatively in PC2 (Figure 3.5C). Notably, the model was particularly robust in predicting apoptosis (Figure 3.5G), though less so in predicting cell cycle effects, proliferation, and autophagy. Because this highly correlated group of four apoptotic signals (cleaved caspase-8, cleaved caspase-6, phospho-DAPK1, and phospho-H2AX) clustered closely with the phenotypic measurement for apoptosis, and because just the subset of four signals was nearly as accurate as the entire dataset at predicting apoptosis (Figure 3.5G,I), we focused on these nodes as critical for the apoptotic response.

Caspase-8 is an initiator caspase, but not usually involved in intrinsic death pathways. It is usually reported as downstream of death receptor activation, but has been reported in apoptosis resulting from EGFR inhibition (Kang et al., 2010; Morgillo et al., 2011), however, erlotinib alone had no apoptotic effect in BT-20 cells. Rather, it was doxorubicin treatment that activated caspase-8, even though doxorubicin usually activates DNA damage-dependent intrinsic pathways typically initiated by caspase-9 (Kim, 2005). Thus, while we were not surprised to find cleaved caspase-9 to be correlated with apoptosis, we were surprised to find cleaved caspase-8 to also be correlated with apoptosis (Figure 3.5C).

3.2.5. Extension of Time-Staggered Treatment to Other Contexts

The BT-20 erlotinib-doxorubicin time-staggered enhanced killing phenotype is promising for TNBC killing, and we wanted to test multiple TNBC lines to see if it is generalizable. To do so, we created a set of ten representative TNBC lines (Neve et al., 2006). The collected cell lines had wildly varying EGFR expression, p53 status, and doubling times, but nine of ten showed an enhanced killing doxorubicin after chronic erlotinib treatment. Of these, only four (including BT-20) showed positive synergy rather than simple additive coopertivity. This synergistic effect was uncorrelated to EGFR expression levels, but was highly correlated to basal level of EGFR phosphorylation on Y1173, a measurement of EGFR activity (Figure 3.6A-B). When we measured caspase-8 activation, we found that the cell lines displaying erlotinib-doxorubicin time staggered synergy were also the only cell lines that cleaved caspase-8. We conclude that the erlotinib-doxorubicin synergy observed in BT-20 may be generalizable to TNBC cell lines with high basal activation of EGFR (not necessarily correlated with high expression or amplification of EGFR), through similar mechanisms involving caspase-8 activation.

Figure 3.6 (Next Page). Time-Staggered Inhibition of EGFR Signaling Enhances Apoptotic Response in a Subset of TNBC Cells and Other EGFR-Driven Cells. (A) Panel of TNBC cell lines with a wide range of EGFR expression levels. Heatmap for total EGFR expression, p-EGFR (Y1173), percent apoptosis, apoptosis relative to DOX alone, and casp-8 cleavage. Apoptosis measured as in Figure 3.1. EGFR and p-EGFR expression are measured by western blotting of untreated cells. Cleaved casp-8 measured by western blot 8 hr after exposure to DOX. (B) EGFR activity, but not total EGFR expression, is correlated with sensitivity to time-staggered ERL→DOX combination. Fold enrichment of cell death observed in E→D relative to DOX alone regressed against total EGFR or p-EGFR (pY1173) as measured in untreated cells for the ten TNBC cell lines shown in (A). R^2 reports the linear fit for each trend line. (C) BT-20 cells grown as xenograft tumors in nude mice. Arrow indicates intraperitoneal administration of indicated drugs. Mean tumor volume ±SEM shown from four animals for each treatment condition.(D–F) Time-staggered inhibition of HER2 in HER2-driven breast cancer cells (D) or EGFR in lung cancer cells (E and F) causes casp-8 activation and sensitization to DOX. Apoptosis measured as in Figure 3.1 for cells exposed to a control RNA (left in each panel) or siRNA targeting casp-8 (right in each panel). Caspase-8 activation was monitored 8 hr after doxorubicin treatment (c-casp8, shown beneath the control RNA plots). Validation of caspase-8 knockdown is shown below the CASP8 siRNA plots. Mean values ±SD of three experiments are shown. (D) HER2-overexpressing MDA-MB-453 cells treated with lapatinib. (E and F) Lung cancer cells treated with erlotinib. (E) NCI-H1650. (F) A-549. (G) A model for enhanced cell death after DNA damage by chronic EGFR inhibition in triple-negative breast cancer cells.
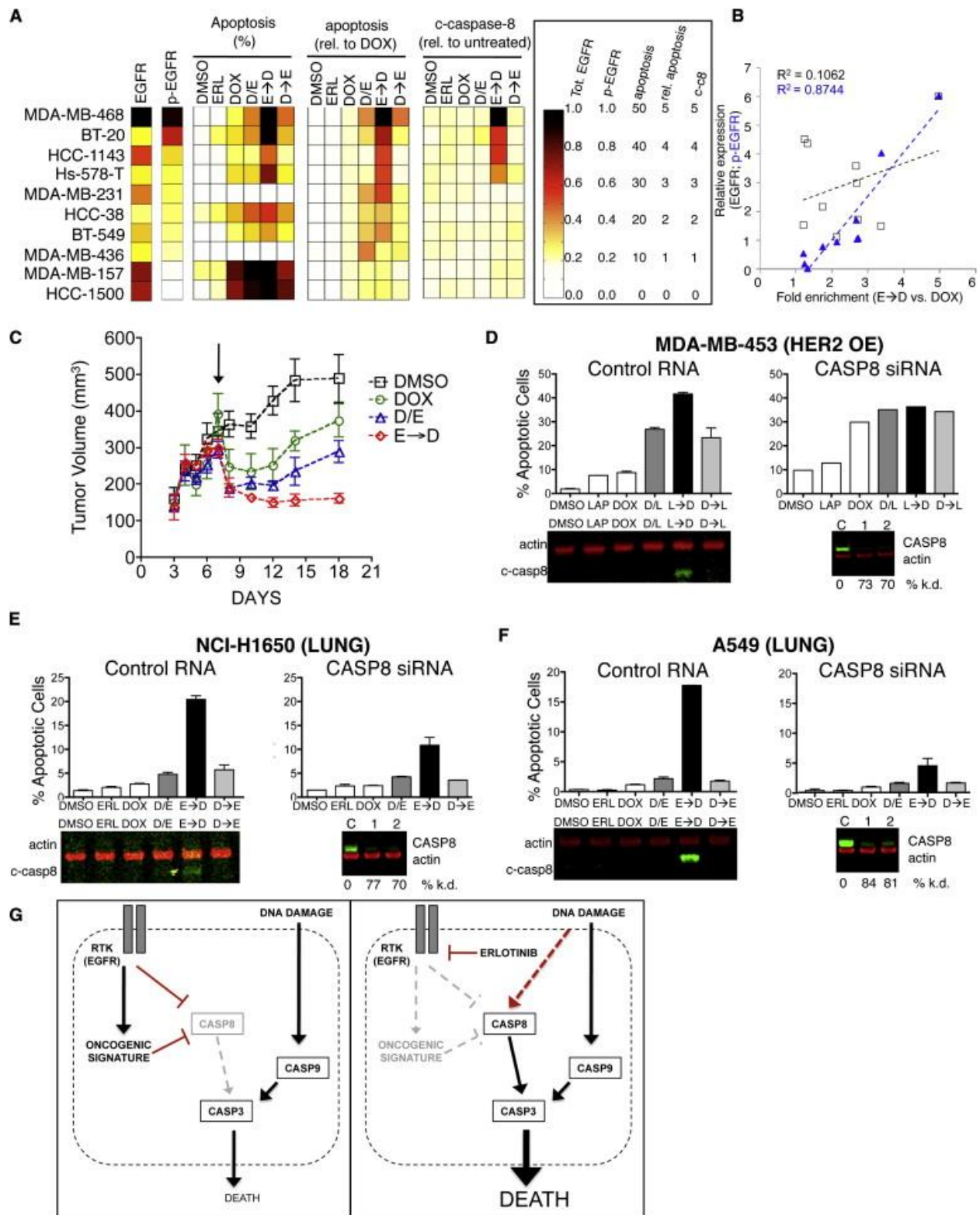
Figure 3.6 (Continued).

110

We were curious to see if the erlotinib-doxorubicin synergy was also efficacious in tumors *in vivo*. To this end, BT-20 cells were injected into flanks of nude mice, and tumors were allowed to form for 7 days before treatment with doxorubicin or erlotinib-doxorubicin combinations (Figure 3.6C). Treatment with doxorubicin alone caused tumor size to shrink for 3 days, after which the tumor began to regrow, reaching pre-treatment volume after 14 days. Erlotinib and doxorubicin cotreatment had a stronger tumor regression effect, and though the regrowth phase was slower and delayed, it nearly also reached pre-treatment volume after 14 days. By contrast, erlotinib given 8 hours before doxorubicin caused a similar rate of initial tumor shrinkage but sustained for longer, and critically, no measured tumor regrowth phase up to 14 days. Thus the pretreatment sensitization effect observed in culture was also present *in vivo*.

Because we had shown pretreatment sensitization with an EGFR inhibitor is potentially generalizable to a subset of TNBC cells and tumors with high basal levels of EGFR signaling, we wondered if analogous concepts could be applied to other types of breast cancers with high levels of growth factor signaling through a different receptor. For example, we had previously shown that erlotinib-doxorubicin timing was anti-synergistic in MDA-MB-453 cells (Figure 3.1G), but MDA-MB-453 is does not have high levels of EGFR signaling. However, MDA-MB-453 does overexpress Her2, and when we treated MB-453 cells with the EGFR/Her2 inhibitor lapatanib, we found a staggered-timing synergy (Figure 3.6D). This synergy was also caspase-8 dependent, indicating that despite the use of a different inhibitor for a different growth factor receptor, MB-453 cells after lapatinib may be rewiring signaling networks analogously to BT-20 after erlotinib.

Lung cancers are also frequently found to have high levels of EGFR signaling, and we wondered if these cancers could also be rewired with erlotinib-doxorubicin staggered timing treatment. We tested NCI-H1650 cells and A549, two commonly used lung cancer cell lines that

have highly active basal EGFR (Diaz et al., 2010; Sordella et al., 2004). These cell lines were resistant to doxorubicin alone, but strongly sensitized to doxorubicin by erlotinib pretreatment in a caspase-8 dependent manner (Figure 3.6E-F). Thus, we conclude that erlotinib pretreatment may be a generalizable mechanism for sensitization to doxorubicin in tumors with high basal EGFR signaling in multiple cancer types.

3.3.Conclusions

The standard of care in oncology at this time remains trial-and-error more often than not. Patients are bounced around from one drug regimen to another until the tumor responds. In the meanwhile, the patient suffers from astronomical medical bills, vicious side effects, and low quality of life. Despite the pharmacopeia of hundreds of cancer drugs, relatively few drugs and combinations can be counted on for a knockout blow. What we learn about one kind of cancer is often not applicable in other cancers, and the lack of uniting principles holds back understanding and treatment of cancer.

We envision several necessary advances to solve these problems. First, "garbage pail" cancer diagnoses must be clarified; triple-negative breast cancers is undoubtedly a heterogeneous cluster of diseases that should be further broken down, so that doctors can more quickly find appropriate treatment regimens for the specific tumor. Secondly, though massive screens for drug combinations have turned up relatively few efficacious cocktails, we find that the additional dimension of time staggering may reveal many more successful combinations. Lastly, we believe that approaches that deeply analyze cellular signaling such as those used in this work can reveal unexpected, exploitable weaknesses that can be generalizable to many types of cancer.

We began by screening drug combinations for efficacy against different types of breast cancer and made the novel discovery that timing is important in combination chemotherapy. TNBCs are poorly defined as a group, tend to be resistant to treatment and carry worse prognoses than other breast cancers. As a result, any way to stratify a standard of care TNBCs based on biomarkers is welcome, as well as efficacious ways to treat TNBCs. We corroborated existing evidence that erlotinib-doxorubicin combination treatment does not significantly kill BT-20 cells, but found that simply applying erlotinib before doxorubicin was efficient to promote apoptosis. Because this

approach appears to be only efficacious in TNBCs that have high EGFR activation, we propose that this subclass of TNBCs may be separate from other TNBCs, and propose clinical testing for the time-staggered approach in human patients.

We also found that this time-staggered phenomenon is not unique to erlotinib and is generalizable to all EGFR inhibitors that we tested. These data seem to suggest that time staggering a growth factor signaling inhibitor with a genotoxic agent is a successful strategy. As we have dozens of both types of drugs, and to our knowledge very little work has been done studying time staggered treatment regimens, we recommend immediate study to see if such combinations are efficacious in humans and if useful combinations have missed in previous screens. Indeed, the evidence that the EGFR inhibitor – genotoxic inhibitor combination is successful in EGFR activated lung cancer gives support to the idea that we may be better served classifying tumors by their internal signaling rather than their parent tissue type.

Finally, over the course of our systematic study of 35 signaling nodes within BT-20 cells, we observed numerous rewiring effects after erlotinib treatment. We also performed gene expression studies that demonstrate massive gene expression changes after erlotinib treatment in BT-20 cells but not MB-453 or MCF7 cells, indicating that our study is probably only scratching the surface of a substantial rewiring phenomenon (Lee et al., 2012). We hypothesize that further experiments along this vein may be rich in insights that are both generalizable and clinically relevant. For example, we identified a possible new role for caspase-8 after DNA damage, which may have been missed without unbiased, multiplexed signaling measurements. Massively parallel experiments are best suited for this type of data collection, for which we believe lysate microarrays are an excellent tool for the future.

3.4. Tables

Condition	BT-20	MDA453	MCF7
DMSO	1	31	61
NCS	2	32	62
Starved	3	33	63
EBSS	4	34	64
Serum Shocked	5	35	65
TNF	6	36	66
DOX	7	37	67
IR	8	38	68
UV	9	39	69
Wortmanin	10	40	70
Tarceva	11	41	71
Sorbitol	12	42	72
D/T8	13	43	73
T--D8	14	44	74
Taxol	15	45	75
Etoposide	16	46	76
Temezolomide	17	47	77
Camptothecin	18	48	78
Cisplatin	19	49	79
Lapatinib	20	50	80
M121	21	51	81
Conflu. (G1)	22	52	82
Aphidicolin (S)	23	53	83
IR 36 hr (G2)	24	54	84
Noco (M)	25	55	85
DTB 0 (eS)	26	56	86
DTB+4 (S)	27	57	87
DTB+8 (G2)	28	58	88
DTB+12 (M)	29	59	89
DTB+16 (G1)	30	60	90

Dilution Series	BT-20 only	Parent Sample #
Serum Shock	91-98	5
NCS	99-106	2
Confluent (G1)	107-113	22
SDS spot	114	---
Aphidicolin (S)	115-121	23
Nocodozole (M)	122-128	25

Table 3.1. Full list of control lysates selected for antibody validation in MCF7, MB-453, and BT-20 cells. Lysate conditions were selected to activate every node for which we had an antibody, in at least one condition. Left: number represents the order in which lysate was printed on arrays. Right: Control lysates and dilution series, using only BT20 sample as parent. DTB = Double Thymidine Block (synchronized in early S phase)

Table 3.2 – Full list of Antibodies Validated for Use in MCF7, MB-453, and BT20 cells			
Antibody Target	Product #	Species	Company
p-S6 (S240/244)	4838	Rabbit	Cell Signaling
p-S6 (S235/236)	AF3918	Rabbit	R&D
pS6K (T421/S424)	9204	Rabbit	Cell Signaling
p-mTOR (S2448)	2971	Rabbit	Cell Signaling
p-4E-BP1 (S65)	9456	Rabbit	Cell Signaling
p-ERK1/2 (T202/Y204)	4376	Rabbit	Cell Signaling
p-p38 (T180/Y182)	9215	Rabbit	Cell Signaling
p-p90RSK (S380)	9341	Rabbit	Cell Signaling
p-MK2 (T334)	3041	Rabbit	Cell Signaling
p-HSP27 (S82)	2401	Rabbit	Cell Signaling
p-SAPK/JNK (T183/Y185)	9251	Rabbit	Cell Signaling
A-Raf	4432	Rabbit	Cell Signaling
p-Akt1/2/3 (S473)	05-736	Rabbit	Millipore
p-MEK1/2 (S217/S221)	9154	Rabbit	Cell Signaling
p-SEK1 (S257/T261)	9156	Rabbit	Cell Signaling
p53 (Total)	9282	Rabbit	Cell Signaling
p-H2A.X (S139)	9718	Rabbit	Cell Signaling
p-DNA PKcs (S2056)	ab18192	Rabbit	Abcam
p-cdc25C (S216)	9528	Rabbit	Cell Signaling
p-53BP1 (S25/29)	2674	Rabbit	Cell Signaling
p-Histone H3 (S10)	06-570	Rabbit	Millipore
p-Wee1 (S642)	4910	Rabbit	Cell Signaling
p-Cycline E (T62)	4136	Rabbit	Cell Signaling
p-BRCA1 (S1524)	9009	Rabbit	Cell Signaling

Table 3.2. Full list of Antibodies Validated for use in MCF7, MB-453, and BT-20 cells. All antibodies were selected from primary screening using control lysates, then individually validated for positive, linear, specific signal in immunoblots.

3.5. Experimental Methods

Antibody Reagents

Pan and phospho-specific antibodies for signaling proteins were purchased from Abcam (Cambridge, MA), BD Biosciences (San Jose, CA), Cell Signaling Technology (Beverly, MA), Santa Cruz Biotechnology (Santa Cruz, CA), and Upstate (Charlotteville, VA). Mouse monoclonal anti-β-actin antibody (clone AC-15) was purchased from Sigma-Aldrich (Saint Louis, MO), rabbit monoclonal anti-β-actin antibody was catalog # 4970 (Cell Signaling Technology (Beverly, MA)). Secondary detection antibodies were purchased from Li-Cor Biosciences (Lincoln, NE).

Cell Culture

All cell lines were obtained from American Type Culture Collection (ATCC) and maintained at low passages (<20) in various medias (See Appendix A).

Cell Response Assays: Apoptosis

Following treatment, cells were washed and trypsinized, saving all floater cells. Fixation using 4% paraformaldehyde at room temperature for 15 minutes was followed by resuspension in ice-cold methanol and overnight incubation at -20°C. Cells were washed in PBST, blocked for 1 hour in BSA/PBST, and stained with antibodies against cleaved-caspase-3 and cleaved-poly(ADP-ribose) polymerase (PARP) (BD PharMinogen). Secondary Alexa-conjugated detection antibodies were used for visualization in a BD FacsCalibur flow cytometer (Molecular Probes). Analysis was done using FloJo, and double-positive cells were counted as apoptotic.

Cell Response Assays: Cell Cycle

Following treatment, cells were fixed in 70% ethanol overnight at -20°C, permeabilized with PBS-Triton for 20 min at 4°C, blocked with 1% BSA, and incubated with antibodies against phospho-Histone H3 (Millipore). After washing, cells were incubated with Alexa-488 conjugated secondary antibody on ice, washed, and stained with 50 µg/mL propidium iodide (PI) prior to analysis. A BD FacsCalibur flow cytometer was used, and analysis was done using FloJo utilizing the Dean-Jett-Fox algorithm.

Cell Response Assays: Viable Cell Count

Cells were plated at 10,000 cells/well in 96-well optical glass bottom white walled plates, then stimulated. Metabolic viability was measured using Cell Titer Glo (Promega) according to manufacturer protocol. Normalization was always to untreated sample.

Cell Response Assays: Autophagy

Cells were stably transfected with pBABE-mCherry-EGFP-LC3B (Addgene Plasmid 22418), which reports activation of autophagy and maturation of autophagic particles to autolysosomes. Expression of this plasmid was determined to have no effect on cell growth rate, apoptosis, or chemosensitivity (data not shown). Cells were seeded onto 18 mm2 coverslips and treated with erlotinib or doxorubicin or both for the indicated times. Cells were then fixed in 3% PFA and 2% sucrose for 15 min at RT, and stained for 10 min with whole cell blue stain according to manufacturer's protocol (Thermo Scientific). Images were collected on an Applied Precision DeltaVision Spectris automated microscope and deconvolved using Applied Precision SoftWoRx software. Deconvolved image projections were analyzed using CellProfiler to identify total cells

as well as autophagic cells. A modified ''speckle counter'' pipeline was used as described previously (Carpenter et al., 2006). Briefly, whole cell blue signal was used to segment each image into individual cells. Number of GFP or mCherry LC3 puncta were counted per cell, and cells were counted as ''autophagic'' if the number of GFP and mCHERRY puncta significantly increased relative to untreated cells (Mizushima et al., 2010). Approximately 100 cells were counted in a double blind fashion per condition, and percent autophagic cells reported from 3 independent experiments.

Western Blotting

Cell lysates were prepared as described previously (Sevecka et al., 2011). Crude lysates were filtered in AcroPrep 96 well 3.0 µm glass fiber/0.2 µm BioInert filter plate (Pall), then normalized for total protein content using the BCA assay (Pierce). Blots were run using 48-well precast gels and transferred using semi-dry fast transfer apparatus onto nitrocellulose membranes (e-PAGE, i-Blot, Invitrogen). Blots were blocked in Odyssey blocking buffer (Li-Cor), incubated overnight with primary antibody, stained with secondary antibodies conjugated to an infrared die, then visualized using an Odyssey flat bed scanner (Li-Cor). Data were calculated as the background subtracted intensity divided by the β-actin signal to correct for loading differences, then normalized to a reference sample contained on every gel, for gel-to-gel normalization. Signal averages were calculated from triplicate experiments. Antibodies that did not report significant variation across treatments were omitted.

Lysate Microarray Fabrication

Lysate microarrays were printed on a fee-for-service basis by Aushon Biosystems. Lysates were printed on 2-pad nitrocellulose slides in technical triplicate and biological duplicate using 333 μm spacing with steel solid 110 μm pins. This resulted in an average feature size of 170 μm. Slides were probed and analyzed as previously (Sevecka et al., 2011).

siRNA knockdown

Silencer Select Validated siRNAs were purchased through Invitrogen. For EGFR, si oligos used were: GAUCUUUCCUUCUUAAAGAtt (sense) and UCUUUAAGAAGGAAAGAUCat (antisense); and CCAUAAAUGCUACGAAUAUtt (sense) and AUAUUCGUAGCA UUUAUGGag (antisense). Oligos for caspase-8 were: GAUACUGUCUGAUCAUCAAtt (sense) and UUGAUGAUCAGACAGUAUCcc (antisense); and GAUCAGAAUUGAGGUCUUUtt (sense) and AAAGACCUCAAUUCUGAUCtg (antisense). For transfection in human cell lines, Lipofectamine RNAiMAX was used according to manufacturer's instructions. Dose titration and time course experiments were performed to determine that optimal knockdown efficiency, which in all experiments was 5nM siRNA for 48 hr.

Computational Modeling and Statistics

Data-driven modeling and the application of partial least-squares to biological data have been described in detail previously (Janes and Yaffe, 2006). PLS modeling was done using iterative algorithms in SIMCA-P (Umetrics). All data were variance scaled to nondimensionalize the different measurements. Model predictions were made via cross-validation. Model fitness was calculated using $R2$, $Q2$, and RMSE, as described previously by (Gaudet et al., 2005). VIP was calculated following (Janes et al., 2008).

Works Cited

Abeloff, M., Wolff, A., Weber, B., Zaks, T., Sacchini, V., and McCormick, B. (2008). Cancer of the breast. In Abeloff's Clinical Oncology, M. Abeloff, J. Armitage, J. Niederhuber, M. Kastan, and W. McKenna, eds. (Maryland Heights, MO: Churchill Livingstone), pp. 1875-1944.

Bosch, A., Eroles, P., Zaragoza, R., Vina, J.R., and Lluch, A. (2010). Triple-negative breast cancer: molecular features, pathogenesis, treatment and current lines of research. Cancer treatment reviews *36*, 206-215.

Carey, L.A., Rugo, H.S., Marcom, P.K., Mayer, E.L., Esteva, F.J., Ma, C.X., Liu, M.C., Storniolo, A.M., Rimawi, M.F., Forero-Torres, A.*, et al.* (2012). TBCRC 001: randomized phase II study of cetuximab in combination with carboplatin in stage IV triple-negative breast cancer. Journal of clinical oncology : official journal of the American Society of Clinical Oncology *30*, 2615-2623.

Carpenter, A.E., Jones, T.R., Lamprecht, M.R., Clarke, C., Kang, I.H., Friman, O., Guertin, D.A., Chang, J.H., Lindquist, R.A., Moffat, J.*, et al.* (2006). CellProfiler: image analysis software for identifying and quantifying cell phenotypes. Genome biology *7*, R100.

Chou, T.C., and Talalay, P. (1984). Quantitative analysis of dose-effect relationships: the combined effects of multiple drugs or enzyme inhibitors. Adv Enzyme Regul *22*, 27-55.

Corkery, B., Crown, J., Clynes, M., and O'Donovan, N. (2009). Epidermal growth factor receptor as a potential therapeutic target in triple-negative breast cancer. Annals of oncology : official journal of the European Society for Medical Oncology / ESMO *20*, 862-867.

Dent, R., Trudeau, M., Pritchard, K.I., Hanna, W.M., Kahn, H.K., Sawka, C.A., Lickley, L.A., Rawlinson, E., Sun, P., and Narod, S.A. (2007). Triple-negative breast cancer: clinical features and patterns of recurrence. Clinical cancer research : an official journal of the American Association for Cancer Research *13*, 4429-4434.

Diaz, R., Nguewa, P.A., Parrondo, R., Perez-Stable, C., Manrique, I., Redrado, M., Catena, R., Collantes, M., Penuelas, I., Diaz-Gonzalez, J.A.*, et al.* (2010). Antitumor and antiangiogenic effect of the dual EGFR and HER-2 tyrosine kinase inhibitor lapatinib in a lung cancer model. BMC cancer *10*, 188.

Gaudet, S., Janes, K.A., Albeck, J.G., Pace, E.A., Lauffenburger, D.A., and Sorger, P.K. (2005). A compendium of signals and responses triggered by prodeath and prosurvival cytokines. Molecular & cellular proteomics : MCP *4*, 1569-1590.

Hanahan, D., and Weinberg, R.A. (2000). The hallmarks of cancer. Cell *100*, 57-70.

Hanahan, D., and Weinberg, R.A. (2011). Hallmarks of cancer: the next generation. Cell *144*, 646-674.

Harper, J.W., and Elledge, S.J. (2007). The DNA damage response: ten years after. Molecular cell *28*, 739-745.

IARC (2008). World Cancer Report
(http://globocan.iarc.fr/factsheets/populations/factsheet.asp?uno=900: WHO).

Janes, K.A., Albeck, J.G., Gaudet, S., Sorger, P.K., Lauffenburger, D.A., and Yaffe, M.B. (2005). A systems model of signaling identifies a molecular basis set for cytokine-induced apoptosis. Science *310*, 1646-1653.

Janes, K.A., Reinhardt, H.C., and Yaffe, M.B. (2008). Cytokine-induced signaling networks prioritize dynamic range over signal strength. Cell *135*, 343-354.

Janes, K.A., and Yaffe, M.B. (2006). Data-driven modelling of signal-transduction networks. Nature reviews Molecular cell biology *7*, 820-828.

Kang, N., Zhang, J.H., Qiu, F., Tashiro, S., Onodera, S., and Ikejima, T. (2010). Inhibition of EGFR signaling augments oridonin-induced apoptosis in human laryngeal cancer cells via enhancing oxidative stress coincident with activation of both the intrinsic and extrinsic apoptotic pathways. Cancer letters *294*, 147-158.

Kim, R. (2005). Recent advances in understanding the cell death pathways activated by anticancer therapy. Cancer *103*, 1551-1560.

Lee, M.J., Ye, A.S., Gardino, A.K., Heijink, A.M., Sorger, P.K., MacBeath, G., and Yaffe, M.B. (2012). Sequential application of anticancer drugs enhances cell death by rewiring apoptotic signaling networks. Cell *149*, 780-794.

Lichter, A.S., and Lawrence, T.S. (1995). Recent Advances in Radiation Oncology. The New England journal of medicine *332*, 371-379.

Mizushima, N., Yoshimori, T., and Levine, B. (2010). Methods in mammalian autophagy research. Cell *140*, 313-326.

Morgillo, F., D'Aiuto, E., Troiani, T., Martinelli, E., Cascone, T., De Palma, R., Orditura, M., De Vita, F., and Ciardiello, F. (2011). Antitumor activity of bortezomib in human cancer cells with acquired resistance to anti-epidermal growth factor receptor tyrosine kinase inhibitors. Lung Cancer *71*, 283-290.

Neve, R.M., Chin, K., Fridlyand, J., Yeh, J., Baehner, F.L., Fevr, T., Clark, L., Bayani, N., Coppe, J.P., Tong, F.*, et al.* (2006). A collection of breast cancer cell lines for the study of functionally distinct cancer subtypes. Cancer cell *10*, 515-527.

Perou, C.M., Sørlie, T., Eisen, M.B., van de Rijn, M., Jeffrey, S.S., Rees, C.A., Pollack, J.R., Ross, D.T., Johnsen, H., Akslen, L.A.*, et al.* (2000). Molecular portraits of human breast tumours. Nature *406*, 747-752.

Sachs, K., Perez, O., Pe'er, D., Lauffenburger, D.A., and Nolan, G.P. (2005). Sachs K, Perez O, Pe'er D, Lauffenburger DA, Nolan GP. Science *308*, 523-529.

Schechter, A.L., Stern, D.F., Vaidyanathan, L., Decker, S.J., Drebin, J.A., Greene, M.I., and Weinberg, R.A. (1984). The neu oncogene: an erb-B-related gene encoding a 185,000-Mr tumour antigen. Nature *312*, 513-516.

Sevecka, M., Wolf-Yadlin, A., and G., M. (2011). Lysate microarrays enable high-throughput, quantitative investigations of cellular signaling. Mol Cell Proteomics *10*.

Slamon, D.J., Clark, G.M., Wong, S.G., Levin, W.J., Ullrich, A., and McGuire, W.L. (1987). Human breast cancer: correlation of relapse and survival with amplification of the HER-2/neu oncogene. Science *235*, 177-182.

Sordella, R., Bell, D.W., Haber, D.A., and Settleman, J. (2004). Gefitinib-sensitizing EGFR mutations in lung cancer activate anti-apoptotic pathways. Science *305*, 1163-1167.

Winer, E.P., and Mayer, E.L. (2007). Optimizing Treatment of "Triple-Negative" Breast Cancer (SABCS 2007: Improving Outcomes in Advanced and Metastatic Breast Cancer).

Part 4

Application of Lysate Microarray Technology

For Understanding the DNA Damage Response

In the Context of Tumor Progression

4.1. Introduction

One of the most problematic features of cancer is that each tumor is unique. Tumor are heterogeneous mosaics, comprising dozens of clones carrying hundreds or thousands of mutations (Samuel and Hudson, 2013). We believe this heterogeneity within and between tumors contributes in large part to the lack of generalized cancer magic bullets. If just a subset of clones within a tumor survive chemotherapeutic treatment, they may regrow and cause a tumor to recur, commonly with heightened resistance to further treatment. Furthermore, as an untreated tumor progresses it is also subject to heritable genetic drift and quickly evolves away from wild-type signaling. For these reasons, it is important to understand in great detail how chemotherapeutics affect cancer cells along the path to tumorgenicity, in order to maximally kill the entire tumor all at once, while minimizing toxicity to surrounding cells.

The MCF10 cell line series represents a tumor progression model spanning the evolution from parental normal tissue to end-stage metastatic tumor. The series of four cell lines were successively derived from a common source, preserving a unique level of genetic relatedness while also simulating the changes through the course of tumor progression. The well-known parental MCF10A cell line was isolated from a patient with proliferative breast disease and spontaneously became immortalized (Soule et al., 1990). This cell line has been extensively used as a "normal control" cell line for comparison with more aggressive lines and does not form xenografts in nude mice. Transfection with T24 H-ras created the MCF10AT cell line, characterized by loss of requirement for EGF, increased invasiveness, and ability to form xenografts in nude mice, mostly consisting of simple ducts and rarely higher grade carcinomas (Dawson et al., 1996). One of these carcinomas was dissociated, isolated, cloned, and cultured to create a cell line known as MCF10AT1K.c12 (Santner et al., 2001). These cells were once again used to create a second

125

generation xenograft. After two additional passes, the final fourth generation tumor was once again dissociated and cultured, and the resulting cell lines designated MCF10CA1 (Santner et al., 2001). MCF10CA cell lines are very aggressive, efficiently forming metastatic adenocarcinomas and killing the host within weeks. For brevity we will refer to these cell lines as A, AT, c12, and CA1 for the remainder of this work.

While the MCF10A series derives from a common source, they are phenotypically quite distinct. Genomic, proteomic, and phosphoproteomic studies have been conducted to identify the molecular basis for these differences. A SNP array analysis of the cell lines found a deletion in CDKN2A in all four cell lines, as well as an amplification of MYC, which may well be the initial immortalizing events (Kadota et al., 2010). A gene expression study showed low expression of estrogen receptor, progesterone receptor, and Her2, indicating the entire series may also be best considered a triple-negative cancer line (Rhee et al., 2008). A phosphoproteomic study found massive reprogramming specifically in metabolism (the "Warburg effect") and cytoskeletal regulation indicative of a possible epithelial-mesenchymal transition (EMT) in the CA1 line (Choong et al., 2010). None of these studies, however, found mutations or major differences in expression between cell lines in DNA Damage pathways, indicating it was ideal to study genotoxic chemotherapy in the context of progression of other cancer-related signatures. We therefore set out to study the differences in intracellular signaling and cellular fates that result from genotoxic treatment of the MCF10A progression line.

We selected four clinically important topoisomerase inhibitors for study. Irinotecan and camptothecin are related molecules that selectively and reversibly inhibit Topoisomerase I, causing single-stranded breaks by intercalating into DNA (Tomicic and Kaina, 2013). Both have been approved for first-line therapy, but also carry significant dose-limiting side effects. Etoposide

and doxorubicin on the other hand are unrelated molecules that poison Topoisomerase II, also resulting in a single-stranded breaks (Pommier et al., 2010). Etoposide covalently modifies TopoII, preventing religation, and has relatively few other effects in cells. On the other hand, doxorubicin at low concentrations (<1 μM) also prevents religation, but at higher concentrations (>10 μM) also intercalates into DNA and interferes with Topo II binding DNA (Pommier et al., 2010). Both are also used in first-line treatment, with significant side effects (cardiotoxicity for doxorubicin, treatment-related acute myelocytic leukemia for etoposide). All such single-stranded breaks induced by topoisomerase inhibition have the potential to progress to double-stranded breaks during S phase as a replication fork passes through.

4.2. Results and Discussion

4.2.1. Multi-parameter Characterization of Cell Fates Downstream of Chemotherapy

We began by asking if the MCF10A progression cell lines show differential sensitivities to Topo inhibitors. We expected that the more aggressive lines would display increased sensitivity. We considered that the major possible outcomes to genotoxic stress include proliferation/survival, apoptosis, and cell cycle arrest. To this end, we challenged all four cell lines with the topoisomerase inhibitor panel and measured markers of cell count, apoptotic cell death, and cell cycle status.

We measured cell number and survival/proliferation using a commercially available luminescent plate-based assay. All four cell lines were grown in 96-well plates to 60% confluence and subjected to a dilution series of each drug for 24 or 48 hours, at which point the plates were harvested for Cell Titer Glo assays (Figure 4.1). Cell Titer Glo assays measure total ATP content within a sample, which we assume to be directly correlated with the number of viable cells. Thus, these data represent some combination of proliferation and survival over the time course of the experiment. Surprisingly, c12 cells were as resistant, if not more resistant, to treatment as the parental A line in nearly all cases. Equally surprising was the fact that AT cells were the most sensitive in all cases except for high doses of etoposide at 48 hours. We conclude from these data that drug sensitivities in the MCF10 progression series is not trivially related to aggressiveness, and considered that the effect may be due to cell cycle checkpoint related arrest.

To measure the effects that topoisomerase inhibitors have on the cell cycle in MCF10 cell lines, we used a FACS technique coupled with a statistical model. Cells grown in 6-well plates, stimulated with 2 doses of each drug and harvested at 24 or 48 hours and fixed. Labeling with propidium iodide for DNA content to distinguish between G1, S, and G2/M, fit using the Dean-
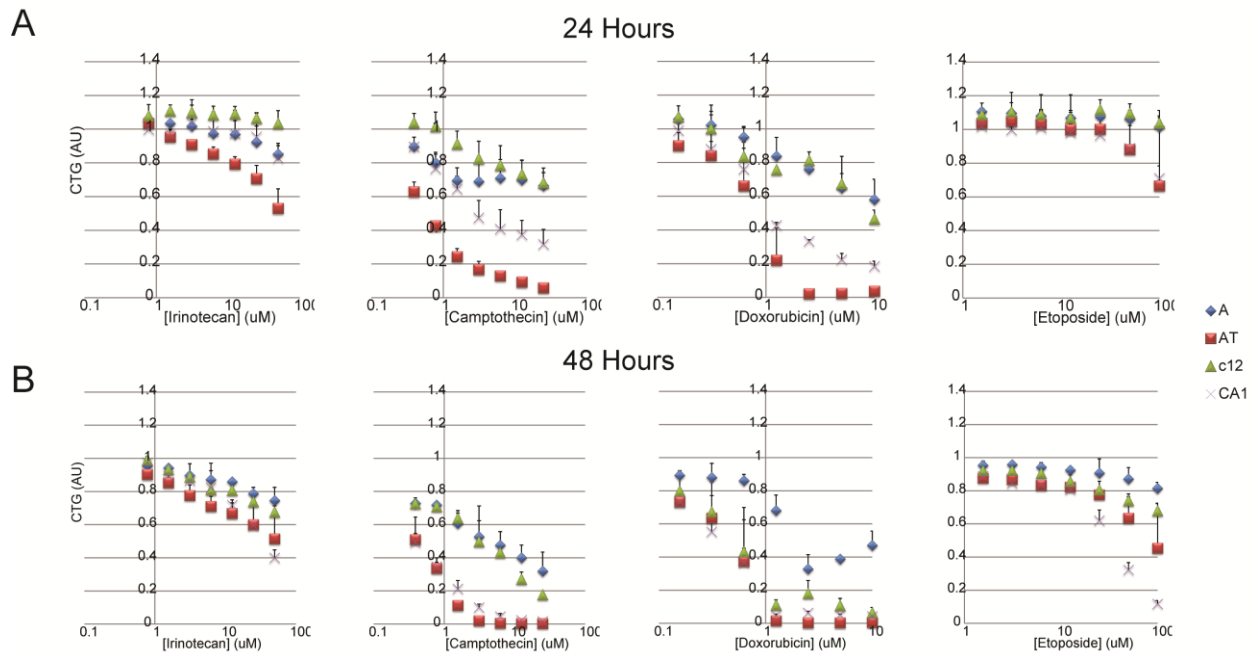
Figure 4.1. The MCF10 progression lines show unexpected trends in proliferation/survival when challenged with topoisomerase inhibitors. Cells were grown in 96-well plates and challenged with serial dilutions of four drugs. After (A) 24 and (B) 48 hours, Cell Titer Glo assays were performed to assess viable cell count. Error bars indicate the standard error of 3 experiments, each of which included 3 biological replicates per condition. All samples were normalized to a matched vehicle control.

Jett-Fox model to fit these populations (Fox, 1980). We also used an antibody against phospho-H3 (S10) to distinguish between G2 and M (Figure 4.2A). Visual inspection of the data revealed that cell lines A and c12 were generally resistant to changes in cell cycle, while cell line CA1 strongly arrested in G2 in response to high doses of drug (Figure 4.2B). In particular, we were struck the similarity of the cell cycle profiles between 24 and 48 hours, indicating that in most cases, cells did not appear to continually accumulate at specific stages of the cell cycle between the time points measured, though notable exceptions did exist (c12, etoposide high dose). These data also did not appear to be correlated or anticorrelated with the cell survival/proliferation data

Figure 4.2 (Next Page). Topoisomerase inhibitors have significant effects on cell cycle in MCF10 progression lines, including checkpoint activation. Cells were grown in 6-well plates and stimulated with 2 doses of each drug for 24 or 48 hours. (A) Samples were analyzed by FACS using p-Histone H3 (S10) as a mitosis marker and DNA content to separate G1, S, and G2/M. A hand-curated Dean-Jett-Fox algorithm was used to approximate number of cells in each population. (B) Cells collected after treatment broken down into phase of cell cycle at time of fixation. Substantial enrichment of G2 phase in AT and CA1 may indicate a less active G1 checkpoint and a compensatory G2 checkpoint. Interestingly, the profiles obtained at 24 and 48 hours are remarkably similar. Data represents mean of 2 experiments.
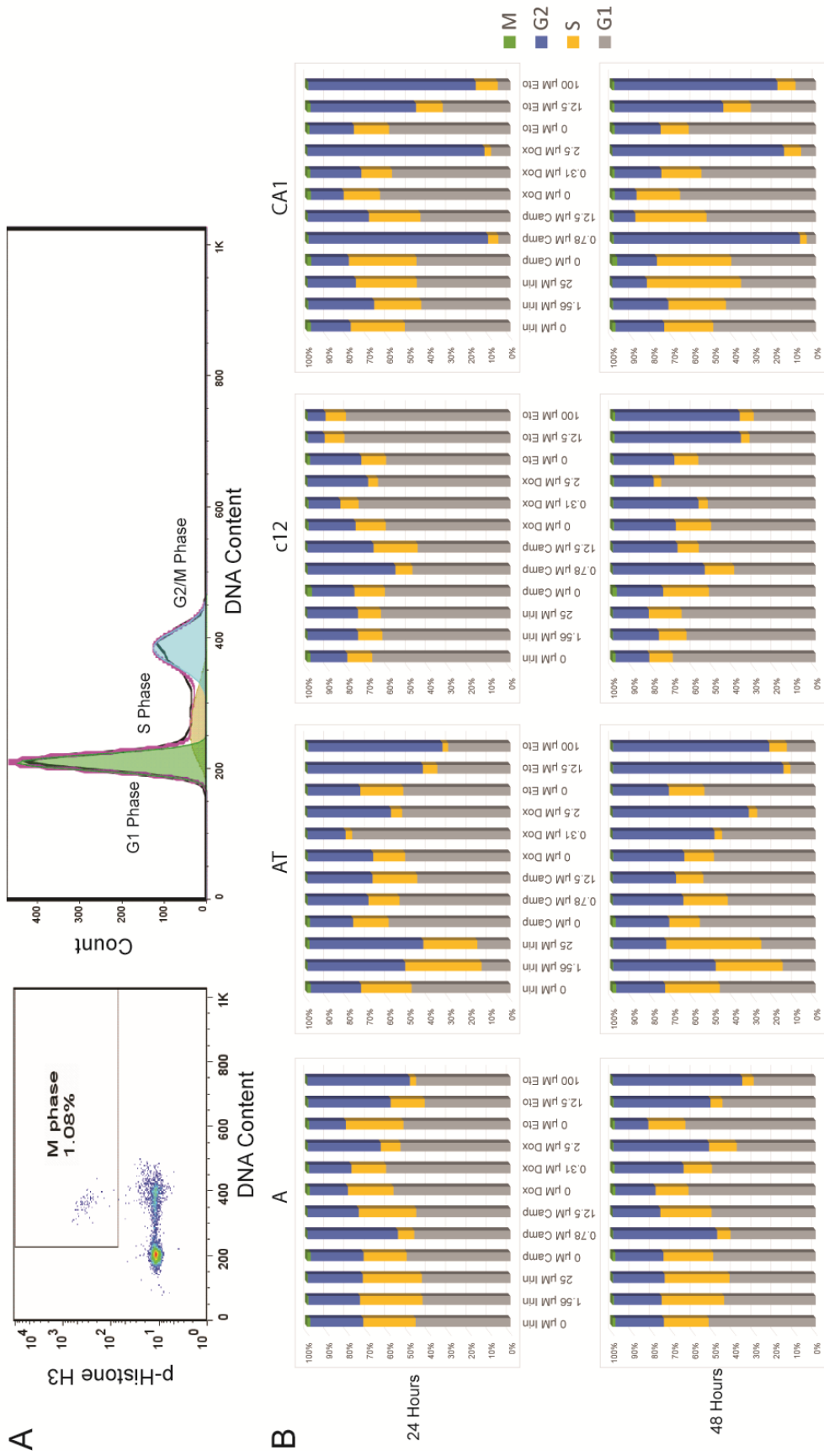
Figure 4.2 (Continued).

obtained from Cell Titer Glo, indicating that survival and cell cycle are capturing different aspects of cell fate.

The final major possible outcome we considered for cells undergoing genotoxic stress is apoptosis. To quantify apoptotic cell death, we again used a FACS-based assay. Cells were grown in 6-well plates and stimulated using the same 2 doses of drug used in the cell cycle assay, and harvested for fixation at 24 or 48 hours. Cells were labeled for cleaved caspase-3 and cleaved-PARP, markers of early intrinsic and late apoptosis, respectively (Figure 4.3A). Visual inspection of this data showed the surprising result that while all cell lines regularly cleaved caspase-3 in response to drug treatment, only AT cells were observed to cleave PARP, and only in select treatments (high dose camptothecin). As a result, as opposed to previous studies, we defined apoptotic cells as those that had cleaved caspase-3 without requirement for cleaved-PARP (Figure 4.3B). Furthermore, the centroid of the presumed non-apoptotic population (low staining for cleaved caspase-3) shifted right with increasing drug concentration, which indicates that cells can cleave caspase-3 to a limited extent, which contradicts the traditional "all-or-nothing" view of apoptosis. c12 cells notably did not cleave caspase-3 in any condition at 24 hours, though significant apoptotic signaling could be observed at 48 hours. AT and CA1 cells showed strong apoptotic response to high doses of both camptothecin and doxorubicin. We did not test for activation of RIP, and it is possible that a subset of this population is fated for death through non-apoptotic means such as necroptosis.

We also attempted to study gross morphology changes as senescence and autophagy can be estimated by their respective characteristic visible changes. Senescence is characterized by a large and flattened cytoplasm and a condensed nucleus, resembling a fried egg. By contrast, autophagy is characterized by a buildup of large numbers or very large vacuoles. We utilized live-cell

Figure 4.3 (Next Page). Topoisomerase inhibitors induce significant apoptotic response in all cell lines, dependent on cellular context and drug dose. Cells were grown in 6-well plates and stimulated with 2 doses of each drug for 24 or 48 hours. (A) After fixation, samples were fixed and stained for cleaved caspase-3 and cleaved PARP. Because cleaved-PARP was only observed in AT cells, we classified cells with cleaved caspase-3 as apoptotic. (B) Full dataset collected at 24 and 48 hours. Cell lines AT and CA1 overwhelmingly committed apoptosis at high doses of camptothecin and doxorubicin, while c12 is totally resistant at 24 hours but not at 48 hours.
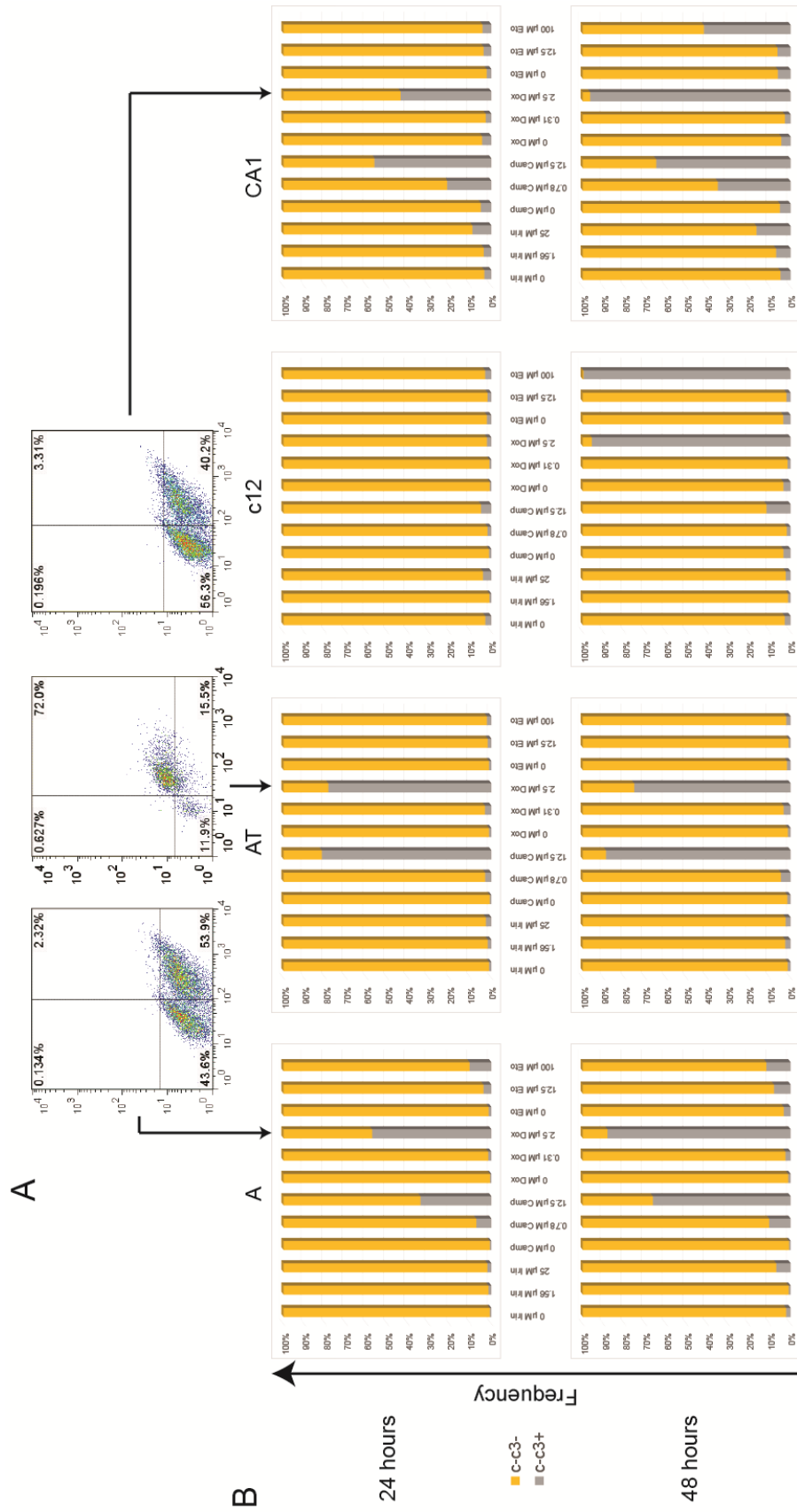
Figure 4.3 (Continued).

automated microscopy to produce time-lapsed image stacks, producing over 10,000 videos in total. In the end, however, we were unable to analyze this data in an unbiased and automated manner, as all software packages we tried failed to identify and track single cells consistently. Even so, we found that c12 cells in particular showed a senescent-like morphology at in response to high dose etoposide at long time points (96 hours or longer). However, attempts to formally assay senescence through β-galactosidase assays were too noisy to interpret. We also observed that AT and CA1 cells seemed to preferentially adopt autophagy-like morphologies with large vacuoles in response to doxorubicin. However, the best formal assay for autophagy is observation of the double membrane structure by electron microscopy. We did observe some such autophagic structures, but electron microscopy is unfeasible for quantification or high throughput methods. FACS screening was not practical as the principal biomarker for autophagy LC3 was not detectible in AT and CA1 cells. Therefore, we were unfortunately unable to extract meaningful information from these live-cell microscopy methods, though we remain hopeful that advances in computer vision algorithms may improve our ability to use these kinds of data in the future.

Having assembled this panel of cellular phenotypes, we next set out to measure internal signaling within the cells that determines cell fate, and find the correlations that explain cellular behavior.

4.2.2. Lysate Microarray Antibody Validation Screen for MCF10A Progression Series

We wanted to understand the molecular events that stem from, and effect the differential survival/death phenotype we had observed. Because we wanted to collect signaling information from as many nodes in as many signaling networks as possible, we performed a reverse screen of

antibodies tested against lysates from all three cell lines. This screen was performed simultaneously and analogously to the screen discussed in Section 3.2.2 of this work.

We designed a set of control conditions, selected such that every node monitored by an antibody is activated in at least one condition. We did not use the same set of 30 used in Section 3.2.2, rather we used a subset of 18 control lysates, produced in each cell line. As several lysates used in the previous work did not give any unique information not replicated in other lysates, we selected the set in Table 4.1.

Also included were serial 2-fold dilutions for 6 of these lysates for cell line A only, for a total of 108 total samples, including all controls. A full list of these lysates is included in Table 4.1. All samples were collected according to established protocol (Sevecka et al., 2011) with modifications to collect apoptotic cells (See Methods Section). These samples were then printed in duplicate onto nitrocellulose-coated glass slides using an Aushon 2470 arrayer and probed with the collection of all available antibodies in the MacBeath and Yaffe labs. In total, this collection numbered 483 antibodies, for a total of 104,328 measurements. Probing was carried out as previously described, with each array being exposed to a unique primary antibody and a standardization antibody (Sevecka et al., 2011). Image quantification was performed using Array-Pro by MediaCybernetics and data analysis was performed in Matlab.

Our selection criteria for passing the screen were stringent: significant signal ($p<0.05$) over background of at least 2-fold or 1/2-fold in at least 1 control lysate. We considered each cell line uniquely, and a particular antibody could be counted as a hit for any or all of the cell lines. Of the 483 antibodies tested, 58 were found to have positive signal in at least one cell line. These were then subjected to further standardization by immunoblotting. Of the 58, 39 were verified by immunoblotting to produce a single band of the expected size in all cell lines, with high linearity

with the screening result (Table 4.2). These antibodies were considered validated for use in lysate microarrays for the purposes of our next experiment.

4.2.3. Gathering a Dataset for Network Analysis of Cellular Signaling Downstream of Chemotherapy

We wanted to understand the signaling events downstream of treatment with chemotherapy drugs. Because we were limited by number of lysates we could print and produce, we selected doxorubicin and etoposide for further study. We selected the Topoisomerase II inhibitors for further study because the cell lines display a range of EC50s for doxorubicin (1 μM-10 μM), and etoposide potently causes cell cycle arrests in all four cell lines.

To find the differences in signaling that explain these differences in cell fates, we collected lysates spanning a long time course after drug treatment. We grew all four cell lines in 10 cm plates to 60% confluence, at which point treatment was administered. Lysates were collected in biological duplicate from treatment with 2 doses of each drug, at 6 time points (1, 4, 8, 12, 24, and 36 hours), along with mock treated controls, for a total of 288 unique lysates. All lysates were created and processed according to established protocol (Sevecka et al., 2011), with modification to collect apoptotic cells (see Methods Section).

These lysates were printed in technical duplicate on nitrocellulose-coated slides along with dilution curves, control lysates, and control spots, totaling 648 spots per microarray. The slides were probed with the set of 38 pre-validated antibodies for a total of 24,624 unique measurements, and quantified using MicroVigene by VigeneTech. Analysis was performed in Matlab. A representative scan of an array is shown in Figure 4.4.

Visual inspection of the lysate microarrays showed data quality was good. Spotting was consistent and technical variation was low: the average range between duplicate spots was 2.7% of the mean. Biological variation was higher than technical variation at 12.8%. Visual inspection also revealed that not every node measured had significant data; as several antibodies measured no change in signal across all treatment conditions. Because we observed this by visual inspection, we later checked for statistical significance in each signal and eliminate those without significant variation.

4.2.4. Statistical Analysis of Signaling and Phenotype Dataset

We wanted to build a model to correlate signaling events with cellular fates. In particular, we focused on applying principal components analysis (PCA) and partial least-squares regression (PLSR) to identify covariance between signals and covariance of signals to cell fates, respectively. As modeling efforts are hampered when data reflects noise rather than biological information, we began by deeply inspecting the data before normalization.

To test for antibodies that reflect biological information, we used statistical techniques to compare control lysates to treated lysates. If an antibody was truly detecting biological change, we expect a comparison of treated samples to mock treated controls to be statistically significantly different. Therefore, multivariate ANOVA was used with a relatively weak cutoff ($p < 0.1$) in order not remove potentially informative data. Non-significant data could indicate either no biological variation in that node in the data collected, or non-specific signal. Continuing to use this data would be misleading at best and confounding at worst after normalization, therefore we excluded these data before normalization. Of the 39 antibodies used, significant variation was
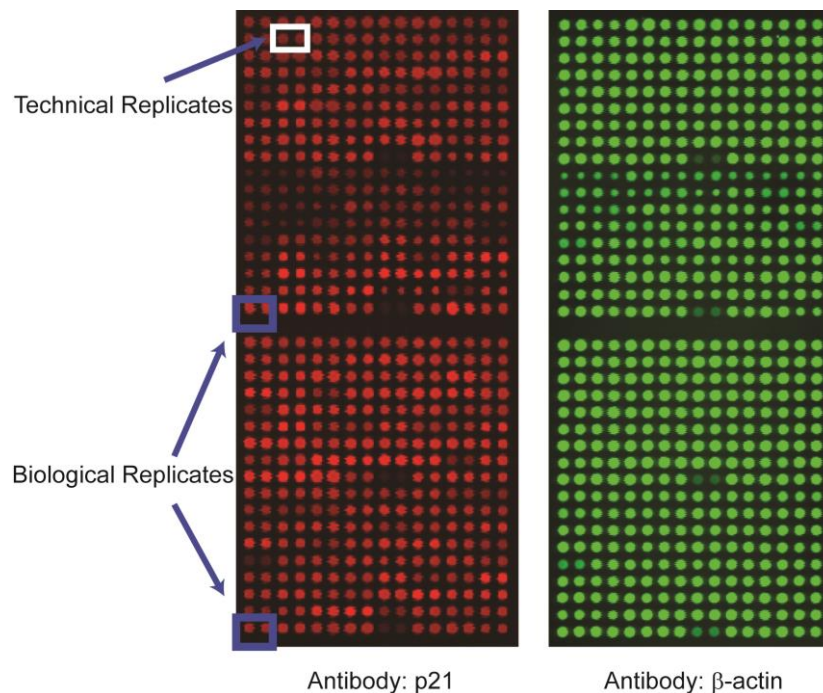
Figure 4.4. Lysate microarrays were used to monitor intracellular signaling after Topoisomerase II inhibitor treatment. Each microarray of 648 spots was simultaneously probed with a single primary antibody and a normalization antibody against β-actin. The microarray shown here was probed with an antibody against p21. Significant variation was observed in p21 upon genotoxic treatment. Lysates were printed as 2 subarrays, each containing 144 unique combinations of cell line, drug treatment, and time point. Biological replicates are found in the same position between subarrays. Technical variation was extremely small (c.v. = 2.7%), while biological variation was larger (c.v. = 12.8%).

found in 22, while no significant signal was observed in 17. All cell fate phenotypes were significant and were also kept. After removal of non-significant data, we then mean-centered range-normalized the data.

In order to highlight the variance in data rather than the absolute value of the signal, we performed several normalization steps for the data from each antibody. First, the mean was calculated for each signal or fate and was subtracted from every measurement. Then, each entry was divided by the absolute value of the highest or lowest value, resulting in a list with mean = 0

with all values between -1 and 1. These values were then put into MIDAS format and DataRail was used to do statistical analysis (Saez-Rodriguez et al., 2008).

Simultaneous visualization of the entire dataset is quite informative (Figure 4.5). We observe that bulk changes in signaling are correlated with progression, that is, cell line A had small changes in signaling in a few signaling nodes, while cell line CA1 had wild changes in many nodes. The amplitude of signaling changes correlated with phenotype severity, perhaps due to a bias in signals measured in the apoptotic pathway.

Our first approach to understand signaling correlations in the dataset was to use PCA. We began with a 2-component model to analyze covariance. Following PCA, we found that cell lines A and AT were projected in opposite directions in both PC1 and PC2, while AT and c12 were about equidistant from both. However, cell lines A and c12 were less positively projected in PC1, while cell lines AT and CA1 were more positively projected in PC2 (Figure 4.6A). This may indicate that PC2 is correlated with apoptotic behavior, as cell lines A and c12 largely resisted apoptosis. When we plotted by stimulus, we found that mock treated controls projected negatively in both PC1 and PC2, while high dose dox projected positively in PC2 (Figure 4.6B). Interestingly, low dose dox projected between low and high dose etoposide. These also formed a positive trend in PC1, indicating PC1 may be a measure of cell cycle dependent effects, as etoposide tended to induce cell cycle arrest.

Finally, analyzing the raw loadings of signals and fates was quite informative (Figure 4.6C). We noticed a cluster in positive PC2 (Figure 4.6C, red) that consists of phospho-ATM, total and phospho-p53, Apoptosis, and G2. We take this cluster to be a measure of DNA Damage signaling, which appeared to correlate strongly with both G2 checkpoint and apoptotic behavior. Interestingly, this cluster did not project closely to the p53 transcription target p21 (Figure 4.6C,
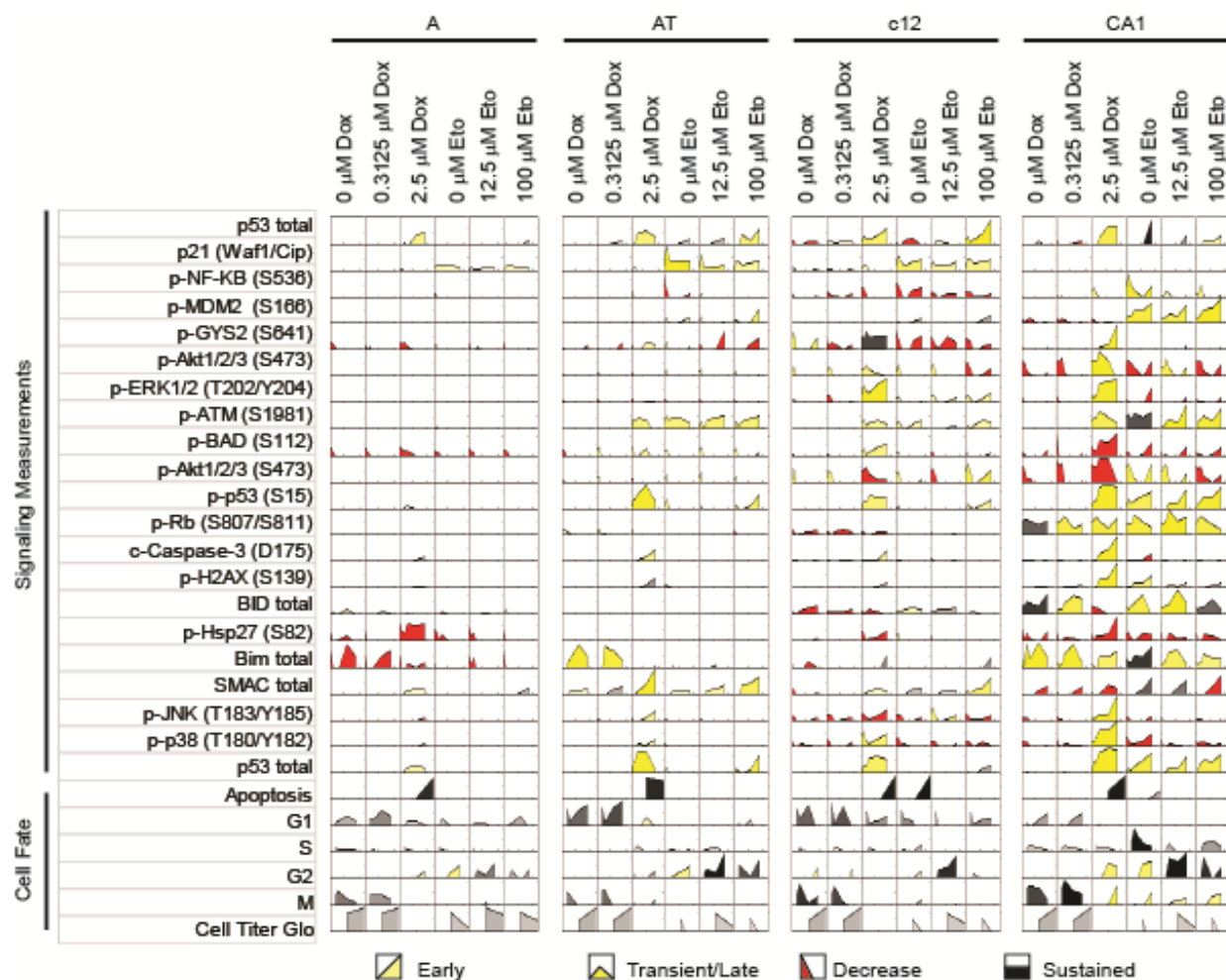
Figure 4.5. Visual inspection of the dataset shows clear differences between cell lines in response to Topoisomerase inhibitors. Time courses obtained from each sample are plotted for all signals and cell fates. Each signaling plot represents the mean of 2 biological replicates over 6 time points. Apoptosis and Cell Titer Glo plots represents the mean of 2 biological replicates over 2 time points, while cell cycle plots represent the mean of 2 biological replicates over 4 time points. Color coding indicates the timing of signaling events: early, transient or late, decreasing, or sustained.

Figure 4.6 (Next Page). PCA analysis of the dataset reveals some surprising insights into the nature of cellular signaling downstream of Topoisomerase inhibitors. The entire dataset including signals and cell fates was reduced to 2 principal components. Scores plots indicate an aggregate measure of all data collected of each type compared to the rest of the dataset. (A) Scores plot separated by cell line indicates that cell line A and CA1 were maximally differentiated, with AT and c12 approximately equidistant between A and CA1. (B) Scores plot broken down by cell line indicate that signaling and cell fates downstream of low dose dox are more similar to both low and high dose etoposide than high dose dox. (C) Loadings for specific measurements are projected into component space. A cluster of DNA damage-related signaling is indicated in red, and is correlated with apoptosis. While this cluster includes total p53 and p-p53, the transcription target p21 (yellow) is not strongly correlated with the DNA damage cluster. p-Akt and p-Rb are closely correlated (green), and together may be informative of cell cycle progression. Notably, however, they are not closely correlated to any of the measures of cell cycle, which are indicated in blue and are themselves not closely correlated with each other.
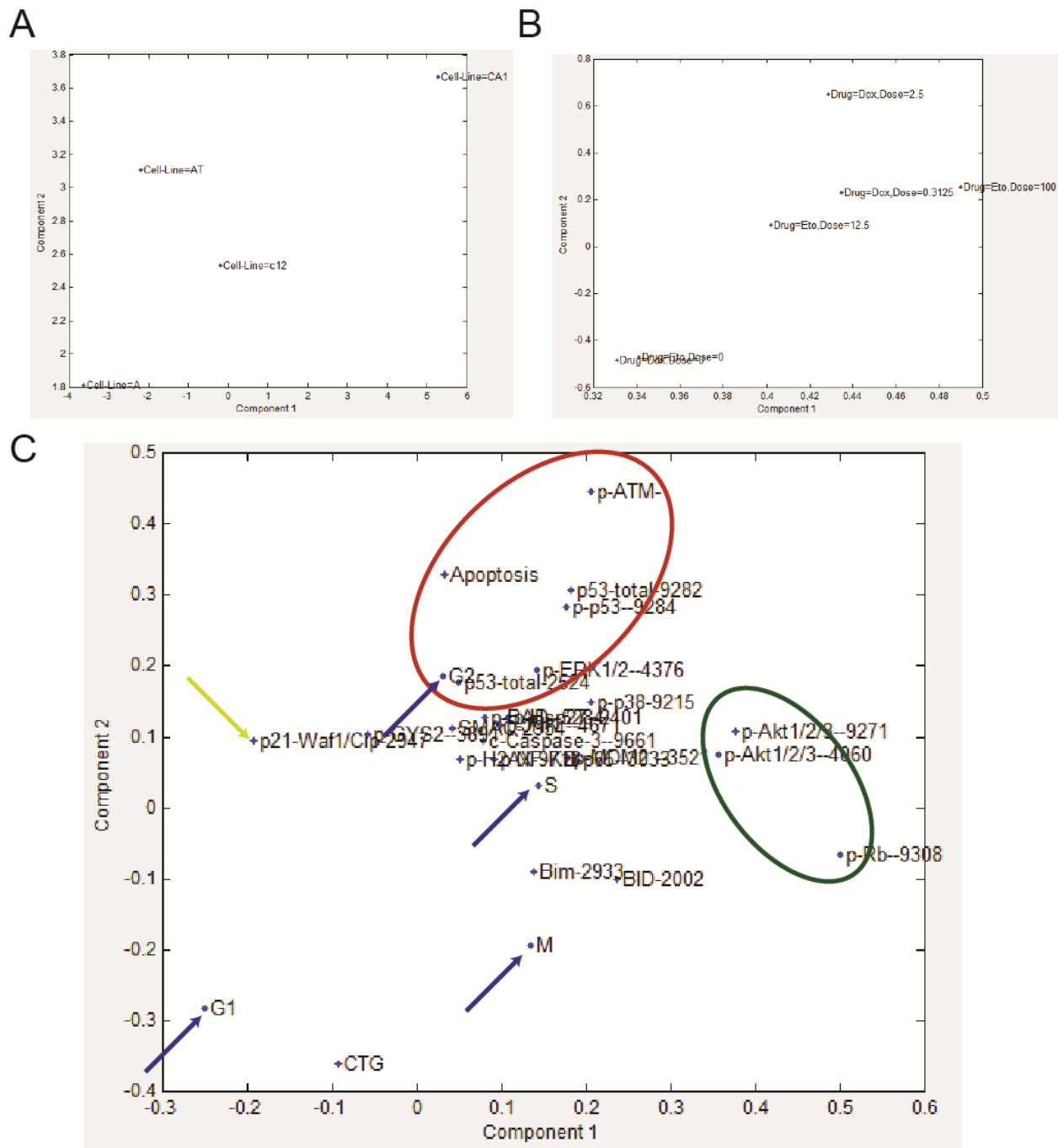
Figure 4.6 (Continued).

yellow), which projected negatively in PC1. By contrast, the proliferative markers phospho-Akt and phospho-pRb were found to project positively in PC1, in agreement with Figure 4.6B. Interestingly, however, neither p21 nor p-Akt/p-Rb was closely correlated to any of the direct measurements of cell cycle status (Figure 4.6C, blue). G1 in particular was projected negatively in both PC1 and PC2, correlating strongly with cell line A, which lends support to the idea that the G1-S checkpoint is quickly lost in tumor progression. Indeed, loss of G1-S checkpoint has been considered as mandatory for cancer development (Foijer and te Riele, 2006).

4.3.Future work

The PCA analysis we have done so far implies that apoptosis and cell cycle effects are not opposites on one axis, but rather orthogonal. This implies that the traditional understanding of cell cycle checkpoints and progression as "survival" and apoptosis as "death" may be incomplete, and that the true opposite of apoptosis may be an alternative cell fate such as autophagy. We would like to test this hypothesis by taking further cell fate measurements in autophagy and RIP kinase as a measure of necroptosis. Furthermore, it is interesting that the G1 checkpoint is active in cell lines A and c12 but lost in cell lines AT and CA1, especially considering that p16 is deleted in all four cell lines (Kadota et al., 2010). Understanding how this G1 checkpoint was lost in AT cells but then regained after xenograft passage through a mouse in c12 cells, then lost again in CA1 cells warrants further study.

At the time of this writing, we have not yet finished analyzing PLSR models of the dataset. We hope to complete this analysis and use it to generate hypotheses based on signals that correlate strongly with apoptosis or checkpoint activation. Because p-Erk was included in the cluster of pro-apoptotic signaling in PCA, we suspect inhibition of Erk may well dampen apoptotic response in. If this is the case, it is possible that giving a patient a cocktail of genotoxic drugs in combination with Erk inhibitors may well be counterproductive. We intend to test this prediction in the future, and hope this dataset may provide insight into the combinations of molecular changes in the DNA Damage Response that corresponds to tumor progression.

4.4. Conclusions

One of the greatest mysteries in cancer is the order in which specific molecular events that cause normal cells to become tumorigenic. In particular, while we know that cancer cells become sensitized to genotoxic chemotherapy over the course of transformation, the mechanism and the timing for sensitization remains largely unclear. Moreover, genotoxic chemotherapies can have severe, even intolerable side effects, and to understand these side effects we should study their effects in normal cells. We believe that in order to answer these questions, the MCF10 progression series of isogenic cancer cell lines is ideal.

We began by screening a panel of clinically used topoisomerase inhibitors against the MCF10 progression lines for efficacy in lowering viable cell count over 2 days, and found that the four cell lines have differential sensitivities. Surprisingly, progression did not directly correlate with susceptibility to chemotherapy, indicating that sensitization to chemotherapy can be a discontinuous process over the course of tumor progression. We therefore believe biomarkers should be measured within a tumor before initiating treatment, as targeted therapy supported by a priori information on internal signaling within the tumor is likely to improve efficacy.

We also used FACS assays to measure checkpoint activation and apoptotic signature. Cell cycle analysis indicated very high G2 checkpoint activation in both AT and CA1 cells, indicating a possible loss of G1 checkpoint and reliance on G2 checkpoint, a hallmark of cancer progression. Curiously, the G1 checkpoint seemed to be very much intact in c12 cells, suggesting a reversion that may be a result of selection pressure from xenograft passage through a mouse. The cell cycle profile at 24 and 48 hours after treatment was mostly unchanged, indicating that cells are probably not suspended in checkpoint indefinitely and can escape after some time. Apoptotic assays demonstrated that the MCF10A cell lines did not stain for cleaved PARP in all but a few

146

stimulations. However, caspase-3 could be observed in response to topoisomerase inhibition across all cellular backgrounds and was therefore used to separate apoptotic cells from non-apoptotic cells. Apoptotic response in A and c12 cells were was limited in all cases except high dose dox, while AT and c12 cells were much more prone to apoptosis. This data supports the idea that the G1 checkpoint is a protective feature of normal cells and loss of G1 checkpoint is correlated with both tumor aggressiveness and apoptotic potential. In cell cycle and apoptosis assays, we observed that doxorubicin was a far more potent drug for apoptosis while etoposide potently activated checkpoints. Perhaps this information as well should guide how these drugs are used in the clinic in the context of MCF10CA1-like, triple negative breast tumors.

Having established that the Topo II inhibitors produce varied signaling responses in the MCF10 lines, we next conducted a multiplexed stimulation with 2 doses of each drug. We validated a set of 39 antibodies against various DNA damage response and apoptosis targets for use in all 4 cell lines. We then collected a set of 144 conditions and measured multiplexed cellular signaling response over a long time course. Finally, statistical analysis has shown some intriguing correlations worth further exploration. PCA analysis indicates that a cluster of ATM/p53/ERK signaling correlate with apoptosis and G2. However, on an orthogonal dimension, p-Akt/p-pRb and p21 are anticorrelated, indicating intracellular cell cycle signaling is statistically distinguishable from apoptotic signaling, and that survival and apoptosis may not be opposites, but rather orthogonal. Inclusion of alternative cell fates such as necroptosis and autophagy may reveal the true complexity of cell fates downstream of chemotherapy.

Over the course of this experiment, we found that lysate microarray technology was useful for gathering datasets for statistical analysis of signaling data. Coupling this technique with others such as FACS and luminescence-based assays is a successful strategy to build rich, informative

147

datasets that give unique insight into biological systems. We believe that to fully appreciate the complexity of biological systems cooperating to make decisions that guide cell fate, we must have techniques that are capable of massively parallel simultaneous measurements. We expect lysate microarrays to continue to be a fruitful tool of the future in such multiplexed research.

4.5. Tables

Table 4.1 – Full list of screening lysates used to antibody validation

Condition	A	AT	c12	CA1
DMSO	1	2	3	4
NCS	5	6	7	8
Starved	9	10	11	12
EBSS	13	14	15	16
Ser Shocked	17	18	19	20
TNF	21	22	23	24
UV (1 hr)	25	26	27	28
IR	29	30	31	32
Dox	33	34	35	36
Conflu. (G1)	37	38	39	40
Aphidicolin (S)	41	42	43	44
IR 36 hr (G2)	45	46	47	48
Noco (M)	49	50	51	52
DTB 0 (eS)	53	54	55	56
DTB+4 (S)	57	58	59	60
DTB+8 (G2)	61	62	63	64
DTB+12 (M)	65	66	67	68
DTB+16 (G1)	69	70	71	72

Dilution Series	A only	Parent Sample #
Serum Shock	73-78	17
NCS	79-84	5
Confluent (G1)	85-90	37
Dox	91-96	33
Aphidicolin (S)	97-102	41
Nocodozole (M)	103-108	49

Table 4.1. Full list of control lysates selected for antibody validation in MCF10 series. Lysate conditions were selected to activate every node for which we had an antibody, in at least one condition. Left: number represents the order in which lysate was printed on arrays. Right: Control lysates and dilution series, using only MCF10A sample as parent. DTB = Double Thymidine Block (synchronized in early S phase)

Table 4.2 – Full list of Antibodies Validated for Use in MCF7, MB-453, and BT20 cells			
Antibody	**Comp**	**Cat#**	**Species**
p53	CST	2524	Mouse
p-BCL-2 (S70)	CST	2827	Rabbit
p21 Waf1/Cip	CST	2947	Rabbit
p-mTOR (S2448)	CST	2971	Rabbit
p-NF-KB p65 (S536)	CST	3033	Rabbit
p-MDM2 (S166)	CST	3521	Rabbit
p-GYS2 (S641)	CST	3891	Rabbit
p-Akt1/2/3 (S473)	CST	4060	Rabbit
p-ERK1/2 (T202/Y204)	CST	4376	Rabbit
p-Wee1 (S642)	CST	4910	Rabbit
p-ATM (S1981)	Epitomics		Rabbit
p-BAD (S112)	CST	5284	Rabbit
p-cdc2 (Y15)	CST	9111	Rabbit
p-SAPK/JNK (T183/Y185)	CST	9251	Rabbit
p-Akt1/2/3 (S473)	CST	9271	Rabbit
p-p53 (S15)	CST	9284	Rabbit
p-p53 (S20)	CST	9287	Rabbit
p-Rb (S807/S811)	CST	9308	Rabbit
p-GSK-3a/3b (pS21/pS9)	CST	9331	Rabbit
c-PARP (Asp 214)	CST	9541	Rabbit
c-Caspase 3 (D175)	CST	9661	Rabbit
p-H2AX (S139)	CST	9718	Rabbit
p-ATM (S1981)	Upstate	05-740	Mouse
p53	CST	2527	Rabbit
BID	CST	2002	Rabbit
p-Chk1 (S345)	CST	2348	Rabbit
p-Hsp27 (S82)	CST	2401	Rabbit
p27	CST	2552	Rabbit
Cyclin D1	CST	2922	Rabbit
Bim	CST	2933	Rabbit
SMAC	CST	2954	Mouse
RIP	CST	3493	Rabbit
p-JNK (T183/Y185)	CST	4671	Rabbit
p-p38 (T180/Y182)	CST	9215	Rabbit
p53	CST	9282	Rabbit
cleaved casp-8	CST	9496	Rabbit
cleaved casp-9	CST	9501	Rabbit
p-cdc25C (S216)	CST	9528	Rabbit
cleaved casp-6	CST	9761	Rabbit

Table 4.2. Full list of Antibodies Validated for use in all cell lines in the MCF10 progression series. All antibodies were selected from primary screening using control lysates, then individually validated for positive, linear, specific signal in immunoblots.

4.6. Experimental Methods

Antibody Reagents

Pan and phospho-specific antibodies for signaling proteins were purchased from Abcam (Cambridge, MA), BD Biosciences (San Jose, CA), Cell Signaling Technology (Beverly, MA), Santa Cruz Biotechnology (Santa Cruz, CA), and Upstate (Charlotteville, VA). Mouse monoclonal anti-β-actin antibody (clone AC-15) was purchased from Sigma-Aldrich (Saint Louis, MO), rabbit monoclonal anti-β-actin antibody was catalog # 4970 (Cell Signaling Technology (Beverly, MA)). Secondary detection antibodies were purchased from Li-Cor Biosciences (Lincoln, NE).

Cell Culture

All cell lines were obtained from the Karmanos Institute (Detroit, MI) and maintained at low passages (<20) in various medias (See Appendix A).

Cell Response Assays: Apoptosis

Following treatment, cells were washed and trypsinized, saving all floater cells. Fixation using 4% paraformaldehyde at room temperature for 15 minutes was followed by resuspension in ice-cold methanol and overnight incubation at -20°C. Cells were washed in PBST, blocked for 1 hour in BSA/PBST, and stained with antibodies against cleaved-caspase-3 and cleaved-poly(ADP-ribose) polymerase (PARP) (BD PharMinogen). Secondary Alexa-conjugated detection antibodies were used for visualization in a BD FacsCalibur flow cytometer (Molecular Probes). Analysis was done using FloJo, and because cleaved-PARP was not always observed, cells positive for cleaved-caspase-3 were scored as apoptotic.

151

Cell Response Assays: Cell Cycle

Following treatment, cells were fixed in 70% ethanol overnight at -20°C, permeabilized with PBS-Triton for 20 min at 4°C, blocked with 1% BSA, and incubated with antibodies against phospho-Histone H3 (Millipore). After washing, cells were incubated with Alexa-488 conjugated secondary antibody on ice, washed, and stained with 50 μg/mL propidium iodide (PI) prior to analysis. A BD FacsCalibur flow cytometer was used, and analysis was done using FloJo utilizing the Dean-Jett-Fox algorithm.

Cell Response Assays: Viable Cell Count

Cells were plated at 10,000 cells/well in 96-well optical glass bottom white walled plates, then stimulated. Metabolic viability was measured using Cell Titer Glo (Promega) according to manufacturer protocol. Normalization was always to untreated sample.

Western Blotting

Cell lysates were prepared as described previously (Sevecka et al., 2011). Crude lysates were filtered in AcroPrep 96 well 3.0 μm glass fiber/0.2 μm BioInert filter plate (Pall), then normalized for total protein content using the BCA assay (Pierce). Blots were run using 48-well precast gels and transferred using semi-dry fast transfer apparatus onto nitrocellulose membranes (e-PAGE, i-Blot, Invitrogen). Blots were blocked in Odyssey blocking buffer (Li-Cor), incubated overnight with primary antibody, stained with secondary antibodies conjugated to an infrared die, then visualized using an Odyssey flat bed scanner (Li-Cor).

Microarray Fabrication and Probing

Custom lysate microarrays were printed in-house using an Aushon 2470 arrayer (Aushon Biosytems, (Billerica, MA)) on 16-pad nitrocellulose-coated glass slides (Grace Biolabs (Bend, OR)). Lysates were printed at 333 μm spacing using steel solid 110 μm pins, which resulted in an average feature diameter of 170 μm. Lysates were printed in technical duplicates. Slides were stored in a dry, dark, room temperature environment until probing. Probing was done according to previous protocol (Sevecka et al., 2011).

Analysis of Microarray Data

Signal intensities from target proteins were normalized using the β-actin signal intensities from the same spot to normalize for spotting variation. Data from duplicate spots were averaged, and the ratio of signal from treated samples to reference control sample computed for each target protein. For each antibody specific to a protein measured, we calculated a value according to Equation 4.1.

$$x = \frac{\text{signal(t)}/\beta\text{-actin(t)}}{\text{signal(ref)}/\beta\text{-actin(ref)}}$$

Equation 4.1. Calculation for upregulation of signal post treatment. "Signal" refers to the fluorescence measured from the variable antibody, "β-actin" refers to the fluorescence measured from the β-actin antibody, "t" refers to the treatment condition being considered, and "ref" refers to a reference condition, a mock treated sample at t=1.

Computational Modeling and Statistics

The dataset was processed extensively before PCA analysis. ANOVA analysis was performed by splitting the dataset into mock treated versus treated samples, then comparison for statistical

significance for variation. Those antibodies without statistically significant variation (p>.10) were

omitted. After ANOVA testing, each signal was normalized by the following equation:

$$y_i = \frac{x_i - \bar{x}}{|x_{max}|}$$

> **Equation 4.2.** Normalization of antibody data to nondimensionalize the different measurements. y is the normalized value, x is the prenormalized value, x_{max} is the measurement most distant from the mean, positive or negative. Applying this equation to an antibody results in a dataset with mean = 0 and all values varying between -1 and 1.

PCA analysis was performed using DataRail using the PCA/PLSR function (Saez-Rodriguez

et al., 2008).

Works Cited

Choong, L.Y., Lim, S., Chong, P.K., Wong, C.Y., Shah, N., and Lim, Y.P. (2010). Proteome-wide profiling of the MCF10AT breast cancer progression model. PloS one *5*, e11030.

Dawson, P.J., Wolman, S.R., Tait, L., Heppner, G.H., and Miller, F.R. (1996). MCF10AT: a model for the evolution of cancer from proliferative breast disease. Am J Pathol *148*, 313-319.

Foijer, F., and te Riele, H. (2006). Check, double check: the G2 barrier to cancer. Cell Cycle *5*, 831-836.

Fox, M.H. (1980). A model for the computer analysis of synchronous DNA distributions obtained by flow cytometry. Cytometry *1*, 71-77.

Kadota, M., Yang, H.H., Gomez, B., Sato, M., Clifford, R.J., Meerzaman, D., Dunn, B.K., Wakefield, L.M., and Lee, M.P. (2010). Delineating genetic alterations for tumor progression in the MCF10A series of breast cancer cell lines. PloS one *5*, e9201.

Pommier, Y., Leo, E., Zhang, H., and Marchand, C. (2010). DNA topoisomerases and their poisoning by anticancer and antibacterial drugs. Chemistry & biology *17*, 421-433.

Rhee, D.K., Park, S.H., and Jang, Y.K. (2008). Molecular signatures associated with transformation and progression to breast cancer in the isogenic MCF10 model. Genomics *92*, 419-428.

Saez-Rodriguez, J., Goldsipe, A., Muhlich, J., Alexopoulos, L.G., Millard, B., Lauffenburger, D.A., and Sorger, P.K. (2008). Flexible informatics for linking experimental data to mathematical models via DataRail. Bioinformatics *24*, 840-847.

Samuel, N., and Hudson, T.J. (2013). Translating genomics to the clinic: implications of cancer heterogeneity. Clinical chemistry *59*, 127-137.

Santner, S.J., Dawson, P.J., Tait, L., Soule, H.D., Eliason, J., Mohamed, A.N., Wolman, S.R., Heppner, G.H., and Miller, F.R. (2001). Malignant MCF10CA1 cell lines derived from premalignant human breast epithelial MCF10AT cells. Breast Cancer Res Treat *65*, 101-110.

Sevecka, M., Wolf-Yadlin, A., and G., M. (2011). Lysate microarrays enable high-throughput, quantitative investigations of cellular signaling. Mol Cell Proteomics *10*.

Soule, H.D., Maloney, T.M., Wolman, S.R., Peterson, W.D., Brenz, R., McGrath, C.M., Russo, J., Pauley, R.J., Jones, R.F., and Brooks, S.C. (1990). Isolation and characterization of a spontaneously immortalized human breast epithelial cell line, MCF-10. Cancer Res *50*, 6075-6086.

Tomicic, M.T., and Kaina, B. (2013). Topoisomerase degradation, DSB repair, p53 and IAPs in cancer cell resistance to camptothecin-like topoisomerase I inhibitors. Biochimica et biophysica acta *1835*, 11-27.

Appendix A: Composition of Solutions

1X Phosphate-Buffered Saline (PBS)
0.8% sodium chloride (NaCl)
0.02% potassium chloride (KCl)
0.144% disodium hydrophosphate (Na_2HPO_4)
0.024% potassium dihydrophosphate (KH_2PO_4)
pH to 7.4

2% SDS Lysis Buffer
50 mM tris(hydroxymethyl)aminomethane hydrochloride (Tris-HCl)
2% sodium dodecyl sulfate (SDS)
5% (w/v) glycerol
5 mM ethylenediaminetetraacetic acid, sodium salt (Na_2EDTA)
1 mM sodium fluoride (NaF)
1 per 50 mL protease inhibitor tablets
1% (v/v) phosphatase inhibitor cocktail
10 mM β-glycerophosphate
1 mM phenylmethylsulphonylfluoride (PMSF)
1 mM sodium orthovanadate (Na_3VO_4), depolymerized
1 mM dithiothreitol (DTT, Cleland's reagent)
pH to 6.8

PBS/Tween (PBST)
1X PBS
0.1% (v/v) Tween-20

PBS/Triton (PBS-Triton)
1X PBS
0.25% (v/v) Triton X-100

Microarray Pre-Wash Buffer
100 mM Tris-HCl, pH 9

Culture Medium for HepG2 cells
90% Dulbecco's modified Eagle's medium (DMEM)
10% fetal bovine serum (FBS)
2.5 µg/mL fungizone
5 µg/mL gentamycin

100 I.U./mL penicillin
100 µg/mL streptomycin

Culture Medium for MCF10A, MCF10AT cells
1X HuMEC basal serum free medium
1X HuMEC supplement kit
100 I.U./mL penicillin
100 µg/mL streptomycin

Culture Medium for MCF10AT1.c12, MCF10CA1.H cells
95% Dulbecco's modified Eagle's medium (DMEM)
5% fetal bovine serum (FBS)
2 mM L-glutamine
100 I.U./mL penicillin
100 µg/mL streptomycin

Culture Medium for BT 20 cells
90% Minimum Essential Medium (MEM) + Earle's Salts
10% fetal bovine serum (FBS)
2 mM L-glutamine
100 I.U./mL penicillin
100 µg/mL streptomycin

Culture Medium for A549, MDA-MB453, MCF7, MDA-MB231, MDA-MB468, MDA-MB436, MDA-MB157 cells
90% Dulbecco's modified Eagle's medium (DMEM)
10% fetal bovine serum (FBS)
2 mM L-glutamine
100 I.U./mL penicillin
100 µg/mL streptomycin

Culture Medium for Hs578T cells
90% Dulbecco's modified Eagle's medium (DMEM)
10% fetal bovine serum (FBS)
2 mM L-glutamine
10 µg/mL insulin
100 I.U./mL penicillin
100 µg/mL streptomycin

Culture Medium for Hs578BST cells
90% Dulbecco's modified Eagle's medium (DMEM)
10% fetal bovine serum (FBS)
2 mM L-glutamine
30 ng/mL EGF
100 I.U./mL penicillin
100 μg/mL streptomycin

Culture Medium for HCC-1143, HCC-1500, NCI-1650, NCI-358, BT-474 cells
RPMI 1640 media
10% fetal bovine serum (FBS)
2 mM L-glutamine
100 I.U./mL penicillin
100 μg/mL streptomycin

Culture Medium for cells
RPMI 1640 media
10% fetal bovine serum (FBS)
2 mM L-glutamine
1 μg/mL insulin
100 I.U./mL penicillin
100 μg/mL streptomycin